Rupture Forces of Split Aptamers

DISSERTATION

zur Erlangung des Grades
"Doktor der Naturwissenschaften“
am Fachbereich Chemie, Pharmazie und Geowissenschaften der
Johannes Gutenberg-Universität Mainz

vorgelegt von

Thi-Huong Nguyen
geboren in Hanoi, Vietnam

Mainz, den 8. April 2013

Tag der Mündlichen Prüfung: 29.04.2013

Zusammenfassung

Die Kräfte für das Aufbrechen von Ligand-Rezeptor Wechselwirkungen, wie sie in Proteinen, Zellen, und lebendigen Geweben vorkommen, wurden erfolgreich mit Rasterkraft-Spektroskopie gemessen. Für diese Messungen wurden Ligand und Rezeptor so modifiziert, dass sie auf einer Spitze und dem Substrat befestigt werden konnten. Ligand und Rezeptor wechselwirken miteinander, wenn die Spitze an die Oberfläche angenähert wird. Diese Wechselwirkungen können durch Messung der Zerreisskraft beim Entfernen der Spitze untersucht werden. Leider ist dieses Verfahren ungeeignet für die Messung kleiner Moleküle, da deren Wechselwirkungen extrem schwach sind. Außerdem kann die Modifikation kleiner Moleküle zur Befestigung an Oberflächen zur Blockade oder Veränderung der Bindungsgruppen führen. Deswegen können die aufgenommenen Zerreisskräfte bei kleinen Molekülen nicht die gesamte Bandbreite der beteiligten Ligand-Rezeptor Wechselwirkungen wiedergeben.

In meiner Arbeit wird ein neuartiges Konzept zur Messung schwacher Ligand-Rezeptor Wechselwirkungen eingeführt das keine Modifikation der beteiligten Moleküle benötigt. Die Zerreisskraft zwischen Rezeptor und Ligand wird dabei nicht direkt gemessen sondern ergibt sich als Differenz aus Messungen in Gegenwart und in Abwesenheit des Liganden. Als Modellsystem wurde Adenosinmonophosphat (AMP) und ein Aptamer, das AMP spezifisch bindet, gewählt. Das Aptamer (Rezeptor) ist ein DNA-Einzelstrang, der teilweise selbst hybridisieren kann und dabei Bindungstaschen für AMP (Ligand) bildet. Die Bindungen zwischen dem AMP und dem Aptamer bestehen aus mehreren Wasserstoff-Brückenbindungen.

In meinem neuen Konzept wird das Aptamer in zwei Teile (Oligo a und Oligo b) geteilt. Ein Teil wird an der Spitze, der andere auf dem Substrat befestigt. Wenn die Spitze an das Substrat angenähert wird hybridisieren Oligo a and Oligo b teilweise und die Bindungstaschen bilden sich. Bei Zugabe von AMP zur Pufferlösung bindet das AMP in den Taschen und zusätzliche Wasserstoff-Brückenbindungen entstehen. Beim Entfernen der Spitze von der Oberfläche konnte die Zerreißkraft dieses AMP-Split-Aptamer Komplexes gemessen werden. Diese Zereisskraft erhöhte sich in der Gegenwart von AMP um ca. 10 pN.

Die Dissoziationskonstante des AMP-Split-Aptamers wurde auf Einzel-Molekül-Ebene (~4 µM) durch Veränderung der AMP Konzentration und Messen der Zerreisskraft bei jeder Konzentration bestimmt. Außerdem wurde die Zereisskraft durch die Erhöhung der Bindungstaschen-Zahl verstärkt.

Die Geschwindigkeitskonstante für die thermodynamische Dissoziation der zwei Oligos war in der Anwesenheit von AMP leicht verringert, was darauf hindeutet, dass AMP das Split-Aptamer mit zwei Bindungstaschen stabilisiert. Die Zerreisskräfte bei verschiedenen Belastungsgeschwindigkeiten folgten keinem logarithmischen Verhalten, das üblicherweise zur

Beschreibung des Verhaltens der Zereisskraft von Oligonukleotiden bei verschiedenen Belastungsgeschwindigkeiten verwendet wird. Für hohe und niedrige Belastungsgeschwindigkeiten wurden zwei unterschiedliche Bereiche gefunden, ein Verhalten welches bisher so nicht beschrieben wurde. Ein Modell, das diese beiden Bereiche mit der Dehnung der Bindungstaschen der Oligos erklärt, wurde entwickelt.

Um den Beitrag einer einzelnen Wasserstoffbrückenbindung zur Bildung der Doppelhelix der Nukleinsäuren zu verstehen wurde die Anzahl der Bindungsgruppen des AMP reduziert, also neue Zielmoleküle dargestellt. Die Zereisskräfte des Split-Aptamers in Anwesenheit dieser Moleküle wurden gemessen. Die Zereisskräfte skalierten linear mit der Anzahl der Bindungsgruppen. Hierbei wurde festgestellt, dass die Phosphatgruppe den größten Anteil an der Ausbildung des Wasserstoffbrücken-Netzwerks zwischen AMP Molekül und Aptamer beiträgt.

Abstract

Rupture forces of ligand-receptor interactions, such as proteins-proteins, proteins-cells, and cells-tissues, have been successfully measured by atomic force spectroscopy (AFS). For these measurements, the ligands and receptors were chemically modified so that they can be immobilized on the tip and on a substrate, respectively. The ligand interact the receptor when the tip approaches the substrate. This interaction can be studied by measuring rupture force upon retraction. However, this technique is not feasible for measurements involving small molecules, since they form only few H-bonds with their corresponding receptors. Modifying small molecules for immobilization on surfaces may block or change binding sites. Thus, recorded rupture forces might not reflect the full scope of the involved small ligand-receptor interactions.

In my thesis, a novel concept that allows measuring the rupture force of small involved ligand-receptor interactions and does not require molecular modification for immobilization was introduced. The rupture force of small ligand-receptor interaction is not directly measured but it can be determined from measurements in the presence and in the absence of the ligand. As a model system, the adenosine mono phosphate (AMP) and the aptamer that binds AMP were selected. The aptamer (receptor) is a single stranded DNA that can partially self-hybridize and form binding pockets for AMP molecules (ligands). The bonds between AMP and aptamer are provided by several H-bonds and pair stacking.

In the novel concept, the aptamer was split into two parts (oligo a and oligo b). One part was immobilized on the tip and the other one on the substrate. Approaching the tip to the substrate, oligo a and oligo b partially hybridized and the binding pockets were formed. After adding AMP into the buffer solution, the AMP bound in the pockets and additional H-bonds were formed. Upon retraction of the tip, the rupture force of the AMP-split aptamer complex was measured. In the presence of excess AMP, the rupture force increased by about 10 pN.

The dissociation constant of the AMP-split aptamer complex was measured on a single molecular level (~ 4 μM) by varying the AMP concentrations and measuring the rupture force at each concentration. Furthermore, the rupture force was amplified when more pockets were added to the split aptamer.

In the absence of AMP, the thermal off-rate was slightly reduced compared to that in the presence of AMP, indicating that the AMP stabilized the aptamer. The rupture forces at different loading rates did not follow the logarithmic fit which was usually used to describe the dependence of rupture forces at different loading rates of oligonucleotides. Two distinguished regimes at low and high loading rates were obtained. The two regimes were explained by a model in which the oligos located at the pockets were stretched at high loading rates.

The contribution of a single H-bond formed between the AMP molecule and the split aptamer was measured by reducing the binding groups of the AMP. The rupture forces reduce corresponding to the reduction of the binding groups. The phosphate group played the most important role in the formation of H-bond network between the AMP molecule and the split aptamer.

Contents

1. Introduction and Motivation

The double helix structure of Deoxyribonucleic acid (dsDNA) was discovered by James Watson and Francis Crick in 1953 [1]. By solving the molecular structure of nucleic acid and its significance for information transfer in living material, they together with Maurice Wilkins were awarded with the Nobel Prize for Physiology and Medicine in 1962.

The dsDNA structure is composed of purine and pyrimidine bases attached to a backbone of a 5-carbon sugar (deoxyribose) alternating with a phosphate group. The purine and pyrimidine bases consist of two units each, i.e. adenine (A) and guanine (G), thymine (T) and cytosine (C), respectively. These bases pair together, A to T and G to C, by based on H-bonds and these are called 'Watson-Crick pairs'. A dsDNA consists of two complementary polyoligonucleotides which are held together by Watson-Crick pairs. Each oligo composes of sugar backbone and nucleotides are attached on it (Fig. 1.1). An oligo is chemically oriented from end to end and follows a rule of directionality, i.e. from 5'- to 3' and for the left strand and from 3'- to 5' for the right strand. When one edge of a base of oligo *1* matches the edge of another base of oligo *2*, the bases are joined by hydrogen bonds (H-bonds, yellow dashed lines) and laid on the same plane. The A-T pair contains two H-bonds while the G-C pair contains three H-bonds. The total H-bonds in a dsDNA depends on the number of pairs in its structure [2]. The double helix structure has a width of 2.0 nm and the distance between bases of 3.4 Å. Each H-bond contributes a small force to stabilize the dsDNA structure and this force is the binding force in the double helix.

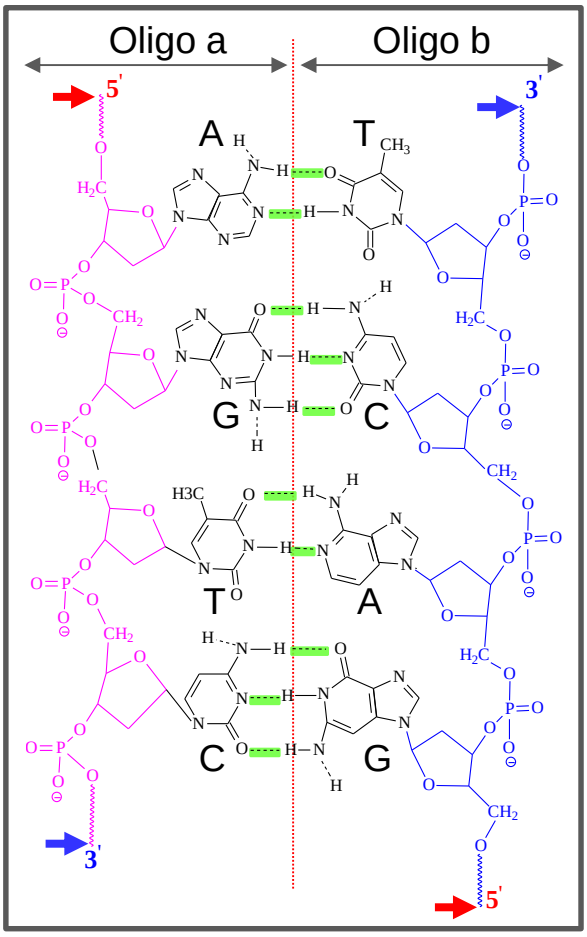

Figure 1.1: Chemical structure of a dsDNA. Two complementary oligos (oligo 1 and oligo 2) are held together by H-bonds (green) to form a dsDNA. The direction of oligo 1 is from 5' (red arrow) - to 3' (blue arrow) end while oligo *2* is from 3'- to 5' end.

Aptamers are short oligonucleic acids (DNA, RNA) evolved in vitro to perform a specific function [1, 2]. They have behaviors that at certain aspects are similar to antibodies which are widely applied in medical studies [3]. However, producing of antibodies normally involves in vivo or in living cell. They can partly self-hybridize to form BP for small molecules or proteins. Aptamers bind to many targets with high affinity and specificity [4]. Figure 1.2 is an example of a DNA-aptamer that binds adenosine monophosphate (AMP).

The procedure to produce aptamer is so called Systematic Evolution of Ligands by Exponential Enrichment (SELEX) by Gold and Tuerk, 1990 [1]. The SELEX process is a technique for isolating functional nucleic acids by screening oligonucleotides for molecular targeting. The targets for SELEX can be varied from small molecules to proteins, cell, and tissues. After the DNA or RNA aptamer bind targets, the DNA- or RNA-target complex is separated from free nucleic acids in the batch by nitro-cellulose filter binding, affinity chromatography, size fractionation on columns, or electrophoresis on native polyacrylamide

gels. This DNA or RNA is then amplified by polymerase chain reaction (PCR). With special adaptation, peptide aptamers have also been found by SELEX.

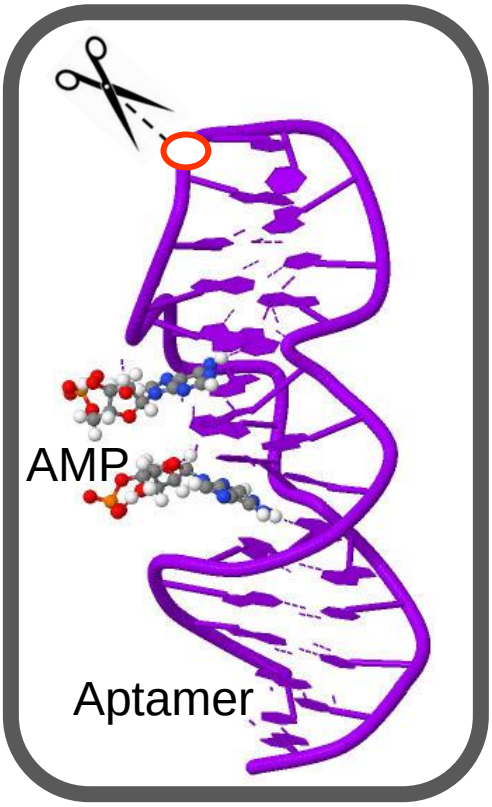

Figure 1.2: Aptamer cartoon (violet) including Waston Crick pairs at two ends and pockets that bind AMP molecules (small balls) at the center. The aptamer is split into two parts for AFS measurement.

Aptamers can be produced by SELEX with high purification and can be modified to enhance their stability, affinity, and specificity because of in vitro process [5, 6]. They can be stabilized by additional modification to involve in medical treatment in vivo [7, 8]. They have high temperature stability and can recover their native conformation after thermal denaturation. In addition, their small sizes can help them penetrate into cells or tissues easily [5, 9]. Recently, aptamers have become very promising candidates in biosensors, analytical and diagnostic applications. The fundamental of the biological systems will be introduced in detail in **Chapter 2.**

To date, a number of methods have been utilized to understand H-bond strength in nucleic acids as well as ligands-nucleic acids interactions. Powerful analytical techniques such as X-ray crystallography, Nuclear Magnetic Resonance (NMR), Absorption spectroscopy, or Electron microscopy have been used to investigate drug-DNA interactions [10]. However, some disadvantages still exist in each. A typical disadvantage is the requirement of significant amount of sample per measurement. In addition, with X-ray technique, the molecular

conformation in the crystal may be significantly different from the conformation in solution [11]. Preparation of the pure crystal sample is challenging and requires hours, days, or weeks of effort. With NMR, the sample needs to be dissolved in a deuterated solvent, and averages the results from all the molecules in the sample. Expertise in NMR is required to interpret the spectra depending on the compound complexity. UV-Vis spectroscopy is simple to conduct, but it contains less information. Electron microscopy can directly image individual molecules. However, stains or contrast agents and vacuum environment are required. These requirements reduce resolution and investigation environment differ from the natural environments, which makes it difficult to transfer the results from the experiment to the conditions in a living organism. In general, detection of protein, cell, and tissue bindings can be facilitated by labeling with fluorescent dyes without changing their properties. By contrast, efficient detection of small molecules suffers from significant changes of chemical properties as a consequence of target labeling and from the relative paucity of binding sites on small organic molecules.

Single-molecule force spectroscopy has emerged as a powerful tool to investigate forces in biological molecules [12, 13]. The most common force spectroscopy techniques are optical tweezers (OT) [14], and atomic force microscopy (AFM) [15]. Both AFM and OT can offer information of drug-DNA interactions in physiological condition [16, 17].

Atomic force spectroscopy (AFS), derived from AFM which was invented in 1986 [21], has been successfully applied to measure the strength of the H-bonds in nucleic acid as well as ligands-nucleic acids interactions [22]. By approaching one strand of a nucleic acid (A) fixed on the tip close to its complementary strand (B) immobilized on the surface, the oligo hybridization will take place (Fig. 1.3). Moving the tip away from the surface, these two strands will be stretched. Eventually, the stress will exceed the binding strength and the strands will be separated. The force needed to achieve this separation is usually called ‘rupture force’. This force represents the total binding force in the dsDNA. More information about AFS will be provided in **Chapter 3**.

From the time the AFM was invented, a number of measurements of separating and stretching structure of dsDNAs have been measured [18-21]. However, the results among those studies provide a large variation in the rupture force of single H-bond. For example, in 1994, one of the first studies of measuring rupture force of H-bonds in nucleic acid was reported by Lee et al who introduced an experimental setup which became a useful method nowadays to measure many molecular interactions in living conditions with AFS [19]. The authors immobilized one part of a DNA strand with different lengths (12, 16, 20 bases) on the AFM tip and its complementary on the substrates. By approaching the tip to and retracting it from the surface, they obtained rupture forces of 830, 1110 and 1520 pN for the corresponding mentioned DNA

strands in ionic conditions (0.1 N NaCl). This means that the rupture force of a single pair (A-T or G-C) is about 70 pN.

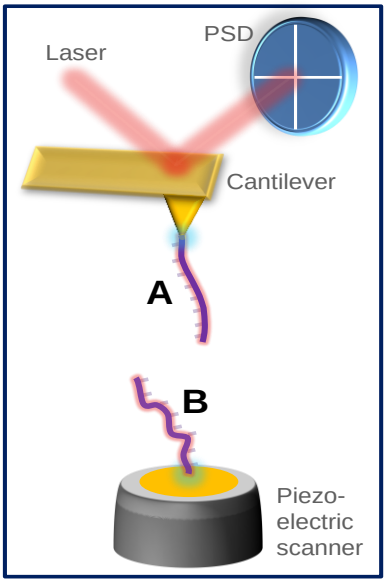

Figure 1.3: Cartoon of the measurement of nucleic acid interaction by AFS. The oligo A is fixed on the tip and oligo B on a piezoelectric scanning stage (gray). Deflection of the cantilever is measured from the displacement of a low power laser (red beam) reflected to the position-sensitive photo detector (PSPD). The piezoelectric scanner moves up and down along the axial direction. The interaction force between oligo A and oligo B is recorded by measuring the deflection of cantilever.

In the following year (1995), Boland et al combed theoretical calculation and measurement by AFS and reported that the required force to break an A-T base is 125 pN and 188 pN for an G-C pair [18]. Few years later, Rief et al reported that the rupture force of A-T pair is 9 ± 3 pN and 20 ± 3 pN for G-C pairs [22] meanwhile Bruno (1998) [23] and Ulrich et al (2002) [24] used optical tweezers to measure the rupture of the pairs and reported a force of about 3 pN per pair. This shows that with improvements of experimental techniques, the rupture forces is reduced compared to the previous studies.

The principal reasons for these discrepancies may also include cantilever spring constant, pulling directionality, loading rate, surface chemistry, linkers used as spacers, buffer, temperature, and/or time scale for sample preparation, etc. Differences in the experimental setup may also provide a different result, e.g. adding a long spacer between the substrate and the oligo may increase the measured rupture force due to spacers stretching and unwinding [25-27]. Chemically immobilizing or only physically absorbing the oligo on the surfaces will give a significant change in the measured rupture force of the pairs [28]. Trying to overcome the influence of using different cantilever spring constant, buffer or long linkers, Sattin et al (2004) reported a significant improvement in this type of measurement by using the same cantilever in the same buffer and short linker for all measurement [21]. They found that the rupture force of AT and GC is approximately equal, although there are more H-bonds in the GC pair than in the AT one. This result contradicts all previous studies in which the force contribution in GC was always greater than in AT. It seems that a clear understanding of the force contribution in the nucleic acids is still challenging and more influencing factors

should be further considered. The influence of factors in rupture force measurement of small molecular interactions will be described in detail in **Chapter 4**.

In order to measure macromolecules-nucleic acids interactions, the modifications that are required for immobilizing the molecules on the surfaces do not significantly change the binding properties of the macromolecules. However, the traditional design as described in the figure 1.3 is not feasible for the detection of small molecules since only a few H-bond binding sites are involved. By fixing small molecule on the surface, their natural binding sites or chemical properties can be lost. At the following, the problem of chemical modification of small molecules will be pointed out in the example of AMP. The AMP-aptamer was isolated by Huizenga et al in 1995 by SELEX [29]. AMP consists of only three specific binding groups (phosphate, amino and imine) which can form a complex with aptamer via few H-bonds. The biotin can be attached to the hydroxyl group at the ribose ring of the AMP [25, 30]. In principle, biotin modification at this position does not influence the phosphate, amino and imine groups for aptamer binding. By modifying the surface with streptavidin, the AMP molecule can be immobilized on the surface via biotin/streptavidin binding. However, immobilization of AMP to the surface may block its functional groups depending on lying angle of the AMP on the surface. The binding ability of the AMP to the aptamer can be altered after immobilization being a major concern. Therefore, a new method to measure the molecular interactions in 'single small molecule level' is necessary.

Aptamers that ind many small molecules have been found by SELEX. However, until now, there is a lack of a powerful experimental setup for measuring the interaction forces. Regarding the measurements of rupture forces of the involved small molecules-aptamers complexes, several studies tried to improve the measurement techniques [31-34] and each of them has some limitations. For example, Ho et al. successfully amplified the signal of small molecule binding aptamer by applying a comparative unbinding force assay (CUFA) (Fig. 1.4) [32]. The split aptamer was connected to dsDNA chains and the fluorophore was attached in between (Fig. 1.4a). The streptavidins were attached on the surfaces and the biotins at the end of the chains. When the probe closed to the substrate, the streptavidin binds the biotin and the chain is fixed between probe and substrate. The pocket of the split aptamer can now capture free ATP in buffer solution (Fig. 1.4b). The ruptures can be measured from the ATP-split aptamer (Fig. 1.4c) or from dsDNA (Fig. 1.4d) and the fluorophore stays either on the probe or on the substrate, respectively. The fluorophore on the substrate can be imaged and the corresponding rupture force is of ATP-split aptamer complex.

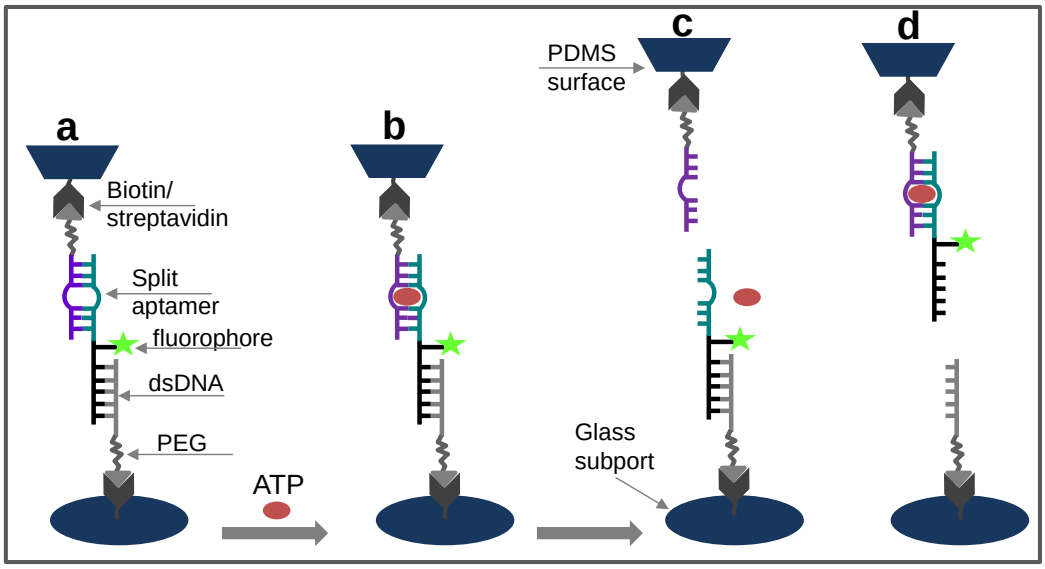

Figure 1.4: Schematic of the comparative unbinding force assay (CUFA) for the detection of small ATP molecules [32]. (a) dsDNA reference and split ATP-aptamers are bound in series via PEG spacers to glass support. A biotin/streptavidin bond is to capture the linker when the PDMS surface approaches the glass support. (b) In the presence of ATP, it binds the pocket of the split aptamer. Two cases of ruptures: from aptamer (c) or from the dsDNA (d) leading to the fluorophore stays on the PDMS surface or on the glass support. Formation of ATP- split aptamer complex increases the rupture force.

The limitation in this study is its low sensitivity. The author reported that it is undetectable if the concentration of the ATP is smaller than 53.5 µM. This method, therefore, may not be feasible for biosensors in detections of the small molecules.

In 2009, Gaub et al. presented another setup to measure label-free copper target binding aptamer (Fig. 1.5a) [31]. Here, they inserted a salicylic aldehyde molecule to the center of two single strand oligos (Fig. 1.5b). The oligos are then brought to the AFM tip and substrate. By approaching the tip to the surface, the oligo hybridization occurs and the copper ion forms a complex with two salicylic aldehyde molecules. Using AFS, rupture of copper-salicylic aldehyde could be obtained. However, there are still some limitations in this method. First, the aptamer needs to be modified with salicylic aldehyde in order to capture the copper. Second, the rupture force of the copper-aptamer could be measured, but copper binds salicylic aldehyde by covalent bonds. The copper-aptamer binding is relatively strong compared to only few H-bonds in small molecular interactions. This system is still possible to measure using AFS without the need of a careful consideration because of high rupture force of covalent bond.

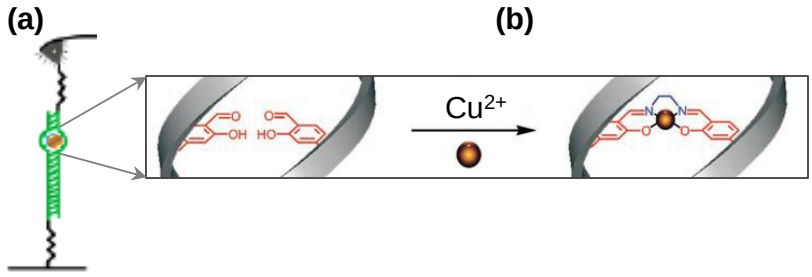

Figure 1.5: Schematic of measuring rupture force of Cu^{2+}-aptamer by AFS. (a) A part of aptamer is fixed on the tip and the other part is on substrate via PEG linker, red sketch presents aptamer self-hybridization while green is the formation of Cu^{2+}-aptamer complex [31]. (b) The copper enters the aptamer via an addition of salicylic aldehyde.

The main task of my thesis is to prove that the 'split aptamer concept' works. For that task, a ssDNA aptamer containing binding pockets (BP) for ligands is selected and is split into two parts. One part is immobilized on the AFM tip and the other one is on the substrate. Adding ligands into buffer solution, the ligands will enter the binding pockets. By measuring the rupture forces in the presence and in the absence of ligand, a difference in these rupture forces can be subtracted and it is attributed to the binding of ligand to the split aptamer. Specifically, we used adenosine monophosphate (AMP) which was introduced in the previous chapter as a ligand. We put our emphasis on this particular ligand because Steinbock obtained preliminary evidence that suggested a force shift in the presence of AMP molecule [35].

In my study, I use a DNA aptamer, 3'-ACTGGA-AGGAGG-AGATGC-GCATCT-AGGAGG-TCCAGT-5', containing two BP at the center (underlined bases) which allows the AMPs entering its pockets. For AFS measurement, this sequence was split symmetrically at the middle (Fig. 1.6). In order to increase the tip/sample distance measured by AFS, 20 adenine bases (A^{20}) were added at the 5'-ends. A thiol linker was added at the 5'-end in order to covalently bind the oligo to the gold surface. The first strand having 18 bases connecting with a spacer 20 adenosine bases (A^{20}) was immobilized on the AFS-tip (oligo a, 3'-ACTGGA-AGGAGG-AGATGC-A^{20}-SH-5') and the second strand was immobilized on the substrate (oligo b, 5'-SH-A^{20}-TGACCT-GGAGGA-TCTACG-3') (Fig. 1.6a). When oligo a was brought into contact with oligo b, partial hybridization between two oligos can take place (non-underline parts) (Fig. 1.6b). Hereby the six center bases do not hybridize (underlined part). They form two BP for AMP molecules. When AMP target molecules are added to the buffer solution, two AMP molecules enter the BP and 8 additional hydrogen bonds are formed at each pocket (red lines) (Fig. 1.6c). Detailed formation of H-bonds in the presence of AMP is indicated by the red dashed lines in the figure 1.6e. Upon the separation of the tip and the sample, the oligo a ruptures from oligo b and the AMPs unbind from the split aptamer (Fig. 1.6d).

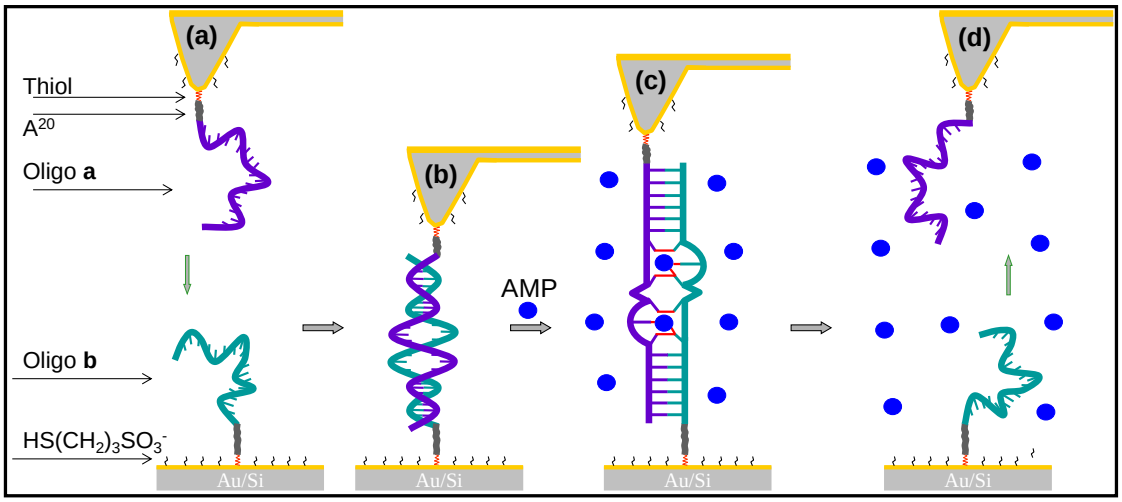

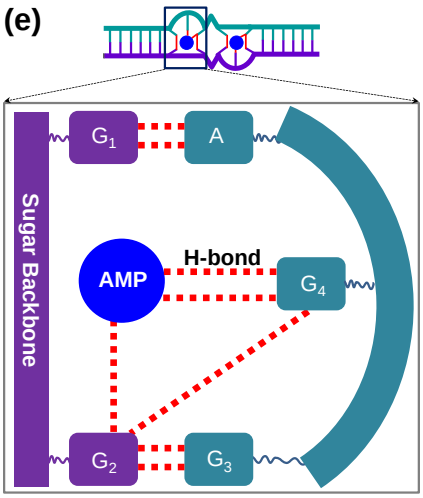

Figure 1.6*:* The split aptamer concept for for AFS measurement. AFM tip stays far away from the sample (a), approaches the sample surface in the absence (b) and in the presence of AMP forming a H-bond network (each red line represents two H-bonds) (c), and separates from the surface (d). (e) Enlargement of a BP with formation of 8 additional H-bonds (dashed red lines) when AMP enters the pocket.

By measuring rupture forces in the presence and in the absence of AMP and subtract the difference between them, the force due to AMP that binds the split aptamer can be obtained. Thus, we can prove that the split aptamer concept works by considering this force difference (**Chapter 5**). First, measurements in the presence- and in the absence of AMP and after washing AMP away were performed. By comparing the rupture forces in those measurements, the rupture force of AMP-split aptamer complex can be deduced. Second, a control experiment using a split aptamer without BP was performed. I also proved that the split aptamer concept works for tetracycline-RNA aptamer and cocaine-DNA aptamer. In order to further understand thermal kinetics of AMP-split aptamer complex, I estimated the dissociation constant by analyzing the rupture force histogram and obtained thermal off-rate by varying the loading rates.

However, the small rupture force of the AMP-split aptamer complex, ~11 pN, is difficult to be measured since many measurement factors are involved. Another question is whether the measured rupture force can be amplified. In order to do that, a series of BP (2, 4-, 6-, 8- and

16 BP) were investigated (Fig. 1.7). The shift in rupture force, x pN, measured from two BP system (top graph) was amplified to 2x pN from 4 BP system (bottom graph). After investigation of multiple BP, the thermal dynamics of these systems will be presented (**Chapter 6**).

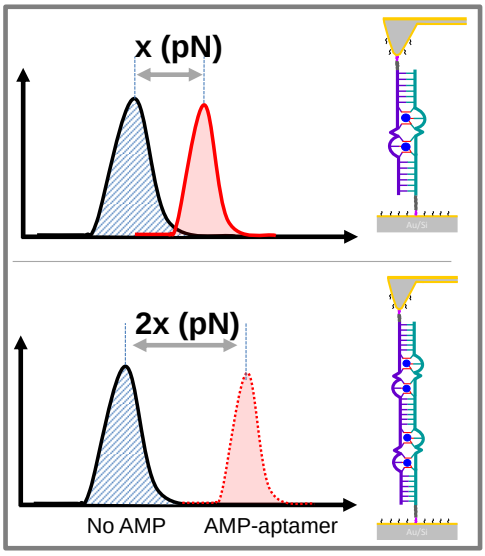

Figure 1.7*:* Cartoon of rupture force amplification by aptamer with additional BP. The rupture force can be amplified from 'x' pN obtained from two BP system to '2x' pN from four BP.

If the split aptamer concept works for the aptamer with additional BP, the lengthen aptamer will be utilized to investigate the contribution of single H-bond in the H-bond network formed between AMP and the binding pocket of the split aptamer. The rupture forces of the split aptamer in the presence of targets with reduction of binding groups can be measured and compared and through which we can estimate the rupture force of a single H-bond (**Chapter 7**).

2.

Aptamers-Targets Complexes

In this chapter, I will first present an overview of basis characteristics, structures, binding abilities of aptamers. Then, the process of producing aptamers by ***S****ystematic* ***E****volution of* ***L****igands by* ***EX****ponential Enrichment* (SELEX) will be introduced. Subsequently, applications of aptamers in life science and medical treatment will be briefly described. Finally, small ligands molecules binding aptamers with the key-lock principles and the importance of small molecules in medical and biosensors studies will be discussed.

2.1. Aptamer History

In 1990, C. Tuerk, and L. Gold [1] and A.D. Ellington, J.W. Szostak [2], developed an in vitro selection and amplification technique and they were the first to find nucleic acids that bind specific targets. They called ‘aptamers’ to indicate the specific nucleic acids which were able to bind non-nucleic acid targets with high affinity and specificity. Aptamers are short single-stranded nucleic acids (DNA, RNA) or peptides, which are typically selected from pools of random-sequence oligonucleotides to bind a wide range of targets from small organic molecules, proteins to cells and tissues. The name comes from the Latin word ‘aptus’ which means ‘to fit’. Their sizes range from 6 to 40 kDa. To date, several hundred to a thousand aptamers have been found to bind specifically to target molecules with a variation of dissociation constant from picomolar to micromolar [4].

Many positive characteristics of aptamers, such as small size, in vitro synthesis, easy modification, and possible penetration into the living cells, drag them to significant

advantages in medical diagnostic applications [36-38] and in biosensors as well [39, 40]. The aptamers shows equal or even better affinity and specificity than antibodies [41-43]. However, simple technique and apparatus are required for isolation of aptamer while complex processes in vivo are necessary for production of antibodies. Famulok et al and Haller et al proved that aptamers have a potential to discriminate among targets which were different only methyl, hydroxyl groups or configuration [42, 44]. Aptamers are interesting in pharmacology since they can bind to certain part of the targets that is possible to inhibit defective molecules. Despite these properties, aptamers so far have reached the marketplace slowly (only one aptamer-based drug receiving approval) [4]. Recently, many studies have used aptamers for cancer cell treatments, drug deliveries, biosensors that may change how nucleic acid therapeutics is perceived. In the near future, it seems that aptamers will become a great promise compared with other therapeutic molecules and modalities because of their above mentioned advanced characteristics.

2.2. Isolation of Aptamers-SELEX

The ***S**ystematic **E**volution of **L**igands by **EX**ponential Enrichment* (SELEX) method was introduced in 1990's by Tuerk et al [45] and Ellington et al [2]. SELEX measures the affinity of transcription factor binding to DNA or identifies the highest affinity recognition sequences for targets [46]. Many aptamers binding target molecules, ranging from small molecules, cells to tissues have been generated by SELEX [47]. SELEX is a combination of a chemistry technique and molecular biology to produce oligonucleotide of either ssDNA or ssRNA that specifically bind to target ligands. SELEX is an attractive method since it can be manipulated in ways which would have been difficult or impossible if organisms involve.

The SELEX process for DNA aptamer (Fig. 2.1) begins with the synthesis of a very large oligonucleotide library (10^{15} oligos) consisting of randomly generated sequences of fixed lengths (step 1). The sequences include four nucleotides (A, T, C, G) for DNA aptamer flanked by 5' and 3' ends which act as primer binding sites for polymerase chain reaction (PCR) amplification. The target molecule is added in the pool for a certain time to produce an aptamer-ligand-complex (step 2). The target, for example, ATP (blue ball) binds to the aptamer (red or orange ribbons) [29]. The oligonucleotides which do not bind the ATP are removed by affinity chromatography (step 3). Then, the bound sequences are eluted (step 4) and amplified (step 5) by polymerase chain reaction (PCR). A double strand DNA pool is generated after PCR and this pool can be either transcribed for RNA selection or strand separated for ssDNA selection to prepare for subsequent rounds of selection. After PCR re

For RNA aptamer by SELEX, the RNA pool is generated by the DNA library which serves as a transcription template. The in vitro transcription requires a T7 promoter sequence and the synthesis of complementary DNA needs a primer annealing site [2].

To enrich the oligonucleotides in the initial pool which show tightest binding to the target, iterative selection and amplification cycles are usually carried out. Up to about 15 cycles depending on oligonucleotides or target concentration, the process is terminated and the selected sequences are isolated. The sequence and the structure of the ligands can be revealed by cloning and sequencing of the selected clones. After that the aptamer is generated by chemical synthesis. The binding activity of ligand-aptamer and discrimination of the loosely bound target molecules and tight bound targets, different techniques such as filter adsorption, non-denaturing gel electrophoresis, immobilization of the target on chromatography beads, immune-precipitation or centrifugation for entire cells have been utilized. The quality assessment of the SELEX experiment is represented by the dissociation constant of the complexes.

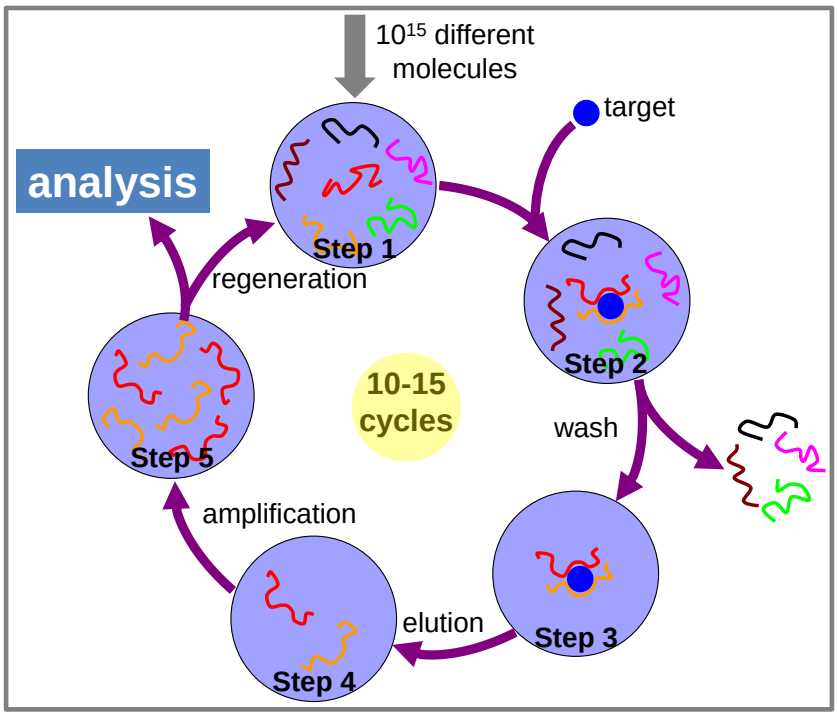

Figure 2.1. Schematic of SELEX in vitro for DNA aptamer. A random pool of nucleic acids is enriched through the selection process.

A great improvement has been done by Ellington lab (http://aptamer.icmb.utexas.edu/) in 2001. Here, the process of *in vitro selection* which was discovered in 1990 was automated and the duration of a selection experiment was reduced from six weeks to three days. There is also useful information of aptamers-proteins in vitro selection in the SELEX-DB [48].

2.3. AMP-Aptamer

D.E. Huizenga and J.W. Szostak (1995) isolated *in vitro* an aptamer that bound adenosine and adenosine triphosphate (ATP) from a pool of 2 x 10^{14} different random single-stranded DNAs [29]. This aptamer was then screened for functional adenosine binding sequences. Analysis of the sequence with ATP indicated that functional groups on both the base and the sugar of ATP were involved in the ATP-aptamer interaction. This analysis also showed that there were two regions with rich guanosine (G base), two invariant adenosine residues, and two regions of predominant Watson-Crick pairs.

Adenosine monophosphate (AMP) (Fig. 2.2) can form a complex with DNA or RNA aptamer [49]. The AMP consists of only one phosphate group while ATP consists of three phosphate groups. The AMP binds to the DNA aptamer by H-bonds formed between three binding groups of AMP such as phosphate (Fig. 2.2, red box), amino (Fig. 2.2, green box) and imine (Fig. 2.2, yellow box) group [29, 49]. In the presence of those groups, highest binding affinity can be observed.

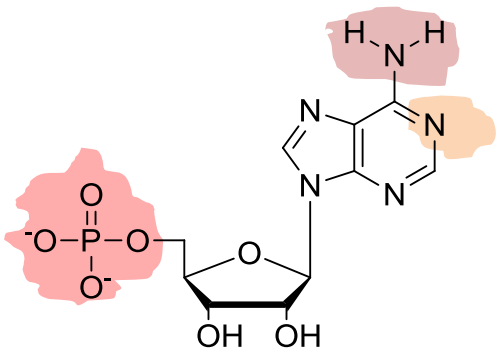

Figure 2.2. Molecular structure of adenosine monophosphate (AMP). AMP can form H-bonds with aptamer via three binding groups (red, green and yellow boxes).

The AMP-aptamer sequence consists of two Watson-Crick areas at two ends (bases from 1 to 6 and from 13 to 18) and two BP at the center (base 5 to 10) (Fig. 2.3). The binding structure of AMP-DNA aptamer was obtained by NMR analysis [49, 50]. The AMP molecule (blue) binds to the DNA aptamer through an H-bond network (Fig. 2.3, red). The binding occurs at the regions with rich guanosine. Nonin et al [49] and Lin et al. [50] have presented the AMP binds the DNA aptamer via 8 H-bonds in each binding pocket (red dashed lines, Fig. 2.3). Two AMP molecules were found entering in two nearby pockets of the aptamer.

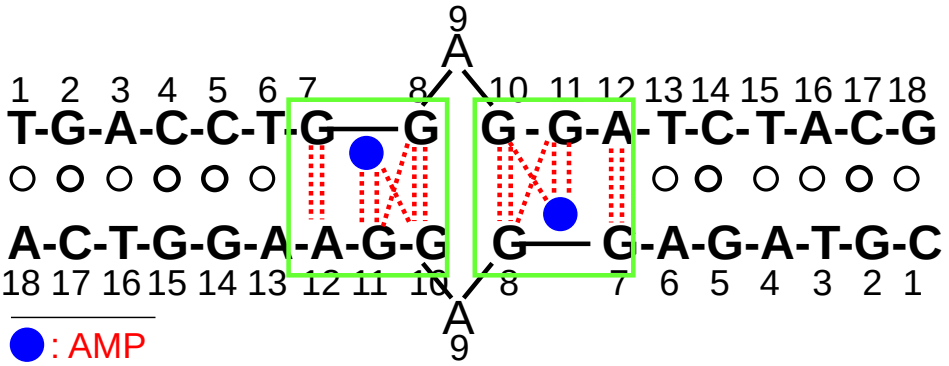

Figure 2.3. Chemical structure of AMP-aptamer. The pockets (green boxes) locate at the center of the aptamer sequence while two Watson-Crick stems are at the two sites of the pockets. The AMPs stabilize the aptamer when they enter the pockets by the formation of eight H-bonds per pocket (red dashed lines).

Detail formation of H-bonds in the absence of AMP for each binding pocket is presented in the figure 2.4. The G-bases at the BP regions stay far away from each other and they become pairs in the presence of AMP. The H-bonds are formed not only between AMP and the G-bases but also between G- and G or G and A bases. The appearance of the new H-bonds pulls two strands in the pockets closely to each other resulting in G-bases pairing. The interaction force in the aptamer in the presence of AMP is therefore higher than in the absence of AMP. By comparing the force in the presence and in the absence of AMP, the additional force to stabilize the aptamer in the presence of AMP can be obtained.

In my study, I measured the rupture forces between two parts of the aptamer in the presence and in the absence of the AMP. By subtracting the difference in those forces, the additional binding force contributed by AMP could be obtained.

Functional groups of AMP play an extremely important role in the formation of AMP-aptamer complex. When the binding groups in the AMP molecules are replaced, the binding ability can be reduced. Huizenga et al. substituted the binding groups of AMP by using Inosine and found no any target-aptamer complex [29]. They presented that AMP-aptamer binding was 70-84% while it is < 5% for target Inosine.

In my study, derivatives of adenosine monophosphate (AMP) such as Inosine, Inosine monophosphate (IMP), 2'-O-adenosine monophosphate (OMA) were used as targets. Those molecules represent the absence of the binding groups in the AMP and have different binding sites which can form different H-bond network with aptamer, and therefore different rupture forces could be measured.

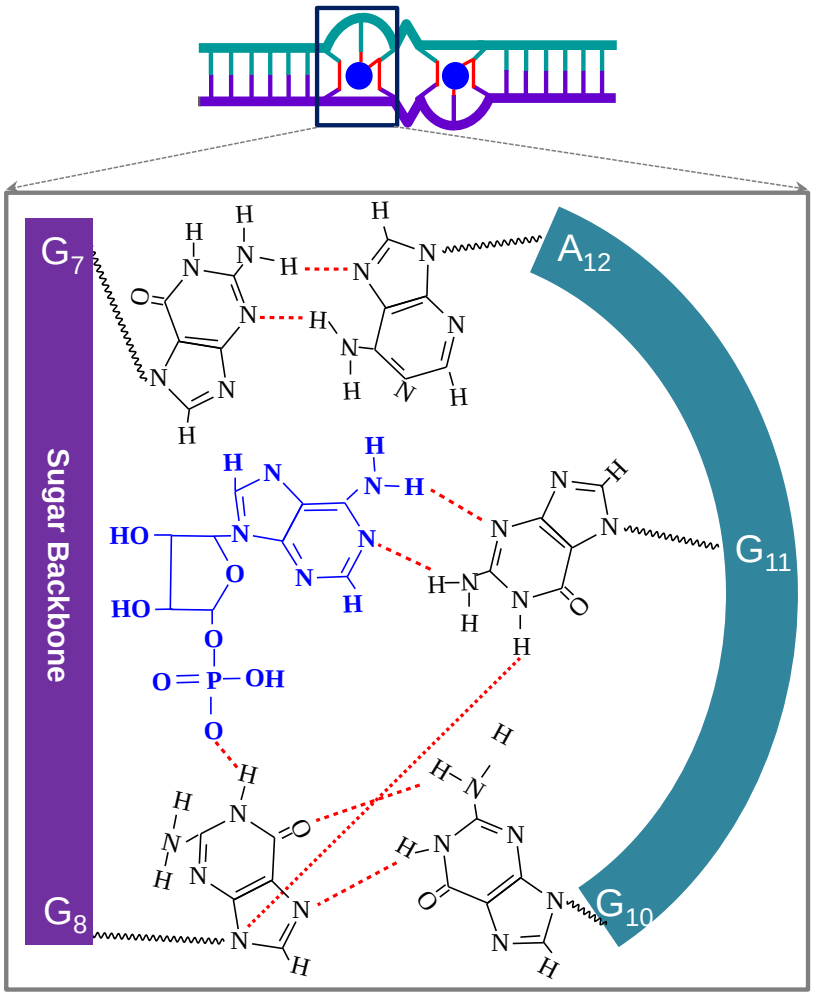

Figure 2.4. Enlargement of H-bond network (red dashes) generated between AMP (blue) and the binding pocket of aptamer on the right site of the sequences (Fig. 2.3).

2.4. Cocaine-Aptamer and Tetracycline-Aptamer

Tetracycline is used against many bacterial infections as an antibiotic. Tetracycline binds RNA aptamer (Fig. 2.5) with nano scale dissociation constants (K_d = 0.8 nM) and the binding is strongly supported by the presence of Mg^{2+} ions in buffer [51]. The binding is formed by the minor grooves of M and the H_1 and H_2 helix via about 37 H-bonds.

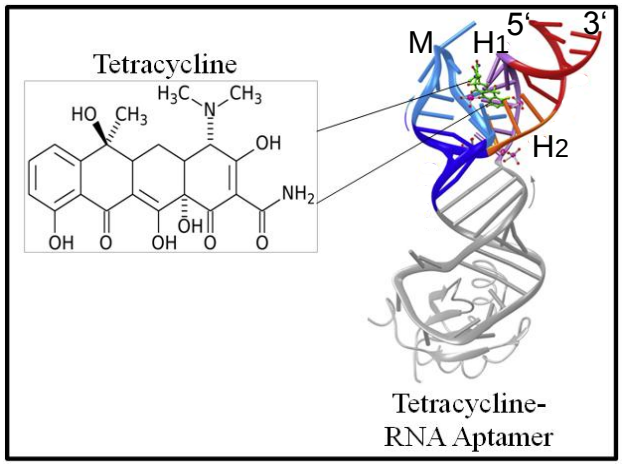

Figure 2.5. Cartoon representation of Tetracycline-RNA aptamer complexes [51]. Tetracycline enters RNA aptamer under the support of the well-ordered magnesium ions and their solvation water (magenta and red spheres, respectively).

Cocaine is a crystalline tropane alkaloid produced by the leaves of the coca plant. The name 'Cocaine' comes from "coca" and the alkaloid suffix -ine. Cocaine is a powerful nervous system stimulant [52]. Cocaine binds DNA aptamer via a hydrophobic pocket formed by a noncanonical three-way junction (Fig. 2.6), with one of the stems structured through currently less well-defined non-Watson-Crick interactions [53]. To date, the binding structure of cocaine to aptamer has not been well understood even though it has been label-free detected in biological fluids [54]. The H-bond network in the cocaine-aptamer or other influences on the formation of this complex has not been as well characterized as AMP-aptamer or antibiotic-RNA aptamer complexes.

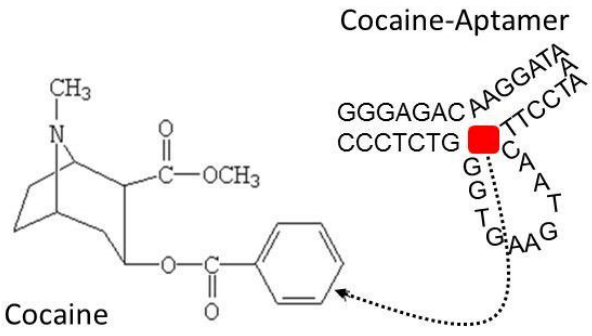

Figure 2.6. Cocaine-aptamer complex. Cocaine binds to the aptamer via a hydrophobic pocket formed by a noncanonical three-way junction.

In my study, cocaine-aptamer and tetracycline-aptamer will be used to test if the 'split aptamer concept' also works for other system.

2.5. Dissociation Constant

The dissociation constant (K_D) is a type of equilibrium constant that measures the direction for a larger complex to dissociate reversibly into smaller components. In biological complexes, dissociation constants normally describe the affinity between ligand and receptor. For ligand-receptor bindings, the analysis is based on the following simple mass action model:

$$\text{Ligand + Receptor} \underset{k_{on}}{\overset{k_{off}}{\rightleftharpoons}} \text{Ligand . Receptor}$$

Ligand and receptor diffuse and collide in solution until they reach the correct orientation, then the binding occurs. The k_{on} ($M^{-1}min^{-1}$) is the association rate constant or on-rate constant, k_{off} (min^{-1}) is dissociation rate constant or off-rate constant. The association rate is k_{on}*[Ligand][Receptor]. The ligand-receptor complex stays in a solution for a random time before dissociation. The dissociation rate is k_{off}*[Ligand.Receptor]. After dissociating, the same ligand and receptor as before exists in the solution. When the rate at which new ligand-receptor complexes are formed equals the rate at which the ligand-receptor complexes dissociate, the equilibrium state is reached and

$$[\text{Ligand}][\text{Receptor}].k_{on} = [\text{Ligand.Receptor}].k_{off}$$

$$\text{or} \qquad K_D = \frac{k_{off}}{k_{on}} = \frac{[\text{Ligand}][\text{Receptor}]}{[\text{Ligand.Receptor}]}$$

where K_D is equilibrium dissociation constant (M^{-1}) [55]. When ligand concentration equals K_D, the concentration of receptor equals the concentration of ligand.receptor. In the other word, half of receptors are free and half are bound to ligand at equilibrium state. The fractional occupancy at equilibrium is 50%.

Dissociation constant can be determined by different methods. The pH meter is to determine the dissociation constant of an acid or base (K_a or K_b) in water by conducting a titration [56]. Spectrophotometer is the method to determine the concentrations of ionized and unionized forms based on their absorbance spectra. It can be obtained by measuring the conductivity of a solution at varying concentrations.

For ligand-nucleic acid, the filtration technique is usually used to determine their dissociation constant. The ligands binding nucleic acids with known concentrations are mixed at 25°C for 30 min. Then, the sample is filled by a filter which has a certain pore size depending on the length of the nucleic acids. High molecular weights are kept on the filter and only free ligand molecules flow through membrane. The filtrate concentration of ligand is then determined by HPLC [57, 58]. However, these methods might provide the K_D value in a large error range.

In my study, a new method to calculate the dissociation constant by analysis rupture force histograms at different AMP concentration will be introduced.

2.6. H-bond Forces

A H-bond is the attractive force arising between donor covalent pair X--H in which a hydrogen atom H is bound to a more electronegative atom X while other covalently bound nearest neighbor electronegative atoms A [59]

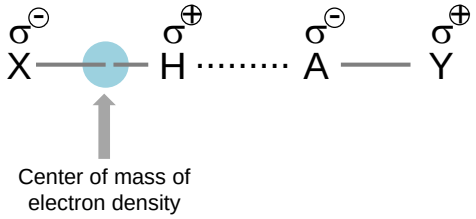

In nucleic acids, H-bonds are important because they help to determine and stabilize the shapes of biological molecules, and stabilize the secondary structure of proteins, enzyme catalysis and nucleic acids. There are different types of N--H bond depending on the hybridization state of the nitrogen. The H-bonds in nucleic acids consists of the following types of bonds

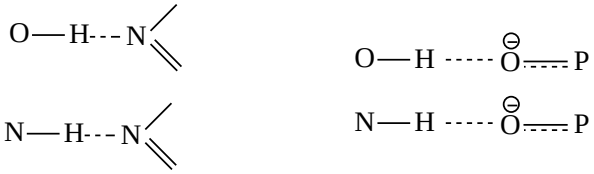

Boland et al estimated H-bond force using the $F = 1/r*E_b/N_A$ [18], where E_b: bond energy, N_A: Avogadro's number, r: bond length. Following this equation, the H-bond force of Watson-Crick pairs A-T and G-C are of 122 pN and 188 pN, respectively. However, the theoretical calculations for those H-bonds are much higher than the one which was measured directly in buffers. For example, Bernie et al. obtained directly total interaction forces of H-bonds in 20 bp dsDNA strands which contained 50% A-T and 50% G-C. The single H-bond force can be induced by averaging the force per total H-bond, resulting in only few pN/H-bond [21].

3. Experimental Methods

3.1. Atomic Force Microscopy (AFM)

Single molecular interactions have been one of the most interesting studies in the last decades [60-62]. Single molecule techniques such as optical and magnetic tweezers and atomic force microscopy (AFM) allow accessing those aspects [63]. Probing intra- and intermolecular forces with high sensitivity in physiological conditions makes AFM a valuable methodology for understanding single molecular interactions. In this chapter, I will first introduce the working principle of AFM and force spectroscopy by AFM. After that, the chemical force spectroscopy will be explained. Finally, the Bell-Evans model will be introduced.

3.1.1. History and Background

The techniques providing information about atomic scale structure generally belong to either the Transmission Electron Microscopy (TEM) or the family of Scanning Probe Microscopy (SPM). Scanning Tunneling Microscopy (STM) which allows imaging conducting and semiconducting surfaces was invented in the early 1980s by Gerd Binnig, Heinrich Rohrer, Christoph Gerber and Edmund Weibel at IBM Zurich, Switzerland [64] and was the first member of SPM family. In 1986, Gerd Binnig and Heinrich Rohrer were awarded the Nobel Prize in physics for this invention. Since STM does not allow imaging of insulating surfaces, Gerd Binnig, Calvin F. Quate, and Christopher Gerber developed another SPM technique named Atomic Force Microscopy (AFM) in 1986 [15].

AFM has become one of the key tools in nanotechnology for imaging, measuring and manipulating matters [65, 66]. It can be operated in different environments, and does not require a complicated sample preparation. It can provide topography images [67-69], kinetic intermolecular interaction [70-72], physical properties [73-75], monitoring biochemical [76], and physiological processes at a molecular resolution [77], and has become a suitable tool for biological application.

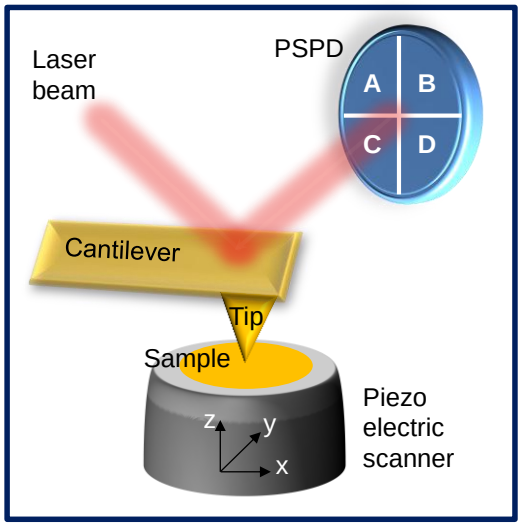

Figure 3.1. The working principle of AFM. Beam deflection system uses a laser and photo detector to measure the beam position. A laser beam is illuminated on the back side of the cantilever, and then it reflects to the PSPD. The piezo electric scanner can move the sample in three directions (x, y, z). The cantilever is bent due to the tip/sample interaction when the tip closes to the surface.

Three main parts of AFM are the piezoelectric scanner, cantilever with a tip at the end and a position sensitive photo detector (PSPD) (Fig. 3.1). The tip scans over the surface in an accurately controlled way on the nanometer scale by a piezo electric scanner. The position of the sample beneath the tip can be well defined in three dimensions. The sample is mounted on a piezoelectric tube scanner which scans in the x-y plane during imaging. The piezoelectric tube scanner also provides the movements in the z-direction. The detection system is based on a laser that is focused on the backside of the cantilever and is reflected back to the PSPD. The PSPD consists of four segments in pairs along the vertical and horizontal axis. When the tip scans over the surface of a sample, the interaction between the tip and the surface makes the cantilever bent up or down and the position of the laser beam on the PSPD shifts. The different voltages of the segments present the deflection signal which is used to control the tip/sample distance. The vertical deflection of the cantilever is the voltages difference $(V_A+V_B)-(V_C+V_D)$ and the lateral signal which presents the torsion of the cantilever is $(V_A+V_C)-(V_B+V_D)$. The piezoelectric scanner is adjusted in z-direction via a feedback control which keeps the tip-

sample distance constant. The tip-sample distance is regulated to reach the initial cantilever deflection. The movement quantity of the piezoelectric scanner is registered. The force acting on the cantilever can be attractive or repulsive. When the distance between tip and sample is less than 0.1 nm, surface atoms on the tip end and on the sample surface repel each other. At ambient conditions, water layer the sample surface produces a capillary force. The electrical forces from work function differences, static surface charges, Van der Waals forces or external applied voltages contribute to the long-ranged force. Van der Waals forces include static and fluctuating dipole-dipole interactions between atoms and molecules of the tip and the sample. According to Hooke's law, the tip/surface interaction force can be estimated by $F = -k*\Delta z$, where k is cantilever spring constant while Δz is the deflection of the cantilever.

There are basically three modes, i.e., contact, non-contact and intermittent modes. The contact and intermittent contact modes work in the repulsive force regime while the non-contact mode works in the attractive regime.

Contact Mode: The tip is in contact with the sample surface while scanning. The repulsive force acting on the cantilever is about 10^{-9} N. In this mode, the tip/surface force is kept constant during scanning by maintaining a constant deflection. The contact mode is useful for hard surfaces, and high-speed atomic resolution scans.

Due to the close proximity to the sample, the tip can touch the water layer on the sample in ambient conditions and a meniscus forms and the cantilever is pulled by surface tension towards the sample surface. The magnitude of this meniscus force is typically on the order of 100 nN depending on the probe geometry. This force, however, can be neutralized by immersing the sample totally in liquid. Further, scanning in contact mode induces shear forces that may distort the sample morphology or contaminate the tip. To avoid the mentioned problems, the non-contact mode was developed.

Non-contact mode: The tip/sample distance in this mode is kept at about 5 to 15 nm. Non-contact (NC) mode works based on an oscillating cantilever in the attractive regime. A stiff cantilever is oscillated close to the sample without touching it. Working in this mode, low forces between the tip and the sample dominate, normally in the order of hundreds pN. During scanning, the attractive Van der Waals forces acting between the tip and the sample are detected. The attractive forces from the sample are usually weaker than the forces used by contact mode. Therefore, NC detection methods are used to detect the small forces between the tip and the sample by measuring the change in amplitude, phase, or frequency of the oscillating cantilever in response to force gradients from the sample. Due to the water layer on the sample surface, attempts to image the true surface with non-contact AFM usually fail when the oscillating probe becomes trapped in this fluid layer.

Dynamic Force/Intermittent-contact/"tapping mode": In this mode a high cantilever spring constant is usually used. The tip is oscillated at high frequency closer to the sample than in noncontact mode. This mode allows high resolution topographic imaging of sample surfaces. Due to the cantilever oscillations at high amplitude, the tip is not captured by the water layer on the sample. When the tip taps the surface, oscillation amplitude of the cantilever is sufficient to overcome the tip/sample adhesion force. Thus, tapping mode operation overcomes problems of friction, adhesion and electrostatic forces. Tapping mode has key advantages compared to the other modes.

The AFM used in this study is a MultiMode PicoForce (Veeco Instr., Santa Barabara, CA, USA) and JPK NanoWizard (JPK, Berlin, Germany). The implementation of a closed loop in those system increases the measurement resolution which exists in both systems. With closed loop, the piezo movement during measurement is defined by the linearized value of height measured rather than the piezo voltage height. Piezo is a short name of piezoelectric elements that are facilitated tiny but accurate and precise movements. The sample is mounted on piezo stage and precise movement of the piezo allows obtaining very small change on the sample surface during scanning. With a closed loop, the nonlinearity and hysteresis of the piezo is therefore corrected during movement. The applied voltage to correct the piezo height is displayed in the error signal channel. Both systems allow doing measurement in liquid with a force resolution in the pico newton range.

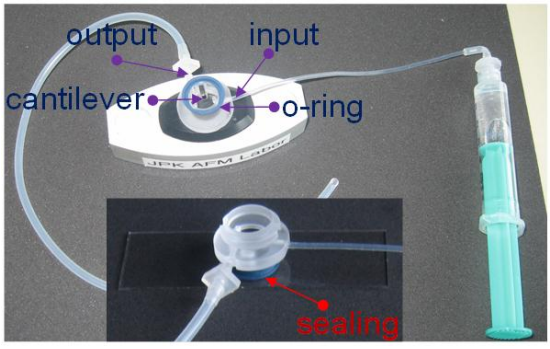

Figure 3.2. Cantilever holder for operation in liquid from JPK. Top figure is the front side of the holder which consists of the cantilever, o-ring, input and output components, and bottom one is the reverted holder of which the o-ring seals tightly the sample to avoid liquid leaking.

Figure 3.2 shows the cantilever holder which is designed by JPK for measurements in liquid. The cantilever is kept at the center of the cell. The surrounding o-ring (blue) is to prevent the liquid leaking out of the liquid cell during measurement. The cell consists of one input and one output which allow injection or removal of the liquid. When the o-ring is sealed with the sample substrate, the cell is closed which avoids the evaporation of liquid during measurement.

AFM Cantilever: AFM cantilevers are commercially microfabricated normally from Si or Si_3N_4 [78]. To enhance reflection of the laser beam to PSPD, the cantilevers are usually coated with a metal layer on the back side. This coating is important for measurements in liquid since the reflectivity is significantly reduced [79]. In force spectroscopy, sharp tips help to immobilize single molecules at the tip end which is a crucial factor in measuring single molecular interactions.

Spring constant of the cantilever allows how much the cantilever can bend up and down during scanning. For imaging, cantilevers with small spring constants are useful for scanning soft samples without damaging them and a stiff cantilever is typically used for dynamic imaging mode. During force spectroscopy measurement, the cantilever probe goes up and down against the sample. By monitoring the cantilever deflection the information of the sample as hardness, adhesiveness and folding force of the protein molecule, single molecular interaction etc. can be obtained.

High force resolution can be obtained by using the cantilevers with small spring constants. In order to achieve the interaction forces of small molecules which are typically formed by only few H-bonds, choosing cantilever with very small spring constant is a key element.

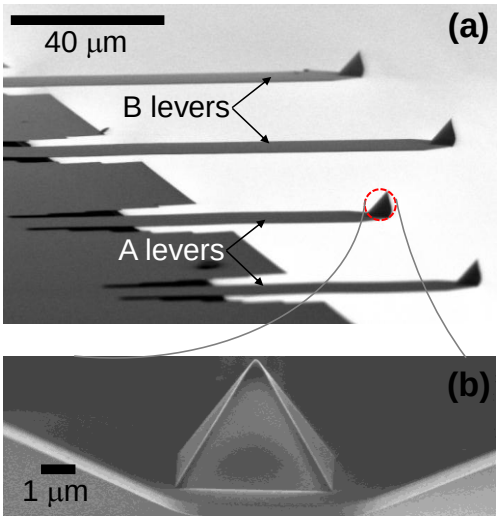

Figure 3.3. SEM images of a Bio-lever with both sites coated with gold taken at MPIP, Germany. Four cantilevers are on one chip (a). Two long cantilevers with low spring constant (6 pN/nm) and the other with higher spring constant (30 pN/nm).

In my study, the cantilevers with small spring constant of ~6 pN/nm named 'the Bio-Lever' (OLYMPUS, Japan) were used. The Bio-Lever is a rectangular silicon nitride cantilever with both-side gold coating. The additional gold coating at the front side of the cantilever is to make the tip easier to be modified using thiol chemistry.

There are two short cantilevers (A levers, spring constant ~30 pN/nm) and two long cantilevers (B levers, spring constant ~6 pN/nm) on each Bio-lever (Fig. 3.3a). Each cantilever carries a pyramidal tip at the end (Fig. 3.3b). I normally used the longer cantilevers (B-levers) in this study to archive the best force resolution.

Cantilever Calibration: In the force distance curve measurements, the Hooke's law ($F = -k\Delta z$) is applied in order to convert the cantilever deflection (Δz) to force. In order to interpret proper images acquired under constant force and mechanical properties of samples from AFS measurement, a precise value of the spring constant of the cantilever (k) is crucial. There are several accessible methods to calibrate the cantilever spring constant.

The first method with the measurements of cantilever geometry such as width (w), thickness (t), length (L) and known Young's modulus of the material is usually used by the manufacturer to calculate the spring constant of the cantilever, $k = Ewt^3/4L^3$. However, the calculated results differ from batch to batch. The nominal value provided by the manufacturer is often inexact and can vary as high as the factor of 4 [80].

The second method, thermal noise spectrum, is the most popular method for cantilever calibration because of its ease of use. This method bases on the fluctuation or diffusion of particles (Brownian motion) in their environments (air or liquid). The thermal noise method following the equipartition theorem is used to describe the motion of particles. Soft AFM-cantilevers are susceptible to thermal fluctuation and the thermal noise method can be used to describe the cantilever fluctuation. The thermal noise spectrum can be plotted against a function of frequency. The greatest amplitude can be seen around the cantilever resonance frequency. Considering the cantilever as an ideal spring, measurement of the thermal noise allows determining the spring constant

$$k = \frac{k_B T}{\langle x^2 \rangle} \tag{3.1}$$

where x is cantilever deflection.

However, in AFM the cantilevers are usually mounted under a certain tilt angle ϕ with respect to the sample surface and the probe geometry are not uniform those make the cantilever cannot be considered as an ideal spring [81, 82]. By carefully considering those factors, Hutter [82] proposed a formula which contains the probe geometry and tilt angle for a precise cantilever calibration,

$$k = 0.8174 \frac{k_B T}{s^2 P} \left[\frac{1 - \left(\frac{3D}{2L}\right)\tan\phi}{1 - \left(\frac{2D}{L}\right)\tan\phi} \cos\phi \right]^2 \tag{3.2}$$

where the numerical factor 0.8174 is a result of the geometry of the cantilever spring, *s* is the sensitivity calibration factor (nm/V), P is the positional noise power (V^2), D is the height of the tip, *L* is the cantilever length, and ϕ is the cantilever tilt angle. In most cases, the term in square brackets is close to unity, so these will not be greatly important.

The available software from AFM system, users determine *s* from the force distance (F-D) curve against a rigid substrate by measuring the slope of the contact portion of the F-D curve (detail of an F-D curve is described in the next section). Then, the power spectral density (PSD) of the noise data should be calculated by identifying the resonant frequency peak which is closest to the one provided by the manufacturer. After that, the PSD as a function of resonant frequency is fitted with a Lorentizian to the peak by

$$P(f) = \frac{A}{(f - f_0)^2 + B} + bg \tag{3.3}$$

where A and B are the variable values, and *bg* is a constant. The positional noise power, *P*, is the area under the fit peak

$$P = \pi \frac{A}{\sqrt{B}} \tag{3.4}$$

Finally, all the parameters are added in the equation 3.2 for determining *k*.

The thermal noise method is limited by the sensitivity of the device used to measure the noise in the deflection signal. The process of determining *s* can provide errors from a force curve against a rigid substrate. In many cases an oscillatory baseline due to interference between the reflected laser beam and laser light scattered from the substrate can lead to an incorrect estimate of *s*. The tilt angle ϕ produces also error in the calibration. The error, typically, varies from 5 to 15% [81, 83].

In my study, I calibrated the cantilevers by thermal noise method. Typically, determination using thermal noise method in air provides the most accurate k value. However, for the functionalization tip with chemicals or biological molecules, the calibration in liquid is necessary since the sample can be damaged at ambient condition. In my experiment, all cantilever calibrations were carried out in buffer T on silicon substrate.

3.1.2. Force Spectroscopy

Besides imaging of sample surface, AFM is a useful tool to study single molecular interaction and achieve information of intermolecular behaviors by generating force-distance curve measurements [84]. The name atomic force spectroscopy (AFS) presents the process of

producing force-distance curves or force spectroscopy measurements by AFM. At a large number of locations force curves can be recorded and an average value of the surface force can be obtained. The AFS has become an important tool to study biomolecular interactions since it works in different living conditions [85].

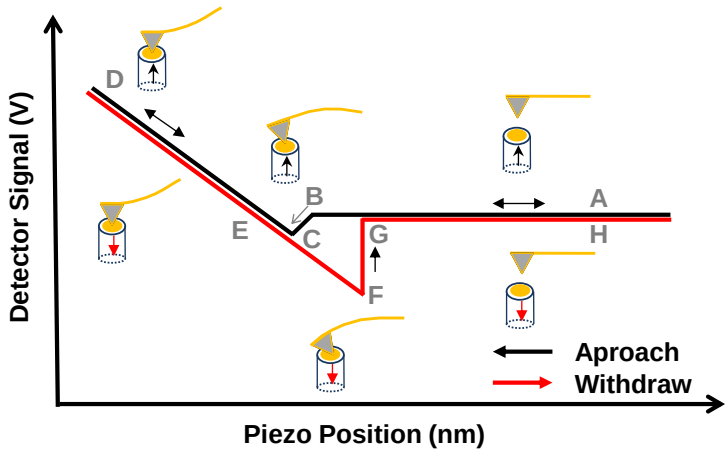

Figure 3.4. Original curve generates by AFS corresponding to the position of the cantilever as the piezoelectric scanner moves up (approach) and down (withdraw). Specific points where the tip jumps-to-contact (B→C), in contact (C→E), withdrawal from the surface (E→F), and jump-off-contact (F→G).

In principle, force distance (F-D) curves are obtained by oscillating the scanner in z-direction while the scanner movement in x and y directions is disabled. In such a way, the deflection signal from the cantilever and the movement of the piezoelectric scanner are recorded. The force is measured as a function of distance. For a local force spectroscopy measurement, the force curve is measured at a particular location on the sample surface. Figure 3.4 presents how a F-D curve is generated using a bare tip on bare glass surface. The cantilever is bent upward or downward corresponding to the different position of the piezo. At the first stage of cycle (A), there is no tip/surface interaction due to the fact that the tip is far from the sample surface. At this position, the cantilever is in a non-interacting equilibrium state. When the piezo moves up, the tip/surface separation decreases, and the tip is brought into contact with the sample at a constant speed until it reaches a point close to the sample surface. When the cantilever moves towards the sample, various attractive forces pull the tip down (long and short range forces). When the tip approaches the substrate, the van der Waals force dominates. The van der Waals force depends on the tip/substrate distance, $F_W = -A_H R/6D^4$ [86, 87], where A_H is Hamaker constant, R the tip radius and D the tip/surface distance. The tip jumps into contact with the sample surface (jump-in contact: B→C) under appearance of F_W.

The tip is in contact with the sample (B→D) while the piezo still moves up. The process from A to D is the 'approach curve'. When reaching the maximum deflection of the cantilever, the piezo stops the extension and starts the retraction process (E→H). The process E→H is called withdraw or retraction curve which means the tip tries to withdraw from the surface. The tip is still in contact with the surface from E to F. The region from E to F is called 'withdraw', adhesion or bonds formed during tip/surface contact makes the tip to adhere to the sample up to some distance beyond the initial contact point on the approach curve. When the piezo continues retracting from the contact point, the spring force of the bent cantilever overcomes the adhesion forces, and the tip pulls off sharply, springing upwards to its non-deflected or noncontact position (G). Finally, the tip completely jumps-out of contact with the surface and goes back to the equilibrium position (H). The difference from point G to point F indicates the adhesion force causing between tip and sample.

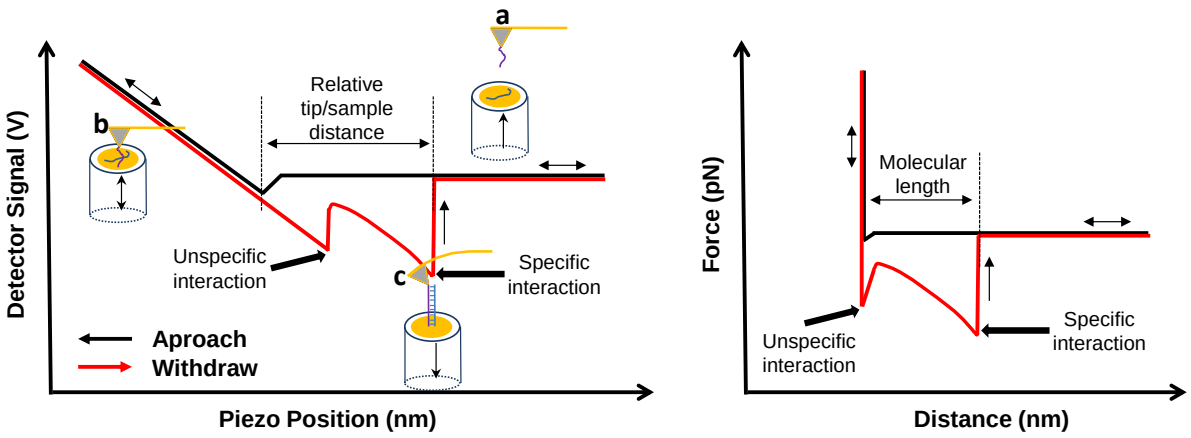

Figure 3.5. Typical F-D curve with an oligonucleotide as a spacer between tip and substrate (left). The tip first ruptures from the surface in a very short distance. The unspecific adhesion peak appears due to tip/surface interaction. The rupture of a specific interaction due to oligo hybridization occurs after rupturing the tip/surface interaction. The piezo position is converted to the real tip/surface interaction by homemade software (right).

When macromolecules such as oligonucleotides attach between tip and substrate, an additional peak appears before the tip jumps out of the surface (Fig. 3.5 left). When the tip approaches to the substrate, the oligo on the tip hybridizes with its complementary on the substrate. During tip/sample separation process, the first-jump-out is unspecific adhesion. When the piezo goes down further, the spacer is stretched first and then the oligo hybridization will be broken leading to the second peak in the withdrawal curve and this is the specific interaction which will be used for analysis of rupture force and rupture distance of molecular interaction. The relative tip/sample distance contains the molecular length between tip and sample. This relative tip/sample distance can be converted to the real tip/sample distance or

the molecular length, which is about 20 nm in our experiment, by considering the spring constant and the deflection of the cantilever (Fig. 3.5 right). This calculation can be automatically done in the homemade software written by Michael Kappl at Max Planck Institute for Polymer Research (MPIP), Mainz, Germany.

Software for data analysis, which selects the largest adhesion peaks, for thousands of F-D curves is available. However, this selection will create incorrect results if both unspecific and specific adhesions appear in one F-D curve and the magnitude of the unspecific adhesion is greater than that of specific one. As a result, I used the mentioned homemade software. The rupture events due to noise (typically very small rupture force) or molecular aggregations (very large adhesion force with short rupture distance) can be eliminated from the batch of force curves by using the homemade software. After viewing all the F-D curves in the batch, the exact final rupture point due to the specific rupture event can be selected. The final rupture events are taken one by one by bringing the cross exactly to the point which the tip detaches from the sample. The rupture forces and rupture distances at those points are then automatically saved for further analysis.

3.2. Dynamic Force Spectroscopy

3.2.1. Bell-Evans Model

When two molecules (X and Y) with mutual affinity are mixed in a solution, their association, XY, is time-dependent [85] which describe the kinetics of the interaction,

$$X + Y \underset{k_{on}}{\overset{k_{off}}{\rightleftharpoons}} X.Y$$

and

$$\frac{d[XY]}{dt} = k_{on}[X][Y] - k_{off}[XY]$$

where k_{on} and k_{off} are the association and dissociation rates of the complex, respectively, and the square brackets stand for the concentrations.

Under an external force to the end of ligand X or receptor Y of the ligand-receptor complex, they are pulled from each other, resulting in their dissociation. The unbinding profile of the ligand-receptor complex is drastically altered by the external force. Bell has described the effects of an applied force on the energy profile of a reaction [88]. An unnatural dissociation of the complex can be described as a thermally activated reaction in the framework of the reaction rate theory.

At equilibrium, molecular interaction can stay at the bound or unbound state and can be described by an energy landscape (Fig. 3.6). When the complex is at the bound state (Fig. 3.6a), their binding energy is described by the depth of the well (point A). Under an external pulling force (*F*), the complex is unnaturally pulled out from each other (Fig. 3.6b) and they finally dissociate from each other (Fig. 3.6c). At the nature dissociation, the complex will be separated at a higher energy barrier ($\Delta G^*(0)$, point B). However, under the external force, Bell predicted that the activation energy is lowered, $\Delta G^*(F) = \Delta G^*(0) - F\Delta x$ (point B, from black to red curve), Δx is the width of the potential barrier along the direction of the external pulling force. And then, the complex is thermally activated to escape from the bound state. The corresponding dissociation rate $k_{off}(F)$ under an external force F increases exponentially:

$$k_{off}(F) = k_{off} \exp\left(\frac{\dot{F}\,\Delta x}{k_B T}\right)$$

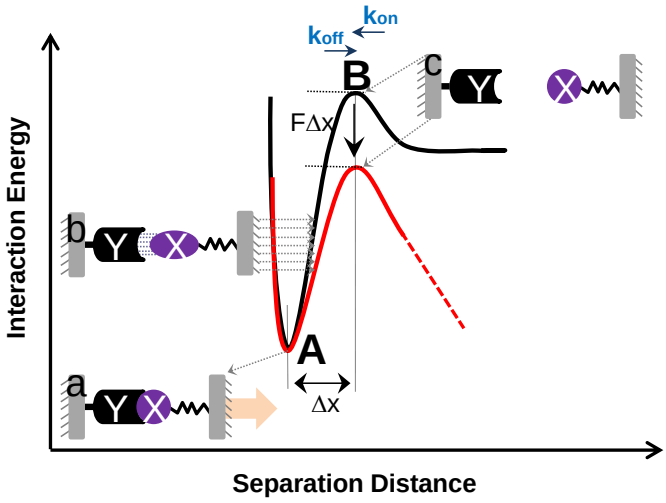

Figure 3.6: Chemical energy landscape governing bond kinetics. (Black curve) normal energy landscape of a complex XY: (a) the molecules are tightly bound at the highest binding energy (point A) and they will dissociate from each other due to thermal fluctuation energy (point B). The dissociated molecules in some cases can also be associated due to the support of thermal fluctuation. (Red curve) under an external force which applies on the complex to pull molecules far from each other (b), the coupling is unnaturally dissociated. The energy barrier is reduced with an amount of $F\Delta x$. Thermal off-rate (k_{off}) and thermal on-rate (k_{on}) present thermal kinetics of the reaction.

The unbinding process crossing over a single and sharp barrier of the complex was then described with a time-dependent force F(t) by Evans and Ritchie [89] which provides us the dependence of the unbinding force on the loading rate. This description was called Bell-Evans model which is based on a series of commonly accepted assumptions such as constant loading rate during a measurement, linear force increase with time ($F = \dot{F}t$),

constant loading rate $\dot{F} = k_{eff}\upsilon$, where k_{eff} is the effective spring constant of the cantilever-complex system, υ the pull-off velocity of the tip which can be selected in AFS measurement and *t* the time [90].

The dissociation of the complex can be obtained by solving the equation for the survival probability *N(t)* in the bound state under an increase of force *F [85, 91]*,

$$\frac{dN(t)}{dt} = -k(\dot{F}t)N(t) \tag{3.5}$$

or

$$N(t) = \exp\left[-\int_0^t k_{off}(t')dt'\right]$$

N(t) connect to the unbinding force probability distribution P(F) by P(F)dF = - S(τ)dτ, where τ is lifetime of the complex

At N(0)=1 the probability in the bound state is

$$P(F) = \frac{k_{off}(F)}{\dot{F}}\exp\left(-\int_0^F \frac{k_{off}F'}{\dot{F}(F')}dF'\right) \tag{3.6}$$

where dF = Ḟdt. By integrating equation 3.6,

$$p(F) = \frac{k_{off}}{\dot{F}}\exp\left(\frac{F\Delta x}{k_BT} + \frac{k_{off}k_BT}{\dot{F}\Delta x}\left(1-\exp\left(\frac{F\Delta x}{k_BT}\right)\right)\right) \tag{3.7}$$

where *p(F)* is a distribution of unbinding force.

The most probable unbinding force or the maximum of the distribution (*F*) at a loading rate (*Ḟ*) is [92]:

$$F(\dot{F}) = \frac{k_BT}{\Delta x}\ln\left(\frac{\dot{F}}{k_{off}}\frac{\Delta x}{k_BT}\right) \tag{3.8}$$

The thermal off-rate k_{off} of the dissociation can be obtained by measuring rupture forces of the complex at different pull-off speeds (υ). At a certain pull-off speed, most probable rupture force distribute within a range and the most probable rupture force can be obtained by Gaussian fit. The rupture forces vary depending on the pull-off speeds. By plotting the most probable rupture force *vs.* pull-off speeds and analyzing by using Bell-Evans model, the information regarding the dissociation of the complexes can be calculated.

In the equation 3.8, the external force (F) is proportional to the loading rate ($\dot{F}$). It can be understood that in the simplest case the parameters governs the dissociation kinetics under an external force. The complex is dissociated under this external force and this external force is measured from force spectroscopy which we call 'rupture force' of the complex. By plotting the most probable force versus the logarithm of loading rate, the kinetic parameters, such as $k_{off} = \dot{F}(F=0)\Delta x/k_BT$ at zero force and $\Delta x = k_BT/m$ (m is the slope of the fit line) can be obtained. Based on k_{off}, the life time of the bond $\tau = 1/k_{off}$ can be calculated. For a complex with known dissociation constant K_D, thermal on-rate $k_{on} = k_{off}/k_D$ of the complex can also be estimated.

Recently, the Bell-Evans model has been used to describe the dissociations of complexes such as DNA-DNA [38, 96], RNA-RNA [97], proteins-DNA [98], proteins-ligands [99, 100], enzymes-drugs and even unfolding of protein domains [102, 103]. As an example of utilizing this model to understand binding kinetic of molecular interaction, the nature off-rate k_{off} and the potential width Δx of Cu-DNA complex is presented [34]. The author split the aptamer into two parts and fixed one part of the aptamer on the tip and the other part on the surface. One base at the center was modified with salicylic aldehyde. When the tip approaches the surface, the hybridization between two parts is formed.

The rupture forces of the oligo hybridization with (red) and without (blue) salicylic aldehyde modification were measured first (Fig. 3.7a). In the presence of the copper, the copper bound the split aptamer via salicylic aldehyde and the rupture force increased (green). By increasing pull-off velocity, the most probable rupture forces increased and followed a logarithm fit. The slopes of the two samples without Cu (blue and red) were almost similar within the error bars while the Cu-DNA-complex sample (green) showed a significantly steeper slope. The slopes were used to calculate the potential widths $\Delta x = k_BT/m$.

The potential widths are of 30 ± 3 Å for the modified dsDNA and only 6 ± 2 Å for Cu-DNA-complex. The short potential width of Cu-DNA-complex means that the interaction between Cu^{2+} and the salicylic aldehyde is localized. The extending figure 3.7a to the left side, the thermal off-rates for the copper-free dsDNA between 10^{-12} and 10^{-13} s^{-1} and 10^{-3} s^{-1} for Cu-DNA-complex which are the intercepts at zero force (Fig. 3.7b). The increase in the thermal off-rate of the Cu-DNA-complex by ten orders of magnitude suggests the thermal stability of the copper complex bond is lower than that of the sample without copper.

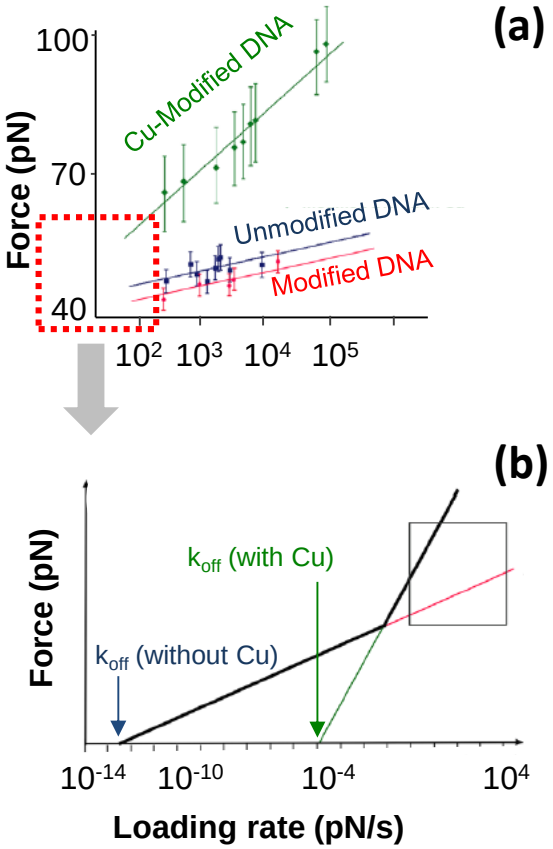

Figure 3.7: Loading rate dependence of unmodified 20-mer DNA in PBS buffer, modified DNA without Cu(II) ions in 0.1 M HEPES buffer and modified DNA with 35 μM Cu in 0.1M HEPES buffer. (a) The most probable rupture forces were plotted against the logarithm of the most probable loading rates and fitted with straight lines. The green line has a steeper slope due to the higher localization of the bond. In the absence of Cu and with mismatch site, the most probable rupture force of modified DNA is lower than that of unmodified 20-mer DNA, whereas the slope is the same. (b) Thermal off-rate can be obtained by an extrapolation of the fit lines with the *x* axis [31].

The dissociation of AMP-aptamer complex in principle is similar to the dissociation of Cu-DNA-complex. However, the binding strength of AMP-aptamer complex is lower than that of Cu-DNA-complex. In order to understand the dissociation of AMP-aptamer complex which only few H-bonds involved, the Bell-Evans model is used in my study.

3.3. Chemical Force Spectroscopy

Regarding single molecular interaction measurements, the AFM-tip and the substrate are usually modified with chemicals to fulfill two tasks, i.e. immobilization of the molecules of interest on the surfaces and reduction of adhesion force between the tip and the substrate. The modification provides a specific chemical function on the surfaces. By approaching the

tip to the substrate, the molecules on the tip interact with their partner on the substrate. The molecular interactions can be obtained in the F-D curves as described in the figure 3.5. This method is called 'Chemical Force Microscopy' (CFM) [93, 94].

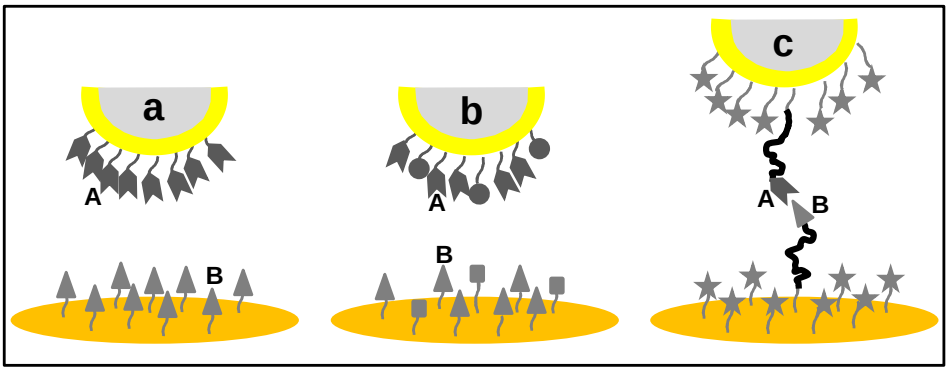

Figure 3.8: Typical surface modifications for measurements of molecular integrations by mean of CFM. A tip and a sample of the atomic force microscope are functionalized with specific chemical functionalities. (a) A species of molecules on the tip (A) and their coupling partners on the surface (B). (b) Active functional groups (A, B) and inactive molecules (circulars and squares) are together on the surfaces. The inactive molecules are to reduce the adhesion force between tip and substrate. (c) Interacting groups with long flexible polymer tethers at very low density (A, B), the free surfaces are passivated by other molecules (stars) which prevent the tip/surface adhesion when the tip closes to the surface. The immobilization with low density can avoid the occurrence of multiple ruptures when the tip approaches the surface. The molecules with specific end groups which are used to fill up the free surfaces must not interact with the molecules of interest to ensure that their functional groups are available to interact with its partner on the tip.

A common way to fix the molecules of interest on the surfaces is to cover the tip end or the substrate by a monolayer of these molecules (Fig. 3.8). For example, if one wants to measure the interaction between two molecules (A and B), a monolayer consisting of these molecules can be brought to the surfaces (Fig. 3.8a). With this modification, interaction of multiple molecules and their partners can be recorded at the same time. To measure the interaction between a single molecule (A) against its partner (B), the free surface can be filled up with the other molecules with specific end groups to prevent tip/surface adhesion (Fig. 3.8b). The molecule of interest can be connected to a spacer and this spacer is one end immobilized on the surface while the molecule of interest is stand outward from the surface (Fig. 3.8c). The free surface is then covered by a monolayer of molecules (Fig. 3.8c, stars) which do not interact with the molecules of interest but the tip/surface can be reduced in their presence.

In 1994, Frisbie et al presented one of the first adhesion force measurement by CFM which the molecules of interest with end groups $-CH_3$ or -COOH were immobilized on the tip or

substrate [95]. By approaching the tip to the surface, the interaction force between those groups could be measured. At the same time, the first measurement of oligonucleic acid interaction was performed by Lee et al [19]. A thiol was attached at 5'-end of the oligo and the oligos were then immobilized on a substrate modified with γ-aminopropylaminoethyltrimethoxysilane. Later on, may other measurements of interactions of oligonucleic acids [35, 86], antigen-antibody [96, 97] and biotin-streptavidin [98] have been carried out.

In order to obtain successful experiments of molecular interactions by CFM, sample preparation and experimental design are crucial steps.

3.4. Sample Preparation

To immobilize the molecules on the surface, avidin-streptavidin and biotin-streptavidin couplings are widely used [25, 85, 99]. For example, streptavidin is covalently bound to the tip while biotin is attached on the molecule of interest which is fixed on the substrate. When the tip approaches the surface, the biotin/streptavidin bond is formed and the molecule of interest is pulled up and the rupture force can be measured. Those methods are simple but have some disadvantage. The couplings are nonspecific adsorption and they may not be strong enough to hold the molecule of interest until it completely ruptures. The biotin/streptavidin may rupture earlier than the other ruptures which results in a difficulty in achieving measurement of rupture force of the molecules of interest. In addition, they can be denatured and degraded when directly bind to an inorganic support.

A typical example for those influence factors to measurements of rupture force of complementary strands DNA were reported by Lee et al [19] and Rief et al [22]. Lee et al obtained the rupture force of ~60 pN for A-T and ~90 pN for G-C pairs while Rief et al reported only 9 ± 3 pN for A-T and 20 ± 3 pN for pairs. These different results are due to different ways of immobilization of the DNA strands. Lee et al used attached a thiol at the 5'-end of each strand and the thiol coupled with silane which was assembled on the tip and substrate. The DNA strands were only physical adsorbed gold surface and a bare tip was used to pick the DNA up from the gold surface in the study of Rief et al. Lee et al expected only the thiol at 5'-end of the DNA strands coupling with the $-NH_2$ groups of silanes on the surfaces. However, later study shown that the DNA itself with negative charge can adhere to the positive charge of silanes on the surface [100]. The tip might peel the DNA strand up from the silane surface before rupturing it which resulted in very large rupture forces reported by Lee et al.

It seems that no chemical involvement in the sample preparation of Rief et al can be an advantage for measurement of rupture force of DNA strands. However, unimmobilization of the DNA strands on the surfaces also has other disadvantages such as movement of molecules during measurement or large variation of molecular lengths due to random picking up by an untreated tip.

In order to assemble oligos on the tip or substrate for the measurement of rupture force of single biomolecules by an AFS, two main points should be considered. First, the involving chemicals should not have deleterious effects on the biomolecules. Second, adhesion force between tip and substrate should be small.

The oligo can be physically adsorbed on the surface or chemically immobilized on the surface using PEG [101-103] or biotin/streptavidin [98] as linkers. Physical absorption of oligos on the surface is normally unstable especially in liquid and is not feasible in sample preparation for single molecular interaction by AFS because the molecules get detached from the surface instead of getting ruptured. When silicon, mica, glass substrates are used, the surfaces are frequently modified with silane or ethanolamine to introduce amino groups to the tip or substrate [104].

Table 3.2. Typical active sites of biomolecules and their corresponding functional groups [105]

Active site of Biomolecule	Functional Group on substrate	Formed Bond
-COOH (carboxyl)	Amine or hydroxyl	Amide or ester
-NH_2(amine)	NHS-ester or carboxyl	Amide or ester
-SH (sulfhydryl)	Maleimide or carboxyl	Thiol-ether or thiol-ester
-CHO (carbonyl)	Hydrazide	hydrazone
-OH (hydroxyl)	Carboxyl	ester
Avidin	Biotin	Avidin-biotin bond
thiol	Au	Au-thiol

The hydroxyl groups on the surface can form covalent bonds with silane reagents, $(OX)_nSi(CH_3)_{3-n}A$. The OX is a hydrolysable alkoxy group and it can form a covalent bond with hydroxyl group on the silicon, mica, glass, i.e. Si-O-Si bond [106]. One end of silane is fixed on the substrate while the other end, *A,* which carries a functional group such as amino or sulfhydryl groups stands upward on the surface. Those functional groups can directly cross-link with the biomolecules of interest or indirectly bind to biomolecules. In the indirect binding of silane to biomolecules, an intermediate linker which carries another functional group needs to be linked between the silanes and the biomolecules. The current favorite intermediate linkers can be glutaraldehyde, PEG, and biotin/streptavidin which can be used

as spacers between tip or surface and the molecules of interest. Depending on the binding groups existing on the biomolecules, corresponding functional groups are selected (Tab. 4.2).

The silane with amine as an end group is usually used to modify the surface prior to the attachment of PEG. However, the DNA molecules can strongly absorb on the substrate due to the opposite charge between the functional group of silane and DNA (Fig. 3.10a). During force spectroscopy measurement, a significant force which needs to peel the DNA molecule off the surface before rupturing it appears in the adhesion peak (Fig. 3.10b).

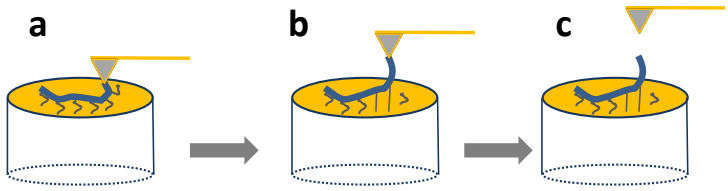

Figure 3.10. Typical reactions between chemically modified surfaces and biomolecules carrying different binding groups.

In this case, the tip only pulls a part of the molecule up from the surface and then detaches from the molecule (Fig. 3.10c) [28, 100]. This adhesion force does not significantly influence the measurements of macromolecular interactions since large specific adhesion peak can be clearly observed (Fig. 3.11a). However, the required force to lift the molecule off the surface is difficult to be distinguished from specific adhesion peaks generated by small molecular interaction (Fig. 3.11b).

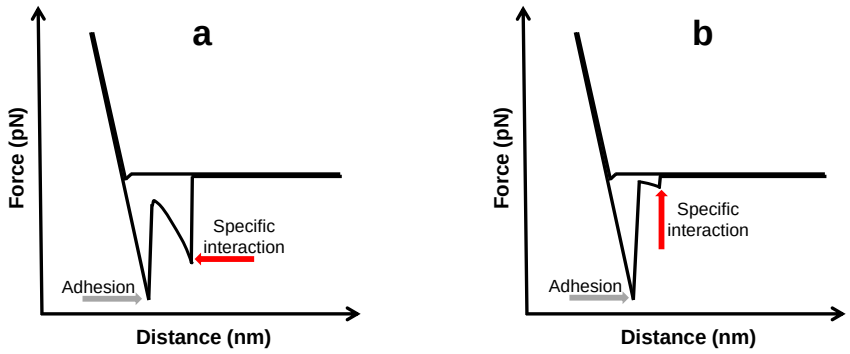

Figure 3.11. Influence of adhesion force on measurement of macromolecular interactions (a) and small molecular interactions (b).

In order to avoid the above limitations, we selected the advantages of those studies to immobilize our oligos on the tip and the substrate. The thiol is attached at 5'-end of oligos and those oligos are covalently bound the gold surface through gold-thiol chemistry.

3.4.1. Immobilization of Split Aptamer

For my specific study, a ssDNA aptamer is split into two parts so called oligo a and oligo b (Tab. 3.1). The oligo a is immobilized on the AFM tip and oligo b is on the substrate. By approaching the tip to the substrate, the oligo a will hybridize with the oligo b and the binding pockets will be formed at the center for AMP binding (Fig. 3.9a). We want to measure the rupture force when AMP molecules bind the pockets (Fig. 3.9b). By measuring the rupture forces in the presence and in the absence of AMP and subtracting the difference from them, the rupture force AMP-split aptamer can be obtained. In the presence of AMP, only eight additional H-bonds are formed which corresponds to small rupture force. The limitations of both mentioned immobilization methods can produce complicated rupture events which brings us to a difficulty in obtaining the rupture force of AMP-split aptamer.

Table 3.1. Split aptamer sequences

	HS-AAAAAAAAAAAAAAAAAAAA(A^{20})-Sequences (5'→ 3')	**Characteristic**
AMP-aptamer	CGTAGA-GGAGGA-AGGTCA-TGACCT-GGAGGA-TCTACG (full sequence)	- Bases/oligo: 18 - Watson-Crick pairs: 12 (6 AT, 6 GC) - Tip/surface distance (nm): 20.7
Split aptamer	CGTAGA-GGAGGA-AGGTCA (oligo a)	
	TGACCT-GGAGGA-TCTACG (oligo b)	

Thiol-modified 5'-end

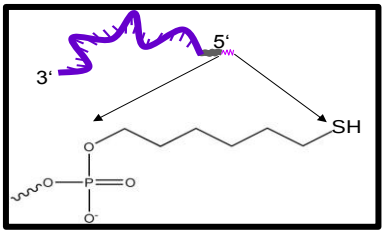

For simplifying the sample preparation protocol, both tip and substrate surfaces are coated with gold. A thiol linker at the 5'-end of oligos will be immobilized on the Au-surface via gold-thiol chemistry. In this experimental design, the bindings of thiol/oligo to the gold surfaces are the strongest, 1.4 ± 0.3 nN, which was measured by AFM at the loading rate 10 nN/s [107]. During tip/sample separation, the rupture force of interest, i.e. oligo hybridization in the absence of target as well as in the presence of the target molecules, is estimated in the range of hundred pN. Thus, the measured rupture force is the oligo hybridization or of target-split aptamer complex.

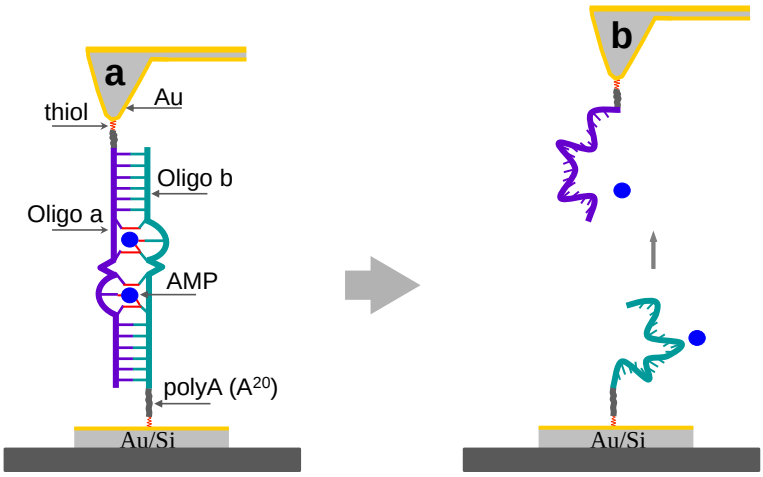

Figure 3.9. Experimental design for measurement of rupture force of AMP-split aptamer. (a) oligo a hybridizes with oligo b when the tip approaches the surface which allows AMP molecules enter the binding pockets. (b) the tip separates from the substrate and the rupture force of the system can be measured in the F-D curve (Fig.3.5).

Gold-thiol chemistry is a simple but efficient method which is well established for immobilizing biomolecules on the solid substrate [20, 21]. Gold surfaces can be easily produced by coating a thin gold layer on the top of any solid substrate such as glass, mica, silicon while gold-coated tips are commercially available. In order to produce a thin gold layer on the Si-substrate, the substrate is first cleaned by plasma cleaning and a very thin layer (2 nm) of Cr is evaporated on the Si-surface prior to evaboration of gold (30 nm). The thiols then bind strongly to gold surface. By measuring the detachment of a thiol-polysaccharide from gold surface, Michel et al. showed that the sulfur-gold anchor ruptured at the force of 1.4 ± 0.3 nN [107]. The other advantage of using gold-thiol is the ease of sample preparation [108], i.e. only 60 min incubation of sample on gold surface.

Since the rupture of small molecule binding aptamer is only few tens of pN, immobilizing oligos on Au-surface is a good selection. Even though, disulfide bond can form in the DNA solution that will produce two ssDNA strand and connect one to another forming unspecific bindings in AFS measurement. Long rupture distances can be obtained from those unspecific bindings. However, Gaub et al presented that disulfide bonds could be broken by adding tris(2-carboxyethyl)phosphine (TCEP) in the DNA solution before incubating it on the surfaces [31, 109] (Fig. 3.12).

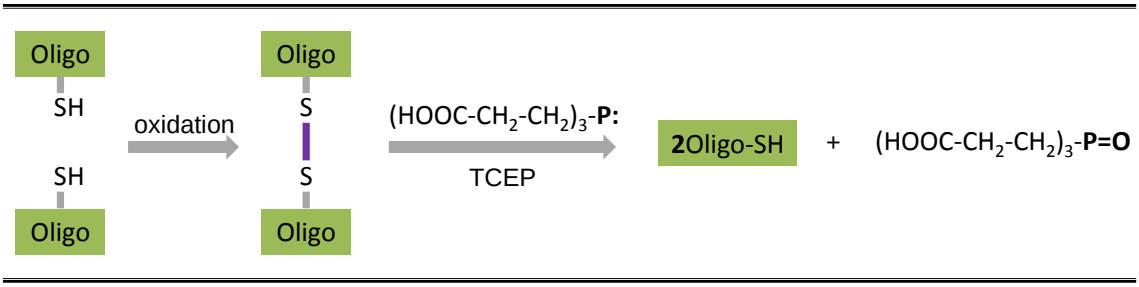

Figure 3.12. Reaction of forming and breaking disulfide bond. Thiol-thiol bond in oligos solution will be broken within 5 minutes at room temperature in the presence of 5 mM TCEP.

The substrate with a thin gold layer was prepared by the following procedure: Si-substrate (1x1 cm^2) was rinsed in turn with acetone and ethanol and then dried with N_2. Subsequently, it was exposed to an argon-plasma for 5 min to remove the organic contaminants. Finally, 2 nm Cr was coated on the surface in order to bind the second 50 nm Au layer on the top by thermal evaporation (Baltec Med 020, Balec, 584 Witten/Buhr, Germany). AFM imaging revealed a roughness of about 1 nm for 1x1 μm^2 Au-surface (Fig. 3.13a). These samples were used within 2 weeks. The surface was always re-cleaned with the acetone and methanol before coating gold onto it for oligo immobilization.

The cantilever used in this study was the Biolever (BL-RC 150VB-C1, Olympus, Japan), nominal spring constant 0.006 N/m, tip diameter around 30 nm, length of 100 μm gold coated both sites (Fig. 3.13b). The first step in the preparation of cantilever was the determination of the spring constant utilizing thermal fluctuation of the cantilever. The spring constant of an individual cantilever calibrated by this method can differ from the nominal value given by the manufacturer by 20-30%. The cantilever was also cleaned before the oligo immobilization. It was first emerged in turn in acetone, in ethanol, and in water to remove contaminants. The plasma cleaning was not used because the soft cantilever bends after treatment.

In addition, the Biolevers are easily folded due to the capillary force during manipulation in and out of the liquid or solvent. Thus, in the tip cleaning process, I simply immersed the cantilever in a drop of acetone, methanol and water for 5 second and repeated this process two more times. A solvent or water droplet was always kept on the cantilevers to avoid the folding problem during cleaning.

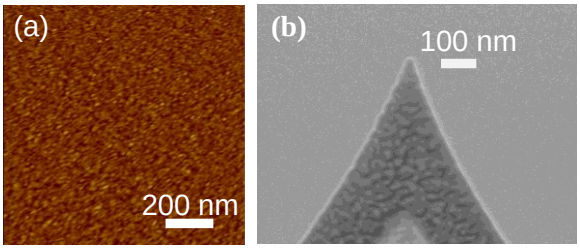

Figure 3.13: AFM and SEM images of Au/Si surface and AFM-tip for AFS measurement. AFM image in intermittent contact mode of the Si substrate coated with 2 nm Cr and 50 nm Au coating with roughness of ~ 1nm (a). A commercial Au coated tip purchased from Olympus (b).

Choosing concentration of oligo for AFS measurement is one of the important steps to achieve a successful measurement to obtain single molecule interaction. Selection of oligo concentrations which allows to obtain only 10% rupture events containing specific rupture events is recommended [110]. For AFS measurement, either of oligo concentrations or their lengths should be together considered. For longer oligos, lower the concentration should be used to avoid cross-linking or aggregation. Strunz et al. prepared oligo sequences of 30, 20 and 10 base pairs with the concentration of 25 µM [111]. However, multiple ruptures were obtained in their rupture force histogram. There 33% of the curves show one rupture event, 20% show two, 15% three, and 7% more than three subsequent rupture events. The small rupture force of AMP-aptamer may be difficult to distinguish if multiple rupture appears. For example, the distribution of the double ruptures may overlap with the one of AMP-aptamer.

I studied some tests of concentration dependence and found that if the concentration is lower than 4 µM, only few rupture events with the specific rupture forces are obtained. When the concentration is higher than 4 µM, multiple rupture appears in the rupture force histogram. Th us, for short sequences of the standard split aptamer, 2 BP, a concentration of 4 µM was used in this study. For 8 or 16 pockets system, the oligo concentration was lowered to 0.5 µM in order to avoid multiple rupture events as well as the crossing among oligos on the surface. Then, the samples were thoroughly rinsed with 100 µl buffer T to remove the unbound oligos from the surface.

3.4.2. Additional Spacer

In many current experiments, long spacer is designed in between the tip and the molecules of interest in order to increase their activity, reduce tip/surface interaction, and lengthen the tip/surface distance in the AFS measurements. This is necessary for measuring small molecular interaction since the short oligos (length ~10 nm) are usually used and this length

can be covered in the unspecific adhesion peak and cannot be detected from the retraction curves. The long linear spacer, typically poly(ethylene glycol) (PEG), is used to connect the molecules to the surfaces [111] (Fig. 3.14). Using PEG, the nonspecific interaction from the specific binding is easy to differentiate and the molecule of interest is more flexibly oriented [112]. In order to attach PEG to biomolecules and on substrates, additional chemicals are required [111, 113].

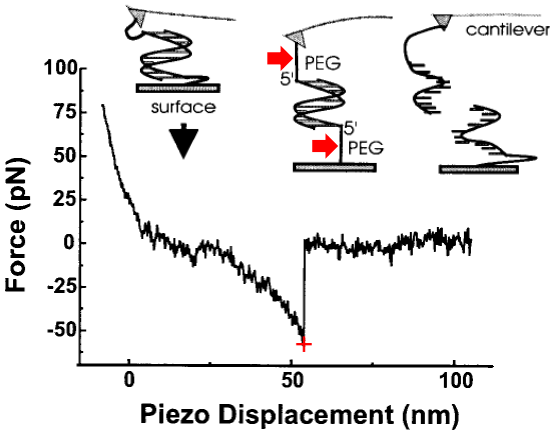

Figure 3.14. Rupture force of complementary strand DNA using PEG linker (red arrows) [111]. Sum of the lengths of PEG (30 nm) and of DNA strands (~10 nm) is a rupture distance of around 50 nm (red cross).

An initial important step is to attach PEG to the molecules of interest. When the molecules need to be immobilized on Au-surface, the PEG end needs to be modified with thiol to form thiol-Au chemistry. When glass or silicon substrates are used, their surfaces need to be modified with the other linker containing $-NH_2$ group at the end in order to form a binding between PEG and substrate. This synthesis is complicated and can harm the samples even though large adhesion force can be generated.

In order to have a simpler protocol of attaching a spacer between the tip or the substrate and the oligos, we here used poly adenine (polyA), 20 bases (A^{20}). A thiol is added to 5'-end of the polyA chain so that the whole chain can be immobilized on the Au-surfaces.

3.4.3. Passivation of Free Surfaces - Reduction of Adhesion Force

The rupture forces of single short complementary strands DNA which are of interest in this study are small compared to adhesion force between tip and substrate. Large adhesion forces and multiple ruptures make us difficult to distinguish the rupture of single molecular interaction. By CFM, one strand of the DNA is immobilized on the substrate and its complementary strand is fixed on the tip. In this step, the density of the DNA strands on the

tip and substrate should be low which allows to measure rupture of single molecular interaction. Together with that, chemicals involve in this immobilization step should be controlled to avoid large adhesion forces.

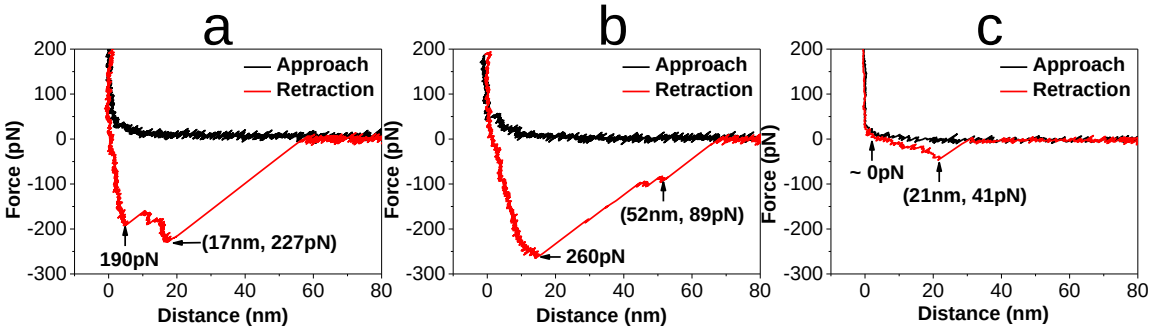

Figure *3.15*: Influence of adhesion force on the expected rupture event. (a) Large adhesion force produces a large rupture force or long rupture distance (b) of the specific event. Small adhesion force provides a reasonable rupture force and rupture distance (c).

If the unspecific adhesions are large, they can hide the specific interaction peaks. Thus, incorrect rupture forces and rupture distances will be produced. For example, three types of adhesion forces (Fig. 3.15) frequently appears in our F-D curve experiments such as large rupture force (Fig. 3.15a), long rupture distance (Fig. 3.15b), and small adhesion force (Fig. 3.15c). The rupture force and rupture distance occurring at small adhesion forces are close to their theoretical values which should be used for further analysis.

Minimizing the unspecific adhesions in order to obtain a successful measurement of rupture force of single small molecules is a crucial task. In order to do that, the tip and substrate are controlled by appropriate surface modification. Chemicals carrying special end groups are usually used to cover the bare tip and substrate surfaces.

Regarding surface modification to reduce adhesion force for single molecular interaction measurement, a number of investigations have been carried out [101, 112, 114-116]. Au-surfaces are usually functionalized with SAMs terminating in different end groups such as ~CH_3, ~OH, ~COOH (for example $HS(CH_2)_{11}OH$) [117]. The thiol at the end of the linker binds the Au-surface while the end groups stay upwards. By modifying both tip and substrate with the same SAM layer and approaching the tip to the substrate, the tip/surface adhesion forces could be measured and the adhesion forces (F) of those interactions are different, $F_{COOH\text{-}COOH} > F_{OH\text{-}OH} > F_{CH3\text{-}CH3}$. Noy et al [117] explained that the ~COOH is a hydrogen-bonding group while the ~CH_3 is a non-hydrogen-bonding groups. In aqueous solution, the ~COOH groups form H-bonds and that creates a greater adhesion force. Noy et al. have also introduced a useful method to avoid gold-tip/gold-surface interaction by adding 16-thiohexadecanol on the surface. By mixing 5'-thiol DNA with 16-thiohexadecanol and depositing them on the tip and substrate

surfaces overnight at room temperature, they could eliminate adhesion force and unspecific binding events [118]. Alkanethiols can also replace other SAM layers of alkanethiols within hours and days [119]. This means that part of the bound oligos or crowded immobilized oligos on the surfaces can be replaced by the alkanethiols. Ling et al. [120, 121] used 3-mercapto-1-propanesulfonic sodium $HS(CH_2)_3SO_3Na$ to cover their free gold surface after immobilization short oligonucleotides and found that the adhesion force was reduced.

The interactions of molecules also vary depending on the buffer. In order to select good molecules to passivate the gold surface and to reduce the adhesion force between Au-tip and Au-surface, I have investigated some good candidates in the AMP-aptamer buffer [122] (see detail in the next chapter). The $HS(CH_2)_3SO_3Na$ was selected for passivation of free gold surface in this study.

The samples with the immobilized oligos were then incubated in 1.2 μM $HS(CH_2)_3SO_3Na$ solution for at least one hour. It is reported that the sample can be incubated in $HS(CH_2)_3SO_3Na$ even up to 15 hours [123]. If the incubation time is too long, the mono layer of oligo can be replaced by the $HS(CH_2)_3SO_3Na$ which results in less oligos on the surface [124]. Finally, the substrate was thoroughly rinsed with buffer T to remove all remaining unbound molecules on the surfaces. The fresh samples were usually used for AFS measurements right after preparation or samples were kept in the buffer at 4 ˚C and used within 3 days.

4. Optimization of Measurement and Analysis

In force spectroscopy measurements, there are many factors such as sample preparations and measurement conditions that influence the specific rupture force. A significant difference in the measured binding force of the same Biotin-Streptavidin system has been reviewed by Lee et al [125]. The binding force of this system varied from 126 pN [126] to 454 pN [127] which is about four times greater depending surface modification and pull-off velocity. In the measurement of rupture force of nucleic acids, a large difference has been obtained. The rupture force of a single A-T or G-C base pair varied from few pN to several hundred pN depending on surface treatment and measurement conditions [19, 24]. Those differences were due to artifacts during sample preparation. The oligo immobilization has been introduced in chapter 3, section 3.3.1. In this chapter, artifacts induced during sample preparation, AFS measurement and data analysis will be discussed in detail. Conditions for sample preparation and method for data analysis will be discussed and the best conditions and methods are then selected for this study.

4.1. Reduction of Adhesion Force

The adhesion force depended on the characteristic of end groups on the tip and on the substrate (Fig. 4.1a). Comparing to the surface without any modification (No linkers), the tip/surface adhesion forces reduce by using the linkers with end groups ~CH_3, ~SO_3^- and ~OH and it increases with end group ~COOH. Significant rupture events with large adhesion force

may be due to the H-bond produced between ~COOH groups when the tip comes closer to the surface [117]. Large error bars in the case of ~COOH termini may be due to the contribution additional H-bonds. Since we have used different cantilevers for each linker, the tip radius were also taken into account. The adhesion force is known to be proportional to the tip radius, $F_{ad} = 2\pi RW$, where R is the tip radius and W is the thermodynamic work of adhesion [117]. By taking SEM image of each tip apex (see an example in figure 4.1b), we estimated the adhesion force per unit tip area. The same trend compared to total adhesion force was observed (Fig. 4.1c).

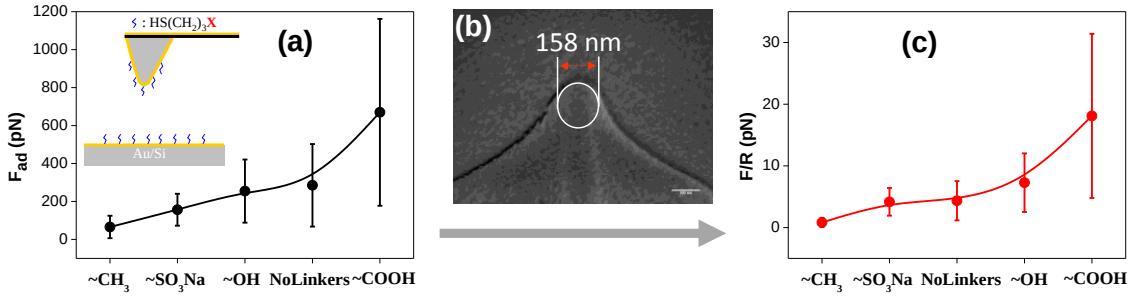

Figure 4.1: Dependence of adhesion force by varying the end group of alkanethiol linker measured in the buffer T. Minimum adhesion force is obtained by the -CH_3 end group and maximum by -COOH group.

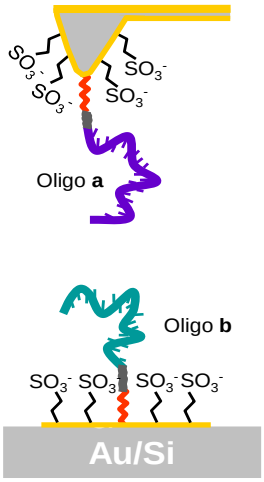

Figure 4.2: Passivation of ~ SO_3^- termini on the free surface after oligo immobilization. Physical absorptions of the oligos on the Au-surfaces are prevented. Sulfurs at the ends of oligos and termini connect to Au-surfaces via S-Au bond with bond strength of 1.4 ± 0.3 nN. The $HS(CH_2)_3SO_3^-$ termini are fully filled the free surface to reduce the tip/surface adhesion force.

The smallest adhesion force is obtained with the ~CH_3 end group. However, the terminus with end group ~SO_3^- is also a good choice to reduce the adhesion forces. In addition, the negative charges of the SO_3^- termini support the oligos to stand upwards the surface. When the tip

approaches the substrate, the oligo a can easily hybridize with oligo b. With this additional advantage of $HS(CH_2)_3SO_3Na$ for measuring the rupture force of small molecule binding aptamer, here I use this terminus to reduce the adhesion force between the tip and the surface (Fig. 4.2). Those termini can firmly attach to the Au-surface via gold-thiol chemistry.

4.2. Optimum Incubation Time

The incubation time for oligo immobilization as well as surface passivation with 3-mercapto-1-propanesulfonic sodium is crucial for a successful experiment. Those steps directly influence the quality of F-D curves. When incubation time is not enough, the molecules may not firmly bind the surfaces, resulting in less rupture events can be measured. In contrast, high density of oligos can form on the surface at long incubation time. The incubation time largely varied in the previous studies. For example, the oligo immobilization on gold surface is varied from 20 min [20], 45-60 min [128], 2 hours [120] and even up to 20 hours [129]. La uren et al. investigated the absorption of sequence-dependent DNA on gold surface and found that the absorption of different oligonucleotides, i.e. polyA (open circles), polyT (black circles), and polyC (gray circles), on the gold surface was saturated after one hour (Fig. 4.3, red bar).

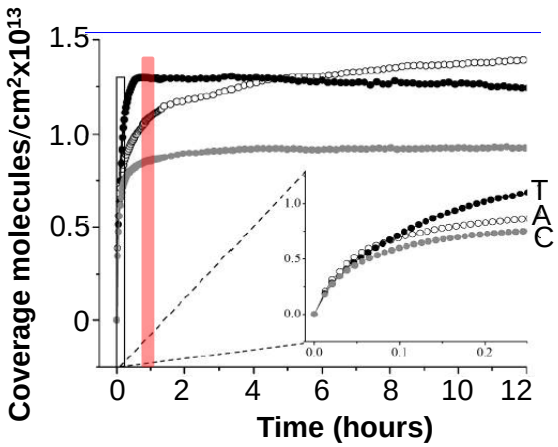

Figure 4.3: Immobilization of different oligonucleotides, (polyA (open), polyT (black), and polyC (gray), on gold surface at different time incubations. The absorption of those oligos on Au surface seems to be saturated after one hour incubation [130]. Inset is an enlargement of the dependence at short time incubation.

The influence of time incubation of both oligos and passivation linkers on the surfaces was also investigated by Lorenz [55]. The author varied the incubation time of oligo on the surface from 20 min to 4h while for the passivation linker it was varied from 20 min to 17h. The author found that short incubation time (20 min) provides a good passivation of 3-mercapto-

1-propanesulfonic sodium linkers to the surface and good quantity (~ 10%) of specific rupture events could be obtained. Increases of unspecific- as well as specific rupture events were obtained at 15h linker passivation time. When the oligo incubation time was raised to 4h, the author obtained less specific rupture events and similar amount of adhesion events (Fig. 4.4). It is worth if we can obtain high quantity of specific events and reduction of the adhesion force. To reach this goal, I have investigated the incubation time to find the best condition.

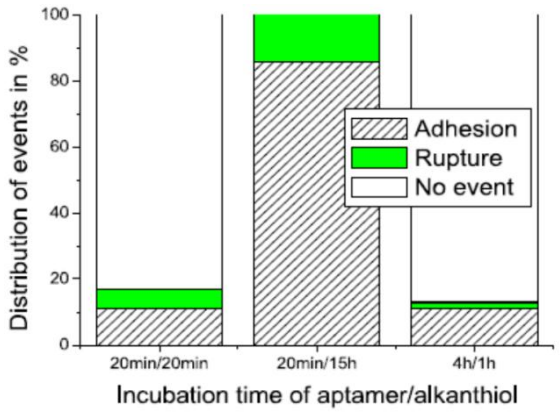

Figure 4.4: Influence of incubation time on the rupture events [35]. With 20 min incubation time for aptamer and 15 h for passivation of ankenthiol, maximum ruptures with specific adhesion events and ruptures with unspecific adhesions were observed (middle green column). The other incubation time provide less specific adhesion events.

In my experiment, I found that the oligos did not stay on the surface for many F-D curve measurements if the incubation time was one hour. There are only few F-D curves (<3%) with specific rupture events could be obtained after 3000 F-D curves measurements. However, with the same incubation time for oligo on the surface but 15 hour for 3-mercapto-1-propanesulfonic sodium linker passivation, I could obtain up to ~80 % of specific rupture events without or with small unspecific rupture events (Fig. 4.5).

In addition, there were only few specific rupture events containing multiple rupture events. By increasing the incubation time to 15h, the 3-mercapto-1-propanesulfonic sodium linkers event replaced some oligos on the surface which resulted in less multiple rupture events [131]. Long time incubation of 3-mercapto-1-propanesulfonic sodium also pushed the loose bound oligos on the surface into the buffer which released more free space for the other oligos to bind to gold surface. As a result, the number of specific rupture events could be obtained even after measuring 10000 F-D curve measurements. Thus, this protocol is found the best and is used for all experiments in my study.

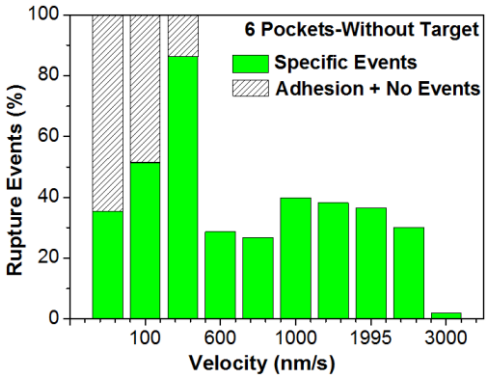

Figure 4.5: Influence of incubation time on the rupture events and stability of oligo on the surfaces. High % of specific rupture events was obtained after 1h incubation time of oligos on the surfaces and 15h passivation of ankenthiol linkers. Rupture events was still obtained at the 10 thousandth measurement.

4.3. Removal of Unbound Molecules

For rupture measurements of ssDNA from its complementary by AFS, removal of the physical absorption molecules on the surface is a crucial step in order to have a successful experiment. If loose bound oligos still stay on the surfaces, they will join each other to form the dsDNA either on the tip or on the surface (Fig 4.6). If this happened, oligo a on the tip cannot hybridize with oligo b on the surface when the tip approaches the surface which results in no any formation of binding pocket. In this case, we do not recognize any (or very few) rupture event that has the expected rupture force.

In the previous studies, the samples are usually rinsed with only buffer and multiple rupture events are often obtained [132, 133]. As a typical example, Liansheng et al. measured the rupture force between the third strand and the double strand within a triplex DNA [129]. Both single and multiple ruptures appear in the retraction curves. When all rupture forces are collected in the histogram distribution, the force varies from few pN to 300 pN. The histogram distribution is fitted with multiple fits. The author claimed that the first peak of 44 pN is due to the rupture of the third strand from the double strand DNA. This value is high enough which the multiple rupture events are distinguishable in the histogram distributions, e.g. two 'third strands' rupture from two dsDNAs at the same time then the force will be 92 pN, and three of them rupture at the same time then the force will be 132 pN, and so on. However, for small molecular interactions, the rupture force is only about 10 pN and the multiple ruptures are normally difficult to be distinguished from the histogram distributions and the mentioned method to analyze rupture force of multiple ruptures is not feasible.

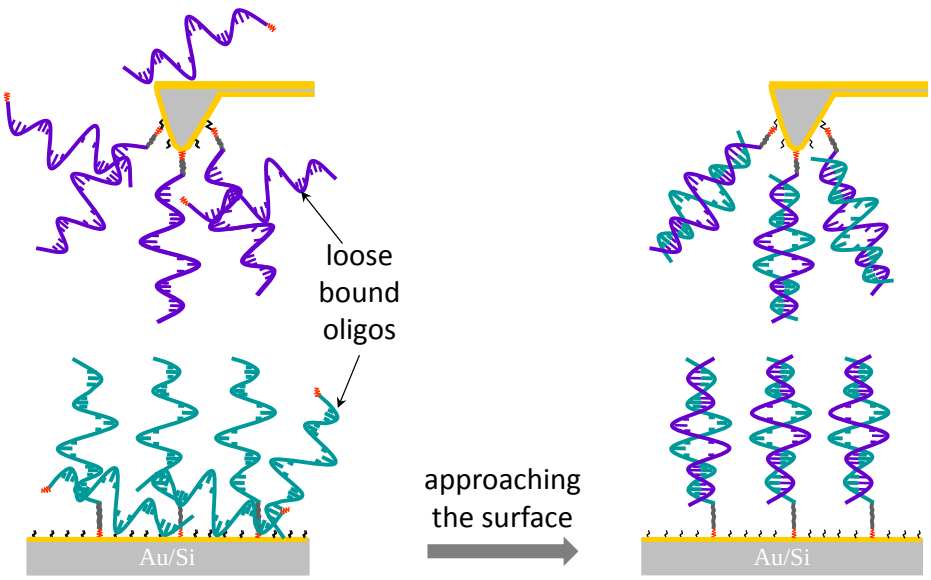

Figure 4.6: Blocking of oligos due to lose bound molecules drifting in liquid cell.

In an ideal rinsing, all unbound oligos are washed away and those multiple ruptures can be originated from the ruptures of multiple oligos immobilized on the tip hybridized with their complementary oligos immobilized firmly on the surface. However, the ideal rinsing is rarely obtained and the oligos are still physically absorbed on the surface. When the tip approaches those loosely bound oligos, the hybridization could be formed and the measured rupture force can be either the rupture of the double helix or the detachment of the oligo from the substrate. For that reason, multiple ruptures in my study need to be minimized as many as possible.

In my sample preparation, a careful rinsing of the tip and substrate after immobilization of oligos on the surfaces is carried out. The tips were rinsed 10 times with 200 µl buffer each while the substrates were kept under a buffer flow for two minutes. However, the loose binding oligos are still trapped on the surface and in AFS measurement, multiple ruptures are still obtained. For example: measurement of the rupture force in the system without AMP molecules, many rupture events appear at high force (Fig. 4.7). The main distribution is at the force of about 27 pN, and the distributions at higher force are ~54 pN, ~81 pN or even ~105 PN. The distributions correspond to the one, two, three or even four rupture events. The high force due to multiple ruptures may contribute to the main single force distribution leading to a broad fit and an inaccurate rupture force from Gaussian fit.

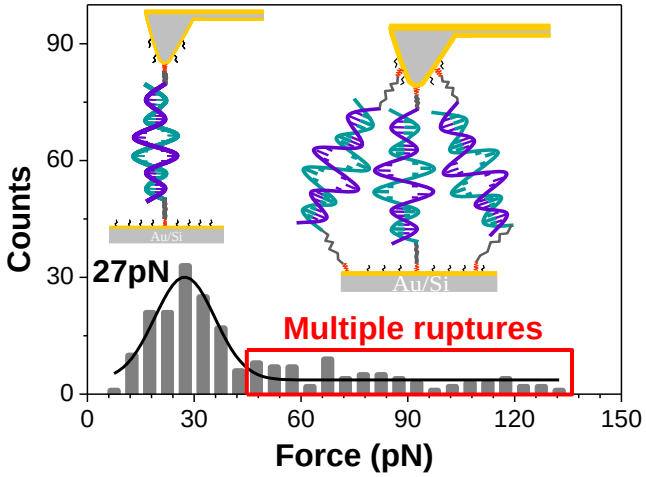

Figure 4.7: Influence of unbound molecule on the rupture force distribution at the first measurement. The main force regime of 27 pN is attributed to the rupture force of single oligo hybridization. Multiple ruptures appear at high force regime (red box).

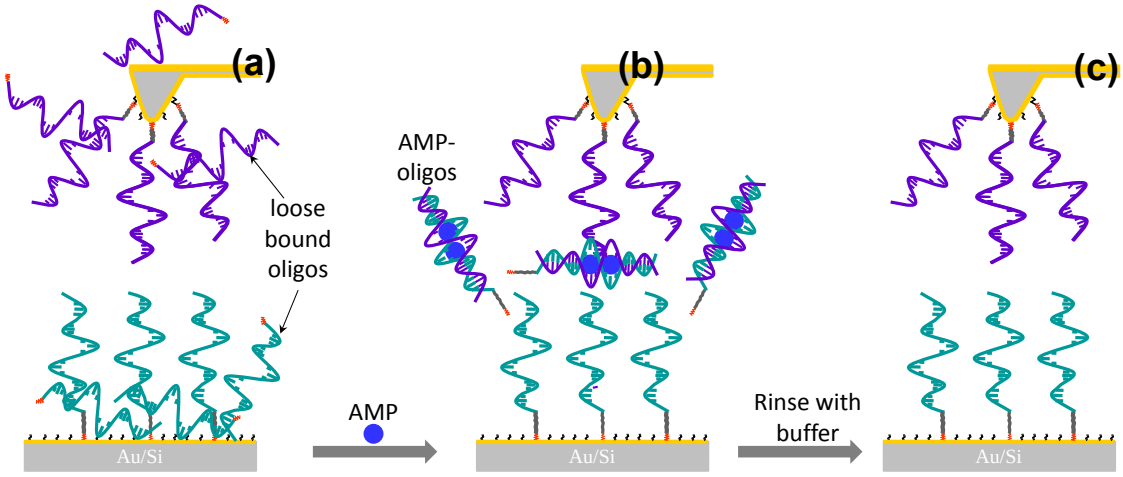

Figure 4.8: Removal of loosely bound oligos by additional washing. (a) Loosely bound oligos on the tip and substrate. Adding of AMP, the oligo hybridization and stabilization by the AMP (b) and the complexes are removed by rinsing with buffer (c).

In order to minimize this influence, the sample after normal preparation is installed in the liquid cell of the AFM (Fig. 4.8a). Then, 1 ml of AMP target molecule is added into it (Fig. 4.8b). The unbound oligos on the tip and substrate can be hybridized and stabilized in the presence of AMP and the complexes can be easily rinsed away. After 10 minutes, the whole liquid cell is rinsed again with 3 ml buffer solution. Then, the first F-D curves are recorded. Following this additional process, the unbound molecules on the tip will be hybridized with the unbound molecules on the substrate with the support of targets molecules (Fig. 4.8b). Then, a rinsing step of the whole system with 3 ml buffer, the unbound oligos can be

removed from the liquid cell. The remaining molecules are only the immobilized oligos on the tip and on the substrate (Fig. 4.8c). Thus, the multiple ruptures in AFS measurement can be minimized. For example, after the additional adding/rinsing steps with 50 µM AMP, the force distribution measured with 2 binding pockets system shows a single distribution and it fits quite well with a single Gaussian fit (Fig. 4.9).

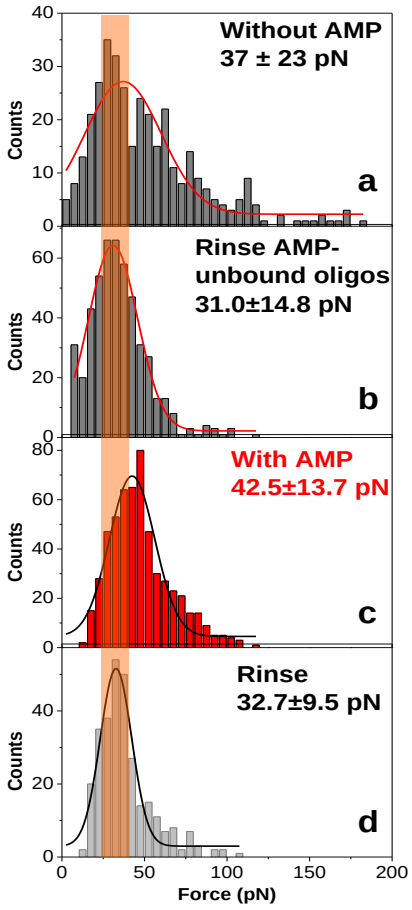

Figure 4.9*:* Minimizing multiple ruptures due to unbound molecules by an additional rinsing step. Top graph is the rupture force distribution of the sample without AMP which is measured right after sample preparation. (a) Many rupture events occur at high force regime which attributed to multiple ruptures. (b) rupture events at high force regime after an additional rinsing with 100 µM AMP and buffer T is reduced. (c) adding AMP again, the force shifts to a higher regime of 42 pN. (d) after rinsing with buffer to remove AMP molecule in the liquid cell, the force goes back to the value of the measurement in the absence of AMP but after the additional rinsing step (b).

4.4. Buffer Selection

In nucleic acids, buffer plays an important role in forming helix structure. In pure water, a ssDNA and its complementary repulses each other because of the negative charge along the sugar backbone. However, when water contains cations such as Mg^{2+}, Na^{+}, the negative

charge along the ssDNA is screened by the positive charge of those ions. As a result, the negative repulsion between two single strands DNA is reduced and the dsDNA can be formed [134, 135]. pH also influences formation of a double helix DNA and on its activity to other biomolecules. A solution which meets these two criteria (salt and pH) is called a buffer. In the first study of finding aptamer that bind adenosine and ATP, Huizenga and Szostak used a buffer with 5 mM $MgCl_2$, 20 mM Tris, pH 7.6, 300 mM NaCl [29]. In the measurements of AMP, ATP and adenosine binding aptamers by AFS, the NaCl concentration is normally lowered to avoid precipitation of salt during measurement while pH of the buffer is always kept at about 7.5 for DNA-ligand interaction. For example, Dorminik et al. measured AMP and ATP binding DNA aptamer with the comparative unbinding force assay in buffer of 15 mM sodium citrate, 150 mM NaCl, 1 mM $MgCl_2$, pH 7.4. Wenner et al. reported that at high salt concentration, the DNA length decreases [136]. To avoid precipitating salt and shrinking the oligos in high salt concentration, in this study, the Tris buffer containing 10 mM NaCl, 10 mM $MgCl_2$, 50 mM Tris-(hydroxymethyl) aminomethan, pH 7.4 (buffer T) was selected. This buffer has the same pH as known in literature but the NaCl concentration is reduced to 10 mM. This salt concentration is enough for formation of the oligo hybridization and establishment of binding pockets.

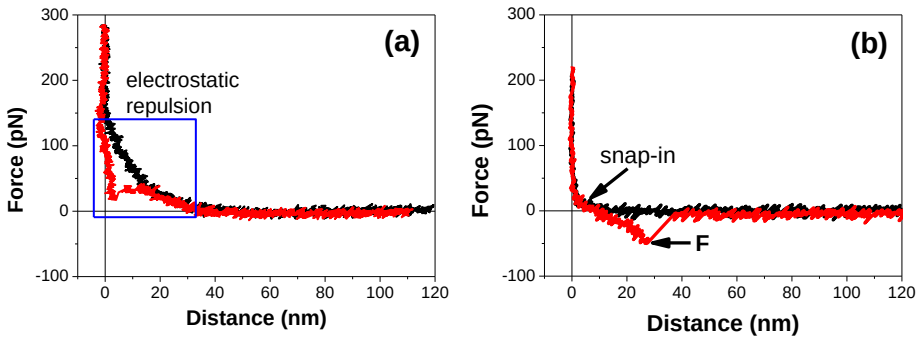

Figure 4.10: Influence of electrostatic force on the rupture force of an oligos hybridization. The rupture force (F) measured in pure water (a) cannot be analyzed due to large electrostatic force. The electrostatic force is removed when the measurement is carried out in buffer T (b).

The other reason to use buffer T for this study was to eliminate electrostatic repulsion between the tip and the sample. In the measurement of single small molecule interactions, the appearance of electrostatic force between the tip and the substrate may provide an inaccurate measured binding force. In pure water, the electrostatic force pushes the cantilever back when the tip approaches the surface (green box, Fig. 4.10a). The specific rupture event and the snap-in point are pushed above the zero line. The electrostatic interactions are reduced in the buffer T containing salt (Fig. 4.10b). This phenomenon has been explained by the appearance of two force contributions using two particles. When they

are close to each other, the van der Waals attraction and the electrostatic double-layer repulsion appear [137, 138]. The electrostatic double-layer repulsion is strong enough to keep the particles apart at low salt concentration. In the presence of significant salt concentration, the electrostatic repulsion is screened.

The rupture force F in water is shifted to a smaller value and it is even unable to determine depending on the magnitude of the electrostatic force. Electrostatic force produces a difficulty in determining the zero line for the calibration of the force curve. In the presence of salt, the electrostatic force can be screened leading to a good determination of the zero line and the obtained rupture force (F) is much more reasonable (Fig. 4.10b).

However, the salt concentration in the buffer should not be too high. Baumann et al. measured the stretching of lamda DNA (λ-DNA) as a function of ionic strength [139]. They found that at low salt concentration (1.86 mM), the required force to stretch the λ-DNA was 649 ± 82 pN. This value increased drastically when the salt concentration surrounding the DNA was increased. In concrete, at 586 mM, the required force to stretch the λ-DNA is 1435 ± 160 pN. At high salt concentrations, the electrostatic attraction dominates and the DNA molecule becomes stiffer. In addition, the DNA fragments in these environments will be looped or condensed [140-143]. As a result, an additional force is required to open the looped or condensed forms of the molecule before it is stretched. The final stretch force at high salt concentration is therefore higher than that at low salt concentration. In addition, Chen et al proved that the contour length of the 40 bp ssDNA is significantly reduced when the salt concentration increases [144]. In our standard split aptamer, the ssDNAs (oligo **a** and oligo b) consist of 38 bp and they can be coiled at high salt concentration. When the tip approaches the sample surface, the coiled oligos may be difficult hybridize, and therefore results in no formation of binding pockets for AMP.

In order to examine the effect of salt concentration on the short oligonucleotides, a simple test was carried out, i.e. rupturing oligo a from oligo b in two different solutions (10 mM NaCl + buffer T and 150 mM NaCl + buffer T). The final rupture forces were collected in each experiment and were fitted with single Gaussian fit (Fig. 4.11). In buffer containing 10 mM NaCl (Fig. 4.11 top), the measured rupture force was about 7 pN smaller than that measured in the buffer containing 150 mM NaCl (Fig. 4.11 bottom).

At high salt concentration (150 mM), the oligo as well as the spacer A^{20} can be folded or coiled. During tip/sample separation, the oligos first need to be extended before ruptured from each other. Therefore, the increase in the force is due to the additional force to open the folding, coiling of the oligos. Therefore, I used the buffer containing only 10 mM NaCl in this study.

The buffer in this study was prepared as accurate as possible. The error in different preparations depends on the accuracy of the amount of salts in it. The balance with an accuracy of 0.1 mg was used and the error of NaCl in the buffer was about 1.7×10^{-4} %. One little of buffer was prepared each time and used within two months to avoid salt precipitation. The same buffer was used for all measurements.

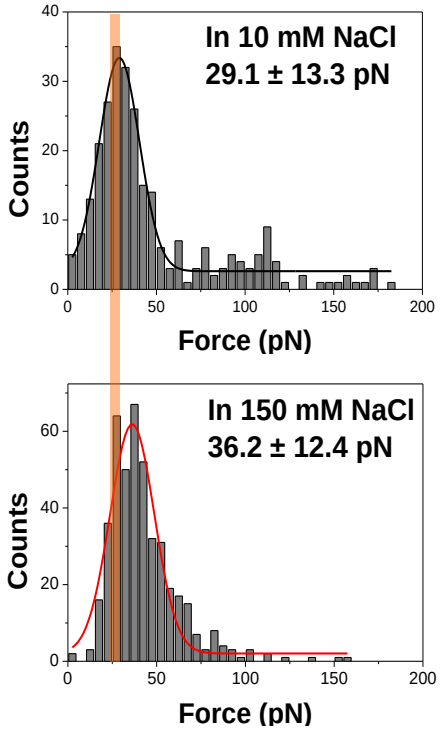

Figure 4.11: Dependence of rupture force of oligo a/oligo b hybridization on salt concentration. One set of F-D curves is collected in solution 1 (10 mM NaCl + buffer T). Then, 3 ml solution 2 (150 mM NaCl + buffer T) is injected into the liquid cell to replace solution 1. After that, another set of F-D curves is collected again. The same tip is used for both measurements.

4.5. Tip/Surface Contact Time

In order to observe a reasonable F-D curve, several parameters should be taken into account. The height and the width of the F-D curve can be adjusted by varying the setpoint value and the Z-length, respectively. The setpoint is a force applied by the tip to the sample and it is the deflection of the cantilever in contact mode. Each cantilever its own spring constant and the magnitude of the setpoint relates directly to it. After determination of spring constant, the setpoint value is provided. The setpoint can be adjusted but it should not be much higher than this given value because the slope regime in the F-D curve will not be linear. The high setpoint makes the cantilever bent or even break. The Z length presents from how far the tip approaches the sample. For short oligos in my study (~20 nm), a Z length of 200 nm was

sufficient to observe the rupture distance in the retraction curves. Also, 200 nm is enough to be sure that the tip is not in contact with any linker when it goes back to the rest position.

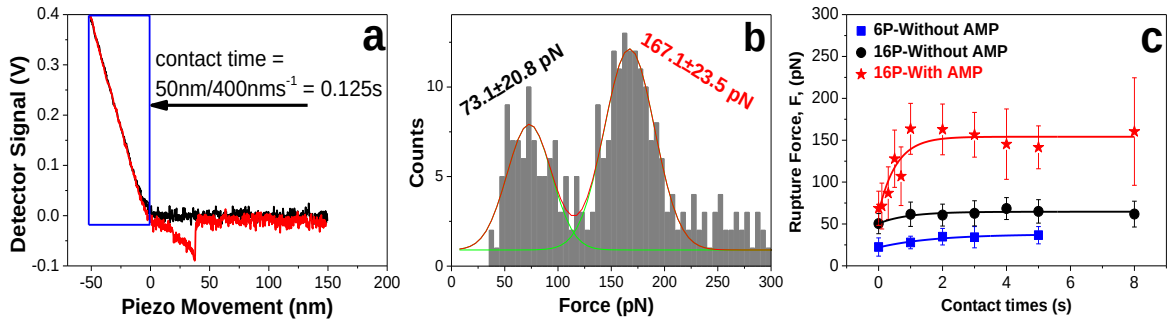

Figure 4.12: Dependence of oligo hybridization on tip/surface contact time. Tip/surface contact time is calculated from the distance of piezo movement and the pull-off speed (a). Histogram distribution of the rupture forces obtains in the presence of AMP with an appearance of both low and high force due to an uncompleted hybridization (b). Variation of rupture force vs. tip/surface contact time (c).

Another parameter that needs to be considered is the contact time. The contact time in force spectroscopy measurement means the time in which the tip is in contact with the surface. The hybridization between oligo a on the tip and oligo b on the substrate may depend on the tip/surface contact time. In the standard pull-off speed of 400 nm/s, 200 nm Z-length, and one second time per F-D curve were selected. This means that the tip/surface contact time is 0.125 s and it depends on the contact distance. The contact time is calculated from the real detector signal *vs*. piezo movement curves (Fig. 4.12a). For the short sequences such as 2- and 4 BP, the oligo hybridization could be completed in nano seconds and no influence of contact time on the rupture force was found. However, in the 16 pockets system which the total numbers of the Watson-Crick pairs increase to 48, a contact time of 0.125 s was not sufficient for completing the hybridization. In the force distribution histogram (Fig. 4.12b), both distributions of low force (without AMP) and high force (with AMP) was observed. This may be due to the uncompleted hybridization which results in an incomplete formation of binding pockets and the AMP could not enter the aptamer. In the presence of AMP, the most probable rupture forces also increase when the contact time increase (red curves, Fig. 4.12c) and it saturates at about 2.0 s for 16 BP and 1.0 s for 6 BP (blue curves, Fig. 4.12c).

However, multiple rupture events were observed for long contact times. For example, the measurement of 6 pockets-AMP complex with different contact time of 0 s (a), 1.0 s (b) and 2 s (c) were investigated (Fig. 4.13). There were three distinguished force distributions at 2s contact time while only two distributions could be observed at zero and one second.

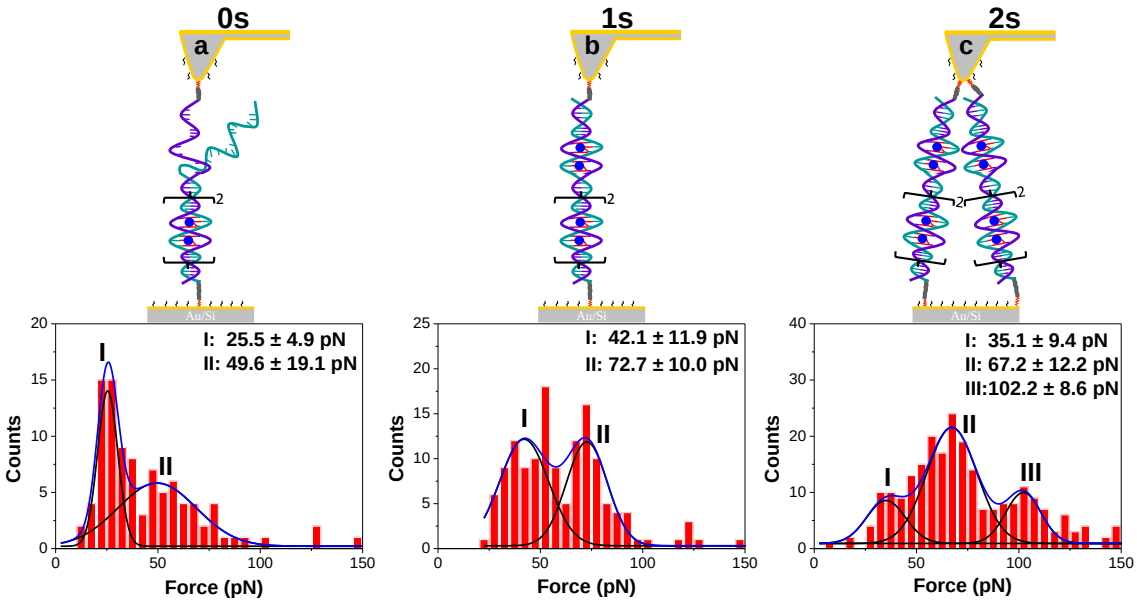

Figure 4.13: Dependence of rupture force distribution on tip/surface contact time for 6 pockets system in the presence of AMP. At zero second (a), about 80% distribution is at low force regime I and 20% is at high force regime II. More rupture force events were obtained in the regime II when the contact time is increased to 1s (b) and 2s (c). At 2s contact time, multiple ruptures appeared (regime III).

The distribution I is the rupture of 'only oligo hybridization' and the distribution II belongs to the AMP-split aptamer complex. At the zero second contact time, the rupture force at the 'distribution I' was significantly low and it was similar to the value obtained from 2 BP system, which might be due to an incomplete hybridization of the oligos (Fig. 4.13a). In this case the binding pockets were partly formed and only several AMP could enter the aptamer and the rupture forces (distribution II) was also low (Fig. 4.13a). At 1 s contact time the oligo hybridization is mostly completed which results in a higher forces of both distribution I and II (Fig. 4.13b). For 2 s contact time, the distribution II dominates and the distribution I reduces to about 20% (Fig. 4.13c). However, the multiple rupture events appear at higher force (distribution III). Therefore, I selected contact time of 1.5 s for 6 BP system. With a similar consideration, I selected contact times for different binding pockets such as 0 s for 2- and 4 BP, 1.5 s for 6- and 8 BP, and 2.0 s for 16 BP.

4.6. Measurement Protocol

After determining cantilever spring constant and setting up the measurement parameters, the tip is approached to the surface and 100 F-D curves are recorded in the scan area of 5x5 μm^2. The tip is then moved by 1 mm on the sample and another 100 F-D cures are again measured. This step is repeated 10 times until achieving 1000 F-D curves. In order to obtain the rupture

force of AMP binding aptamer, three systems, i.e. without AMP, with AMP and after rinsing are always measured in turn. After measuring the force curves on the system without AMP, the buffer solution that contains AMP molecules is added to the liquid cell to replace the first solution and after 30 minutes the force curves are measured again. Finally primary solution is added into the cell to remove AMP molecules for the last measurement of the force curves. For other target molecules such as Inosine, IMP and OMA, the same procedure is used.

For the series of experiments at different AMP concentrations (from 0.01 μM to 100 μM), the measurement was first recorded in the buffer without AMP, and then 1 ml AMP solution was injected into the liquid cell in order of ascending concentration and 1000 F-D curves were recorded at each concentration. The measurements were taken from low to high AMP concentration. In total, five cantilevers were used for this series of experiments.

4.7. Background Measurement

In order to be sure that the rupture forces collect from the retraction curve are due to the rupture of the oligo a/oligo b hybridization, two background measurements were carried out (Fig. 4.17). The first one was measured with a system where only oligo a was immobilized on the tip and the substrate was modified with $HS(CH_2)_3SO_3^-$ without oligo b (Fig. 4.17a). The second one was with oligo a on both tip and substrate. The free surface was also passivated by $HS(CH_2)_3SO_3^-$ (Fig. 4.17b). With those systems, there is theoretically no any specific interaction between the tip and the surface. By taking F-D curves on those systems and analyzing the results, only less than 5% of the F-D curves containing the specific rupture events. Therefore, the specific rupture events between oligo a and oligo b in the presence and in the absence of AMP are reliable.

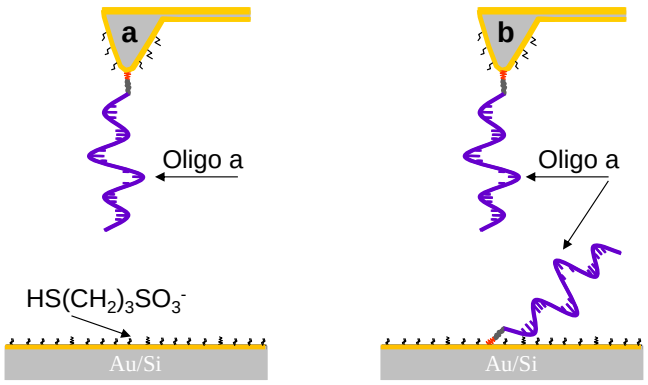

Figure 4.17: Background measurements. (a) oligo a on the tip interacts with the gold surface modified with $HS(CH_2)_3SO_3^-$ and (b) oligo a on the tip interacts with the other oligo a on the substrate. Only few specific adhesions were obtained in both cases.

4.8. Data Analysis

4.8.1. General Aspects of Rupture Force

Four typical types of F-D curves were usually observed in one set of measurement (Fig. 4.14), i.e. no any adhesion between tip and surface (Fig. 4.14a), specific rupture event which was attributed to the rupture of oligo a from oligo b (Fig. 4.14b), specific rupture event together with nonspecific adhesion event (Fig. 4.14c) and multiple rupture events (Fig. 4.14d). The F-D curves shown in Fig. 4.14b or Fig. 4.14c were selected for further analysis. Selection of the F-D curves similar to the one shown in the figure 4.14c which containing the nonspecific adhesion event, should not be very large compared to the rupture force of the specific adhesion events. I selected the F-D curves which contained adhesion force smaller than 100 pN. At this adhesion force, the rupture distances of the specific events did not significantly vary compared to their theoretical value. The rupture force *F* and rupture distance *L* were collected from each individual F-D curve and were plotted in a histogram. The rupture length of ~21 nm or the length of the molecule normally equals to the distance between the tip and the Au-surface. This length was theoretically calculated by multiplying the number of base pairs by the length of a single base pair (3.4 Å). The thiol linker (thiol-$(CH_2)_6$) at the end of each oligo was approximately 1 nm.

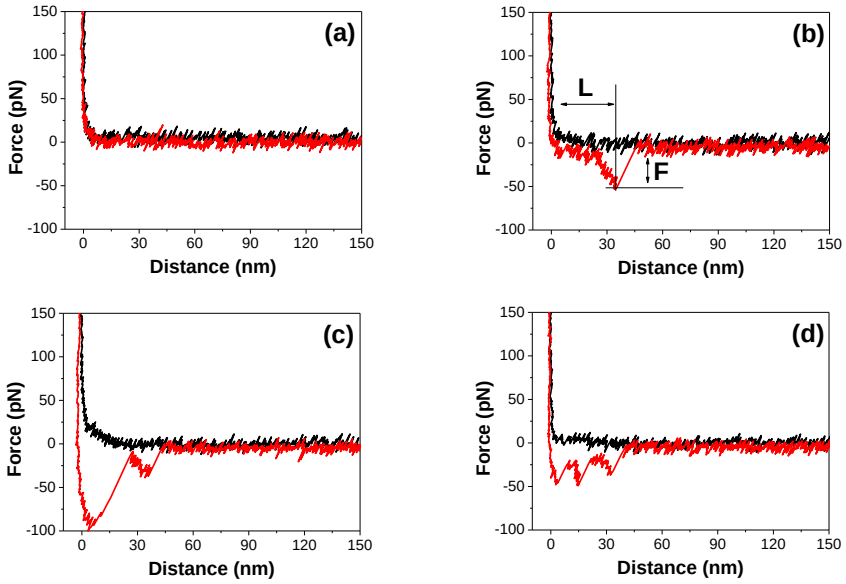

Figure 4.14: Typical F/D curves in AFS measurement. Specific event (a), specific without adhesion (b), specific with large adhesion (c) and multiple ruptures (d) due to oligo hybridization or AMP-aptamer binding. Black and red curves show the approach and retraction traces of AFM cantilever towards and away from the substrate surface, respectively.

4.8.2. Removal of Drag Force

In the study of ligand-receptor interactions by AFS, the pull-off velocity in the regime from few nm/s to few μm/s is usually selected to obtain thermal kinetics information of the complexes at around equilibrium. Although higher speeds are desirable for more complete investigation but the drag force appears. The drag force is proportional to the velocity of the object. The drag force (F_d) on a moving object due to a fluid is [145]:

$$F_d = \frac{1}{2}\rho \upsilon^2 C_d A \tag{3.9}$$

where ρ is the density of the fluid, υ, the velocity of the moving object, C_d, the drag coefficient and A, the cantilever area.

Janovjak et al. found that the hydrodynamic drag force acting on the AFM cantilever linearly dependence on the pulling speed (Fig. 4.15). The author notices that this force could reach the same order of magnitude as the molecular interaction forces at above 10 μm/s pull-off speeds [146].

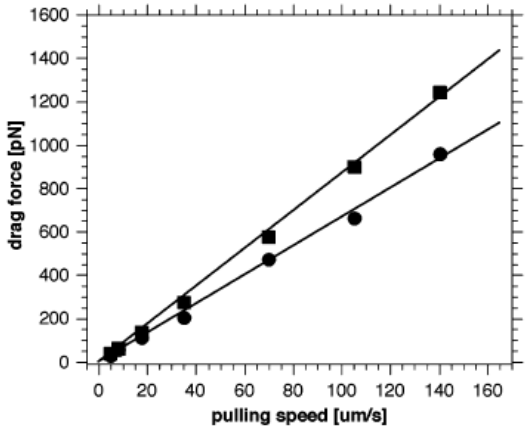

Figure 4.15. Hydrodynamic drag force acting on an AFM cantilever in PBS (squares) and in water (circles) [146].

In my measurements of rupture forces at different loading rates, the drag forces are removed by analysis of the F-D curves (Fig. 4.16). The F_d does not appear at low loading rate (Fig. 4.16a) and it is significant at high loading rate (Fig. 4.16b), $F_d = F_s - F_r$. In our experiments, we even observe the drag forces at low velocities. These forces increase proportionally to the increase of pull-off speeds (Fig. 4.16c). For simplification for removal of F_d during data analysis, the withdraw curves at free position are selected for zero line calibration instead of approach curve. By doing this, the drag force is removed.

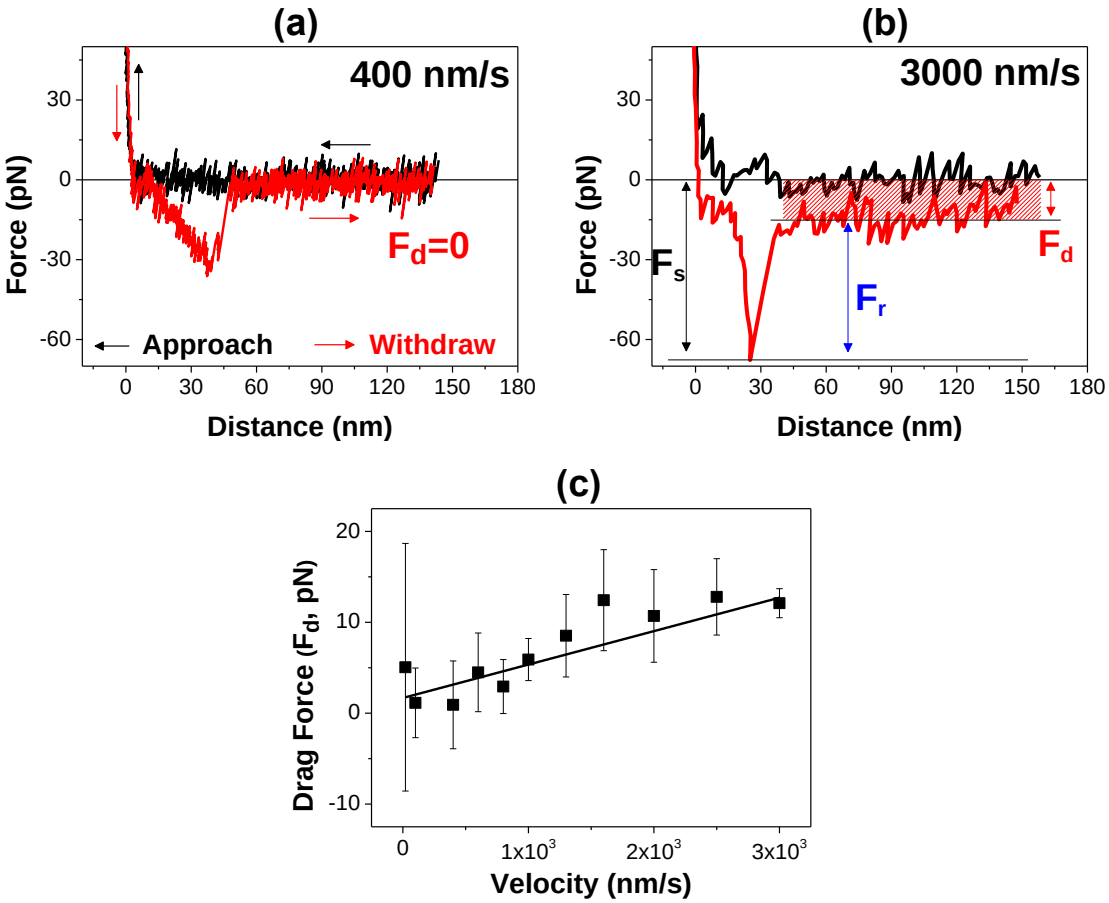

Figure 4.16. Hydrodynamic drag force acting on cantilever. (a) no drag force (F_D) was obtained at low pull-off speed (400 nm/s) and (b) it appeared at high pull-off speed (3000 nm/s). The measured force (F_s) including the drag force (F_d) did not present correctly the rupture force of oligo a from oligo b (F_r). (c) Linear dependences of the drag forces obtain from 2 BP system in the presence (red) and in the absence (black) of AMP.

4.8.3. Pulling Angle

Regardless of the method used to anchor the molecule of interest, it is typically and tacitly assumed that the pulling direction is always axial to the extension of the molecule, so that the force applied to the molecule is identical to the force deflecting the AFM cantilever (Fig. 4.18a). However, the actual pulling geometry may be more complicated than the ideal situation in which the attachment point on the substrate may not coincide with the normal projection of the attachment point on the tip, resulting in the molecule being pulled at an angle (Fig. 4.18b). In such a case, the force measured through the deflection of the AFS cantilever, F_z, is only a component of the force applied to molecule, F. Similarly, the measured extension, L_z, is only the projection of the distance between the two anchor points. The relation between F and F_z or L and L_z and the pulling angle α is $F_{measure} = F_z = F\cos(\alpha)$ or $L_{measure} = L_z = L\cos(\alpha)$ [147]. For

example, for stretching o molecule with the theoretical length of 30 nm, the rupture distance L~30 nm at zero pulling angle while it is only ~15 nm at a pulling angle $\alpha = 60^0$.

The pulling angle affects the force-extension measurements such as rupture force and rupture distance which we collected from the retraction curve to analyze the binding of target molecules to aptamer. The rupture force and rupture distance are in inverse ratio to the pulling angle (Fig. 4.19). Measuring the rupture forces and rupture distances at different pulling angles among 1000 F-D curves provide a variation of the data which distribute in the histograms. The error bars of the Gaussian fits of those distributions depend on the pulling angles.

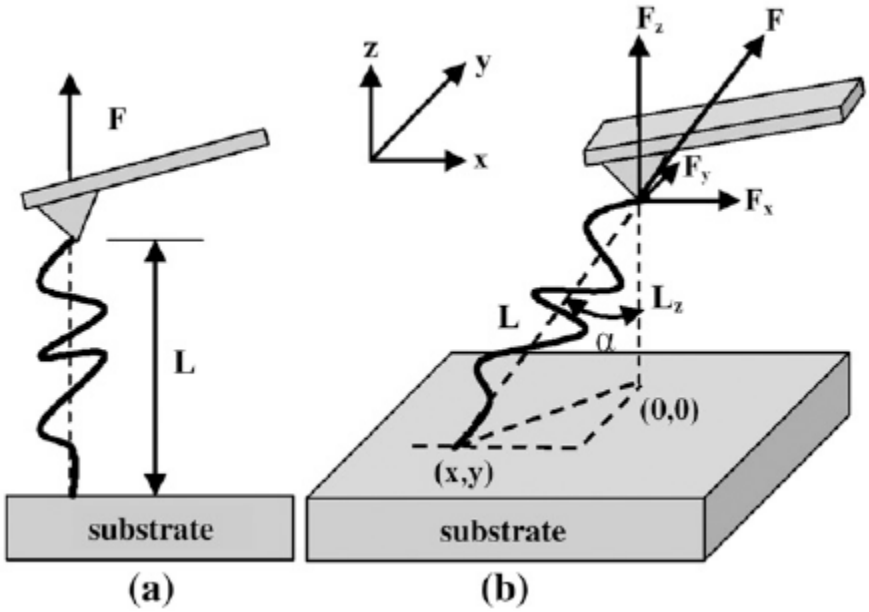

Figure 4.18: Schematic diagram of possible pulling situations in AFS measurement: Ideal situation (a) and general situation (b). The corresponding F/D curves present the difference in the measured distance in those different situations [148].

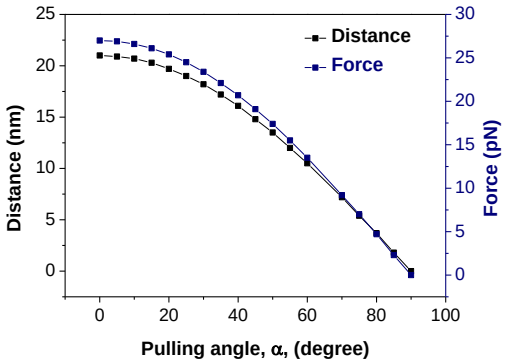

Figure 4.19*:* Theoretical calculation of the dependence of rupture force and rupture distance on pulling angle. Both rupture force (blue) and rupture distance (black) reduce when the pulling angle increases.

In a set of measurement, all rupture distances were collected in a histogram distribution and fitted with Gaussian model. The variation of the most probable rupture distance is presented by the error of the fit. The influence of pulling angle could only be recognized in the measurement of long oligos. For example, a data set from a measurement of 6 BP in the presence of AMP was analyzed at different regime of the rupture distances (Fig. 4.20).

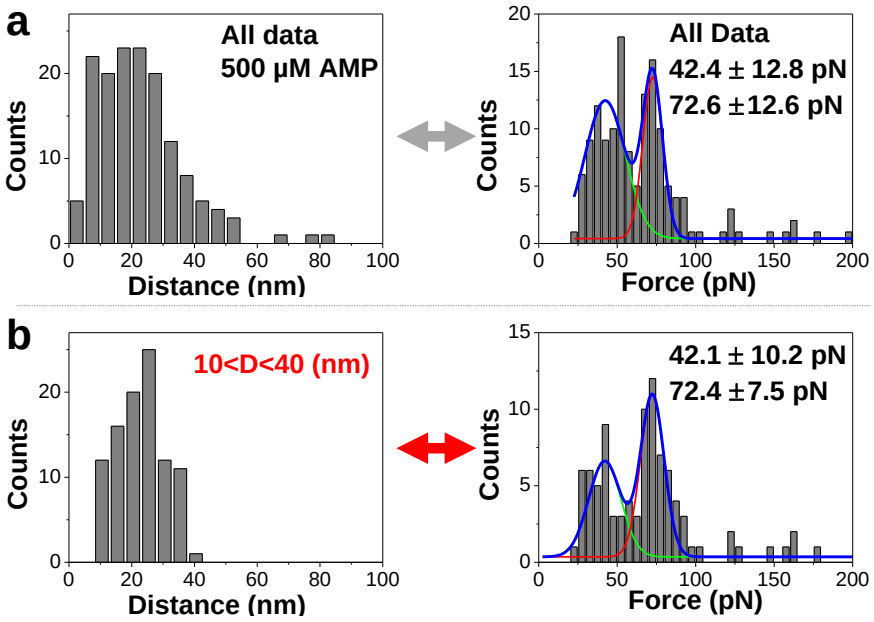

Figure 4.20: Histograms of the rupture distance and rupture force distributions which were recorded from 6- BP system in the presence of 500 µM AMP with 1s retract delay time. (a) All data collected from 1000 F/D curves measurements. The rupture distance ranges from 5 to 85 nm while the rupture force is from 20 to 200 pN with 2 distributions. The selected rupture forces in the range from 10 to 40 nm rupture length (b) reduce the rupture events at the low force regime.

The rupture distance (left) and the rupture force (right) from every F-D curves with specific adhesion peaks at different rupture distances were collected (Fig. 4.20a). The rupture distances varied from 0.3 nm to 85 nm (Fig. 4.20a-left) and their corresponding rupture forces from ~20 to ~200 pN. Two distributions in the rupture force graph present the unbound (low force regime) and bound (high force regime) of AMP to the aptamer. In this data set, about 60% rupture events at the low force regime and the remaining at the higher force regime were observed. It meant that there was only 40% AMP binding aptamer in this data set. The low binding efficiency of AMP to aptamer was obtained even at high AMP concentrations and long contact times. However, when the rupture force was selected in a certain range of rupture length (from 10 to 40 nm), the rupture events at the low force regime was reduced to 40% and rupture events at the high force regime was increased to 60% (Fig. 4.20b). The 40% rupture events at low force regime in this case are higher than that from 2 and 4 BP system (~30%). This may be due to some pockets which were not filled with AMP molecules resulting in smaller

rupture forces. This data suggests the pulling geometry and data analysis directly influence the force histogram obtained by AFS. For longer DNA sequences, this effect will be increased.

4.8.4. Bin Size Selection

The histogram is the probability distribution of rupture forces in a graph. Each column includes a group of data and the interval between columns is called bin size. In the histogram, the height of the column in y-axis is proportional to the class frequencies of the data and the width of the column in x-axis is proportional to the class which the variable has been divided. For example, among 100 data points of rupture forces, there are 30 data points with the magnitude from 25 pN to 30 pN. A column with the width at x-axis is in the region of 25 to 30 pN and the column height in y-axis appears in between 0 to 30 depending on the data. The total area of the histogram is equal to the number of the rupture events. The width and height of the column can be varied by changing the bin size (Fig. 4.21).

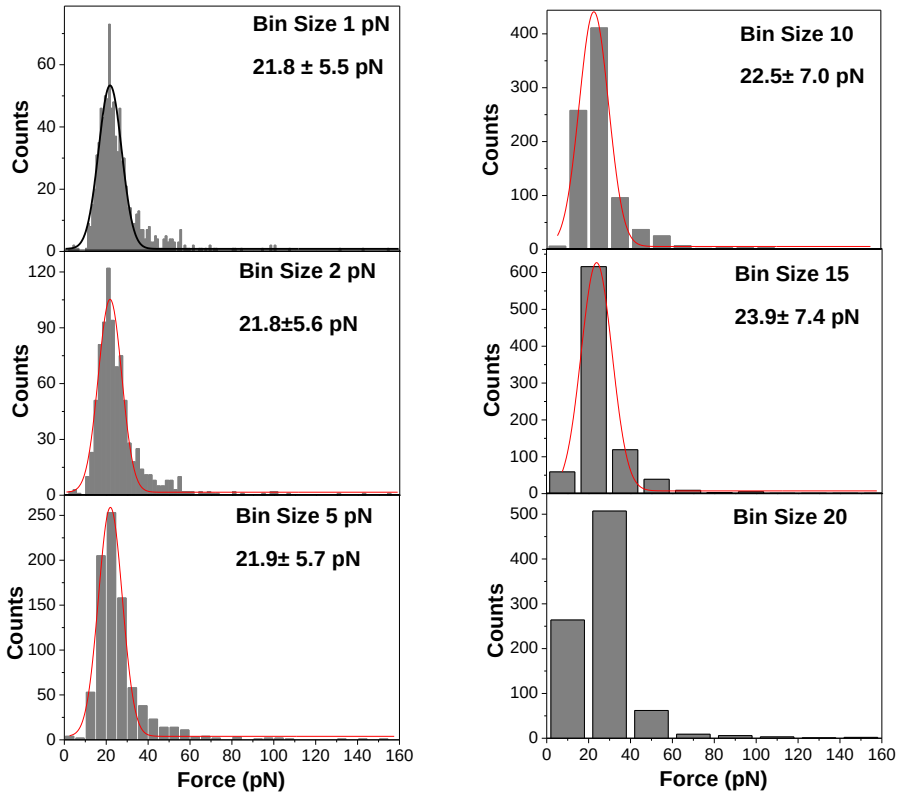

Figure 4.21: Variation of bin size for the data set obtained from 2 BP system in an absence of target molecules. The same average value and standard deviation is for the bin size smaller than 5 (left). The average value and standard deviation slightly increase for the bin size greater than 5 (right). Bin size unit is in pN.

The data is obtained from a defined system in the absence of target molecules. By varying the bin size from 1 pN to 5 pN, the average rupture force is around 21 pN. The average force increases slightly when the bin size is up to 20 pN. For measurement of unbinding force of small or complicated molecular interactions, detailed force distribution may provide additional information. For example, two force distributions which may present two transition steps of the complex can be observed at small bin size but they will be hidden in a broad distribution if a large bin size is used. However, the noise level in AFS measurement is about 5 pN. Therefore, it is meaningless to discuss differences in force when bin size is smaller than 5 pN. If the bin size is too large (~20 pN), the data do not even fit with Gaussian. In conclusion, I always keep the bin size 5 pN for all data analysis in this study.

4.9. Best Analysis Conditions

In this chapter, I presented the steps and artifacts during sample preparation and data analysis which influence directly the rupture force measurements by AFS and summarized all the steps and factors which are crucial for rupture force experiments (Tab. 4.1).

Table 4.1: Best steps and conditions for rupture force analysis

Condition	Purpose	Step
I	Less involved chemicals for oligo immobilization	Using Au-thiol chemistry
II	Oligo Immobilization Passivation of $HS(CH_2)_3SO_3^-$	1h incubation, 4 µM for 2 BP and lower for longer oligos 15h incubation, 1.2 µM
III	Minimize electrostatic force	The same buffer for all investigations (using Buffer T)
IV	Removal of unbound molecules by an additional washing with target molecules	1. Carefully rinse with buffer before installing in AFM 2. Rinse with 1 ml of 100 µM target molecules prior to the first measurement
V	Tip/surface contact time	0s for 2 and 4 BP, 1.5s for 6 and 8 BP, and 2s for 16 BP
VI	Constant pull-off velocity	400 nm/s
VII	Removal of drag force	Retraction curve as zero line calibration
VIII	Selection of F-D curves for analysis	Exclusion of uncommon F-D curves with unspecific adhesion force higher than 100 pN and multiple ruptures
IX	Constant Bin Size	Bin size 5 pN for all analysis

5. Rupture Force of Split Aptamer

I followed the optimum steps of sample preparation and analysis as mentioned in table 4.1, chapter 4 for the measurement of rupture force of adenosine monophosphate (AMP)-split aptamer complex. The standard aptamer here contained two pockets. In this chapter, I am going to present and discuss the results of rupture forces of this system.

5.1. Analysis of Rupture Force

This aptamer was split into two parts, 4 μM concentration, and each part was immobilized on the tip or the substrate, 1h immobilization time and 15h incubation in 1.2 μM $HS(CH_2)_3SO_3Na$. The samples were rinsed with 100 μM AMP prior to measurements of F-D curves at 400 nm/s pull-off speed and zero second tip/substrate contact time. The retraction curves at free positions were selected as zero line for calibration of the F-D curves. Typical F-D curves from AFS measurements in the presence (red) and in the absence (black) of AMP are presented in the figure 5.1. The rupture forces (F) and the rupture distances (L) from those F-D curves were collected to form rupture force histogram distributions for further analysis.

The probability distribution of the forces (F) was plotted in the histograms (Fig. 5.2). In pure buffer solution without AMP, the most probable rupture force F = 27.3 ± 5.4 pN was determined from a fit of the main peak in the histogram by a Gaussian distribution (Fig. 5.2-top). The error bar represents the standard deviation (1σ) obtained from the Gaussian fit. This most probable rupture force is associated with 30 hydrogen bonds formed by 50% G-C (6 bp) and 50% A-T (6 bp) in the hybridized system and it is comparable with the measured rupture force ~30 pN of

26 H-bonds formed by 60% GC (6 bp) and 40% A-T (4 bp) at 400 nm/s in PBS by Strunz et al. under comparable conditions [31, 111]. Even though their oligo has 4 H-bonds less than my split aptamer system, their measured force is few pN higher than mine and this tiny difference may be due to the fact that the measurements were carried out in different buffers or the error in cantilever calibration.

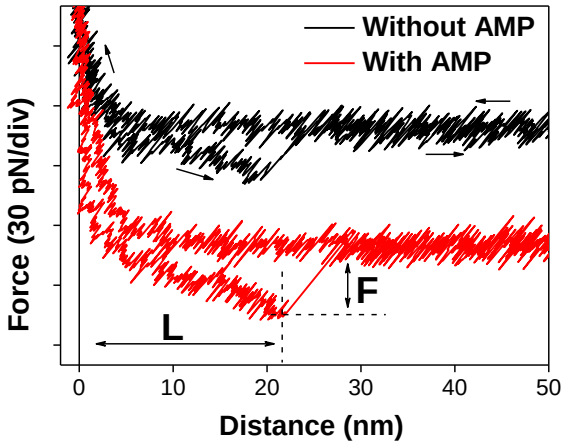

Figure 5.1: Typical force distance (F-D) curves measured in buffer T at pull-off speed 400 nm/s. The individual force distance curves resulted in a rupture force of ~39 pN in buffer containing 100 µM AMP (red) and ~27 pN in pure buffer (black). The measured mean rupture distance (L) of 17.4 ± 5.2 nm is in agreement with the calculated contour length of the designed oligos (21 nm).

The special oligo sequences in my study consisted of two BP, 6 bases, at the center which cannot form the Watson-Crick pairs. Each binding pocket consisted of four G-bases which distributed equally at the center of both oligo a and oligo b. In principle, those parts do not form hybridization, resulting in a smaller rupture force being observed.

After measurement in the absence of a target molecule, AMP solution was added to the cell to replace the pure buffer solution. Since the dissociation constant of AMP-split aptamer is 6 ± 3 µM [29], I choose a high concentration (100 µM) to achieve a high possibility of AMP entering the BP. By analyzing 1000 F-D curves measured in the presence of 100 µM AMP, I found an increase in the most probable rupture force to 38.8 ± 5.2 pN (Fig. 5.2-middle). After that the AMP molecules in the cell were rinsed away with buffer T and additional measurements were recorded. Under pure buffer condition, the force distribution shifted close to the original value as measured before adding AMP (Fig. 5.2-bottom).

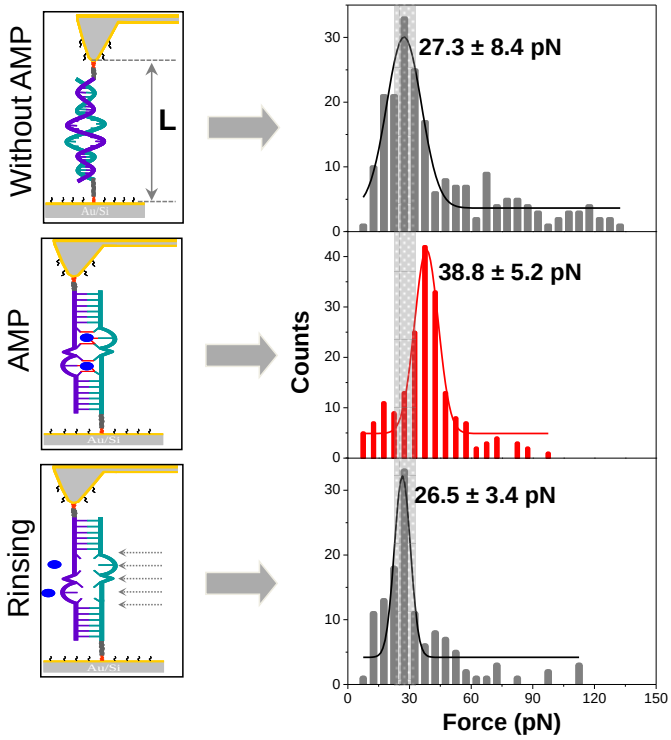

Figure 5.2: Histograms of the rupture force distributions which were recorded at speeds of 400 nm/s. Typically, 1/4 of the recorded 1000 F-D curves exhibited a rupture event. (top) In the absence of AMP, (middle) at 100 µM AMP and (bottom) after rinsing the AMP away with the corresponding histograms. The length of the molecule (L) is the distance between the tip and the sample. The histograms were fitted by Gaussian distributions, which define the rupture force values and the associated errors, i.e. one sigma.

From this set of measurement, I conclude that the most probable rupture force shift is due to the presence and absence of AMP molecules. In the presence of AMP, these molecules enter the BP and 16 additional H-bonds are formed between the two oligos. As a result, the rupture force in the presence of AMP is about 11 pN greater than that in the absence one.

5.2. Control Experiment

The measurement after rinsing the AMP molecules away can be considered as a control experiment. However, the unbinding force of AMP-split aptamer is quite small; therefore, two additional control experiments were carried out using modified sequences (Tab. 5.1). Split aptamer sequences (a and b) formed two BP (underline bases) at the center can bind AMP molecules. Oligos c and d are mutated at the center (bold and underline bases) so they cannot form the AMP binding pocket at the center. Oligos a and oligo c are immobilized on the AFM tip while b and d are fixed on Au-substrates.

Table 5. 1. Mutated BP in the split aptamer sequences

Oligo	HS-A^{20}-Sequences (5'→ 3')	Remark
a	CGTAGA-**TT**A**TT**A-AGGTCA	mutated G bases by T bases
b	TGACCT-**CC**A**CC**A-TCTACG	mutated G bases by C bases

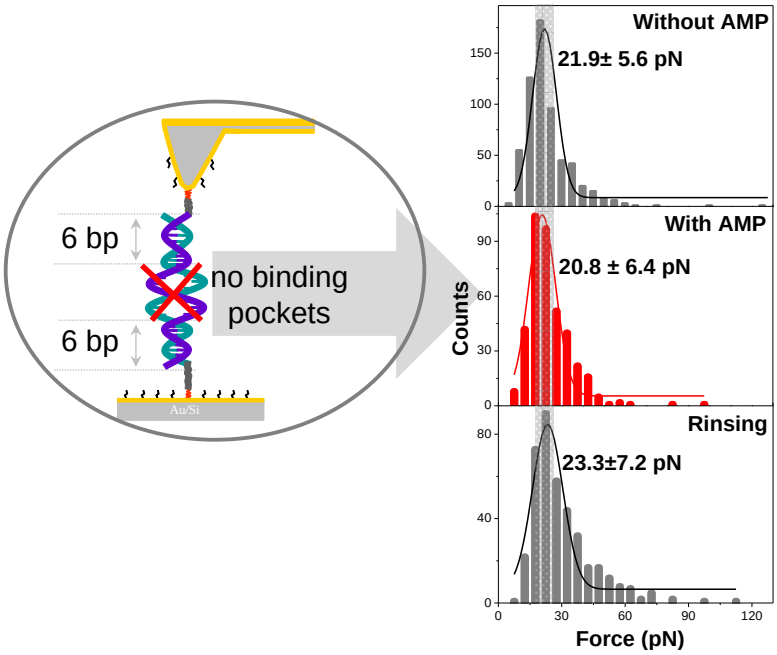

Figure 5.3. Histograms of rupture forces obtained from the mutation pockets. Red cross presents the substitution of G bases at the pocket areas. There is no significant change in rupture forces in the presence and in the absence of AMP. One cantilever was used for each comparative study.

As the control experiment, mutated binding pockets were designed in which the G bases of the BP were replaced at different positions (Tab 5.1). Changing of G bases by T or C units, the BP were destroyed and the specific binding sites which can bind AMP are removed. As a result, the AMP molecule cannot enter between the two oligos. Therefore the rupture force distributions with AMP should be almost the same in the presence or in the absence of AMP, which is what I found in my experiments (Fig. 5.3).

5.3. Analysis of Rupture Distance

The theoretical rupture distance corresponds to a length of about 21 nm: it is a sum of 1-hexanthiol, spacer A^{20} and oligo's length, in which the distance from base to base is 0.34 nm. In the ideal situation, the measured rupture distance reaches the theoretical length of the system (Fig. 5.4a). Under an applied force, the linker between the tip and the surface is first pulled upward until it reaches its contour length. The cantilever still moves up from the

surface which leads to the extension of the tip/surface linker. The spacers A^{20} will be stretched first because they are the softest parts in the system. Thus, the rupture lengths longer than 21 nm may consist of stretching of the spacer A^{20} (Fig. 5.3b). In the ideal case, the oligo lies perfectly under the tip end and the pulling angle (α) is zero. However, when the tip approaches the surface, there will be a high chance of picking up molecules which lay in a certain angle (α) with the tip. The measured rupture length in those cases is $L_z = L\cos(\alpha)$, L_z is shorter than L if α is not zero (Fig. 5.3c). The other possibility is that the oligo on the tip is not immobilized exactly at the tip end but on the tip-side. Under influences of pulling angle and site immobilization of the oligo on the tip, the measured distance will be shorter than the theoretical value.

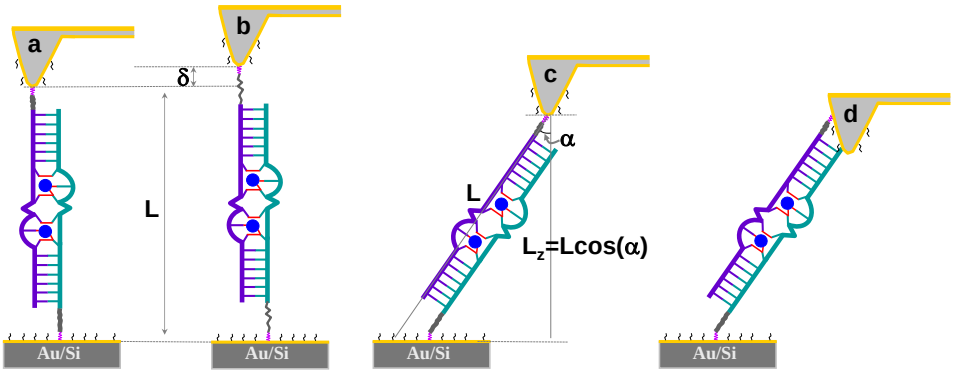

Figure 5.4. Sketch of different scenarios where the tip pulls the molecule from the surface. The rupture distance can vary depending on the conditions, i.e. (a) ideal rupture distance (~21 nm), (b) longer rupture distance due to stretching of spacers A^{20} and (c) short rupture distance under the effect of a pulling angle.

In my experiment, the rupture length often varies from few nm to about 60 nm (Fig. 5.5). This long rupture distance caused due to the formation of a thiol-thiol bond between two oligos in buffer solution. This long oligo absorbs on the surface and the tip can pull it up and stretch it. All the rupture distances are collected in a histogram and fitted with Gaussian fit from which the measured value and its error are determined. In the absence of AMP molecules, the average length is of 17.4 ± 6.2 nm (Fig. 6.5a-top) and increases to 20.6 ± 3.9 nm in presence of AMP (Fig. 5.5a-middle). This increase of ~3 nm can be explained with stretching of the involved oligonucleotides at the higher rupture force values [149].

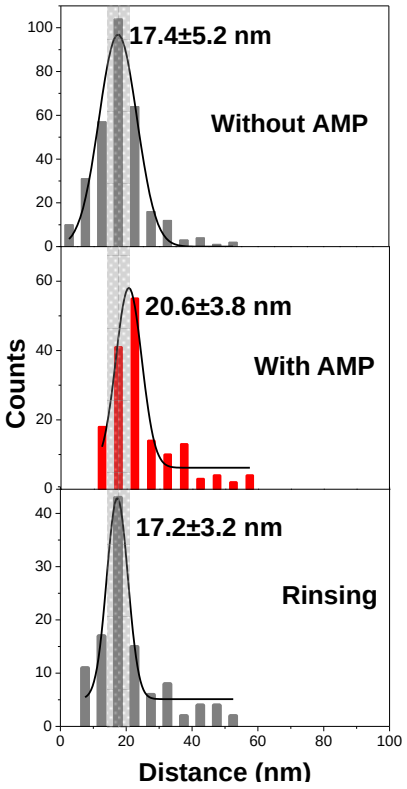

Figure 5.5. Probability distributions of the rupture distances from 2 BP system in the absence of AMP (top), in presence of AMP (middle), and after the AMP molecules were washed away by buffer (bottom). These measurements correspond to the measurement of rupture forces that was provided in figure 5.1. One cantilever was used for this comparative study.

5.4. Cocaine and Tetracycline Binding Aptamers

In order to test if the split aptamer concept can be used for other aptamers as well, I used cocaine-aptamer and tetracycline-aptamer and performed similar experiments. To date, the number of H-bonds between cocaine or tetracycline to their aptamers were not quantified clearly even though they have been broadly used as a target for different purposes such as biosensor [150] or colorimetric tests [151, 152]. Therefore, it could be interesting to understand the different behaviors of those molecules to their aptamers.

The cocaine-aptamer complex is an interesting system used in biosensors or gold nanoparticles conjugate studies [152, 153]. In order to better understand the interaction between cocaine and the aptamer in terms of binding force, the rupture force of the cocaine containing aptamers was measured by AFS. Since the well characterized structure of AMP-aptamer as well as the rupture force quantity have been determined before, an estimation of the cocaine-aptamer binding in terms of the number of involved H-bonds should be possible from AFS measurements on cocaine-aptamer-systems.

Table 5. 2. Cocaine-, Tetracycline-Split aptamer sequences for AFS measurements

Oligo	HS-A^{20}-Sequences (5'→ 3')	Remark
Cocaine-aptamer	CCCTCTGGGTGAAGTAACTTCCAT-AATAGGAACAGAGGG	Full sequence
a	AATAGGAACAGAGGG	Cocaine-Split aptamer
b	CCCTCTGGGTGAAGTAACTTCCAT	
Tetracycline-aptamer	GAGCCUAAAACAUACCAGAGA-UCUGGAGAGGUGAAGAAUACGACCACCUAGGCUC	Full sequence
c	GAGCCUAAAACAUACCAGAGA	Tetracycline-Split aptamer
d	UCUGGAGAGGUGAAGAAUACGACCACCUAGGCUC	

The cocaine-aptamer and tetracycline-aptamer sequences were also split into two parts at the red dashed positions for AFS measuements (Tab. 5.2). The splitting position is to make sure that the binding pockets and Watson-Crick pairs can be formed then the tip approaches the surface. The thiol and A^{20} were added at 5'-ends for immobilizing on gold. Then, one part (oligo a) was fixed on the tip and the other part (oligo b) was on the Au-surface following the standard protocol for AMP-split aptamer.

The measurements were then carried out in buffer T only to find out if the tetracycline binds the tetracycline-aptamer. Investigation of different buffer in order to archive the proper buffers for those systems should be the future studies. The binding constant of the cocaine-aptamer is 100 ± 9 μM [154] while it is only 0.8 nM for the tetracycline-aptamer [51]. The concentrations of cocaine (1.0 mM) and tetracycline (1.0 μM) were selected very high compared to their dissociation constants in order to obtain a maximum number of binding events. Rupture forces in the absence (black columns) and in the presence of cocaine or tetracycline (red columns) were collected and analyzed (Fig. 5.7). The rupture force increased by about 21 pN when cocaine is added in the buffer and about 25 pN when tetracycline is added in the buffer. The increase in rupture force in the presence of cocaine and tetracycline means that the rupture forces of cocaine and tetracycline from their corresponding split aptamer can be measured. The increases in the rupture force in the presence of cocaine or tetracycline allowed me to conclude that the split aptamer concept also works for other systems.

However, there were still significant ruptures events at low force regimes which indicate that the cocaine or tetracycline did not bind to their split aptamer in every measurement. This may be due to the influences of the buffer solutions on these molecular bindings. For example, the tetracycline-aptamer binding depends strongly on the concentration of Mg^{2+} in the buffer [51].

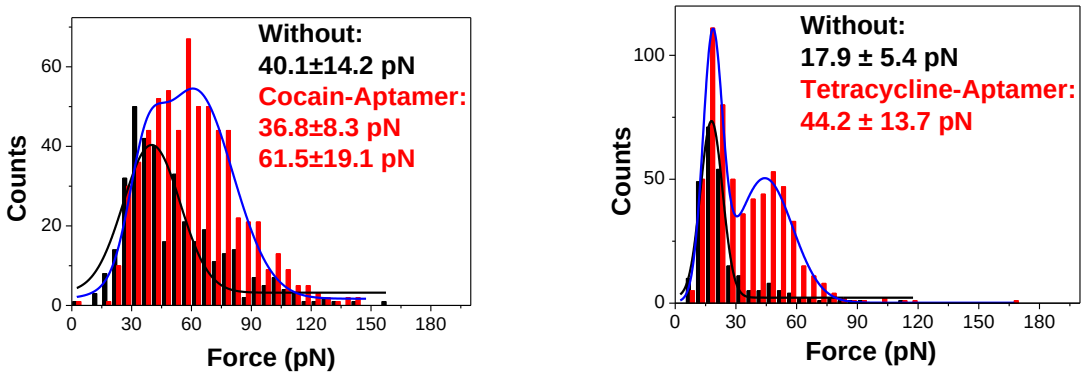

Figure 5.7. Histograms of the rupture force distributions which were recorded from cocaine-split aptamer (left) and tetracycline-split aptamer (right) at a speed of 400 nm/s. The force distribution at lower regime (black column) is due the rupture of oligo hybridization and the distribution at both high and low force is the combination of oligo hybridization and cocaine or tetracycline binding split aptamers (red).

Even though deeper investigation for those systems is still required, two conclusions can be made. First, the split aptamer principle can be applied to detect other small molecules. Second, a quantitative unknown number of H-bonds in the cocaine- or tetracycline-split aptamer can be determined from the standard AMP-split aptamer system. For example, the force of a single H-bond can be estimated from measuring the probable rupture force and the well-known number of H-bonds between AMP and split aptamer. The bindings of cocaine or tetracycline to their aptamers depend on not only H-bonds but also many factors such as buffer and cations in the buffer. However, considering only the aspect of H-bonds, the number of H-bonds in those unknown binding structure can be roughly estimated to be about 30 H-bonds for cocaine- and 35 H-bonds for tetracycline-split aptamer complex (Tab. 5.3).

Table 5. 3. Mutated BP in the split aptamer sequences

Target	H-bonds	F_b (pN)	f_b/H-bond (pN)
AMP	16	11	0.7
Cocaine	**30**	21	
Tetracycline	**35**	25	

5.5. Determination of Dissociation Constant by Rupture Force Analysis

5.5.1. Principle of Determination of Dissociation Constant

In order to determine the dissociation constant K_D of the AMP-split aptamer, sets of F-D curves are recorded at a certain range of AMP concentration which is very far from the

equilibrium. The distribution of rupture force due to oligo hybridization (OH) only and AMP-split aptamer complex (AA) changes when the AMP concentration changes (Fig. 5.10). In the absence of AMP (first graph), the rupture forces represent 100% OH and zero % AA. At low (in nM range) concentration of AMP (+AMP, right-top graph), a second peak appears at higher force (red curve) while the OH reduces (black curve) which is attributed to few ruptures of the oligo with AMP staying in the pockets.

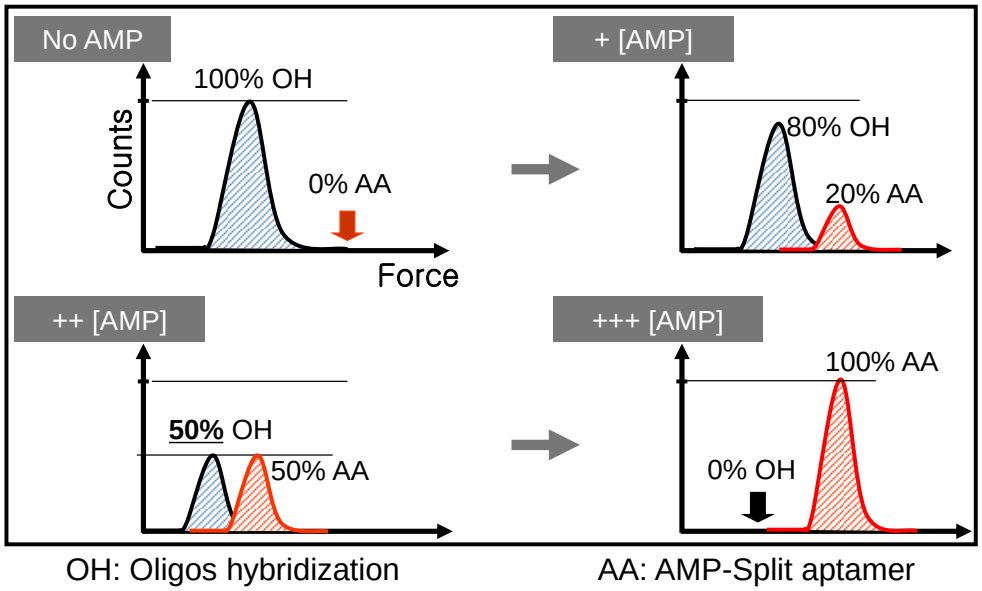

Figure 5.10. Variation of rupture force distribution depending on AMP concentration. Distribution of rupture force of AMP-split aptamer complex increases when AMP concentration increases while it is reversed for oligos hybridization. Number of '+' indicates the concentration of AMP.

The rupture events associated to the second peak increases when the AMP concentration increases. Each histogram of the rupture forces is analyzed by fitting simultaneously two Gaussian distributions to the peaks corresponding to "only oligo hybridization" and to "AMP-split aptamer complex", respectively. With increasing concentration of AMP, the peak corresponding to "AMP-split aptamer complex" becomes more pronounced, i.e. more rupture events at higher forces are present. Simultaneously, the peak corresponding to "only oligo hybridization" is composed by fewer rupture events. The percentages of oligos hybridization (%OH) and AMP-split aptamer complex (%AA) are calculated by considering the total counts under the corresponding peaks. The concentration where equal rupture events (50%) of OH and AA can be achieved corresponds to the dissociation constant of the system (++AMP, left-bottom graph). At high concentration of AMP (+++AMP, right-bottom graph) which is far from the equilibrium, all rupture forces distribute at high force region. At this concentration, all rupture events are from AMP-split aptamer complex.

5.5.2. Dissociation Constant of AMP-Split Aptamer

The dissociation constant of AMP binding split aptamer is determined by carrying-out a series of experiments with AMP concentrations ranging from zero to 100 µM. The data set were recorded in buffer T and then in buffer T containing AMP with different concentrations (Fig. 5.11). In this investigation, fifteen different concentrations were measured and 1000 F-D curves were measured at each concentration. Unfortunately, the tip was not functioning after 3000 or 4000 F-D curve measurements. After these amounts of measurement, the retraction curves which contain specific adhesion peaks decreased significantly. Thus, different cantilevers had to be used in order to complete these sets of data. A difficulty in using different cantilevers is the error in determination of the cantilever's spring constant by thermal tune. The rupture forces shifts causing by the use of different cantilever can be up to ~4 pN (Fig. 5.11). For example, for the measurement of the same oligos hybridization with two different cantilevers, two different most probable rupture forces can be achieved, i.e. ~27 pN and ~ 31 pN. Such shifts cannot be tolerated in measurements of single small molecular interactions since the increase in the most probable rupture force can be either caused by different cantilever spring constants or by the rupture of the target-split aptamer complex.

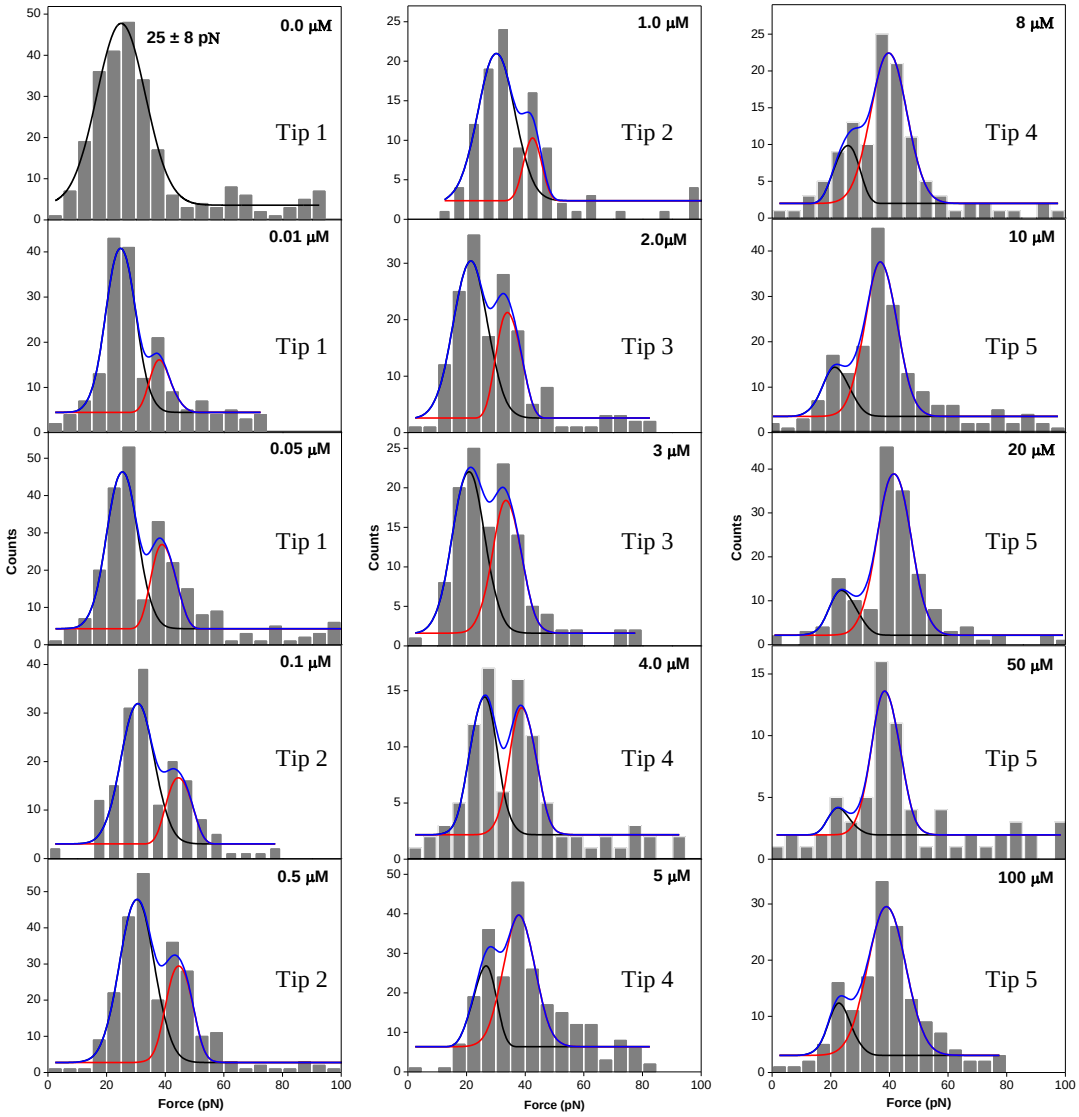

Figure 5.11. Quantitative analysis of the oligo hybridization and AMP binding split aptamer at various AMP concentrations via two Gaussian fits. The series of rupture force measurements were obtained by using five different cantilevers.

For the series of measurements, here, five different cantilevers were used. Thus, an analysis of the histograms was chosen which is independent on the accuracy of spring constant of the cantilever (Tab. 5.4). The first histogram shows the ruptures of only oligo hybridization (25 ± 8 pN) (black curve). When a low concentration of AMP is added to the system, the second peak appears at higher force (red curve) which is attributed to the ruptures of AMP-split aptamer. The rupture events associated to the second peak increased when the AMP concentration increased. A reverse trend is observed for the first peak of oligo hybridization.

Table 5.4. Data from 2 Gaussian fits

Con. (μM)	Cantilever		A_1 (counts)	A_2 (counts)	$A_1 + A_2$ (counts)	% OH	% AA
	No.	k (pN/nm)					
0.0	1	5.6	225	0	255	100	0
0.01	,,	5.6	211	88	299	71	29
0.05	,,	5.6	148	76	224	66	34
0.1	2	5.9	149	82	231	65	35
0.5	,,	5.9	178	103	281	63	37
1.0	,,	5.9	96	50	146	66	34
2.0	3	5.6	122	79	201	61	39
3.0	,,	5.6	80	65	145	55	45
4.0	4	5.8	44	43	99	50	50
5.0	,,	5.8	148	198	346	43	57
8.0	,,	5.8	50	97	147	34	66
10.0	5	5.6	67	135	202	33	67
20.0	,,	5.6	30	118	148	20	80
50.0	,,	5.6	18	41	59	25	75
100.0	,,	5.6	35	116	151	23	77

A_1, A_2: number of counts under the first and second peaks, respectively

OH: Oligo hybridization, AA: AMP-Split aptamer

The rupture events under each peak at each individual concentration are listed in the table 5.4. The percentages of oligos hybridization and AMP binding split aptamer are calculated by considering the counts A_1 and A_2. With an assumption that total counts is $A_1 + A_2 = 100\%$, the % of OH and AA can be calculated. For example, at 4 μM AMP, number of rupture events due to OH is 44 and that of AA is 43 (Fig. 5.6), and the total counts is $A_1 + A_2 = 87$. The amount of OH at 4 μM is 44 x 100/87 ~ 50% and AA is 43 x 100/87 ~ 50% or 100% - 50% (OH) = 50%. By doing the same calculation, the percentages of OH and AA at different concentrations are obtained (Tab. 5.4). However, at highest concentration, 100 μM, not all the rupture events shifted to the higher force region. Around 29% of rupture events still stay at the OH region. Those events may be due to unspecific adhesion between tip and surface forming the background of the measurements. Both fractions were determined for each histogram recorded at different AMP concentrations, and these values are plotted in figure 5.12. This figure presents the variation of percentages of OH and AA at different concentrations. For example at 4 μM AMP, the %OH is 50 and %AA is also 50 which are plotted in y-axis as %binding and x-axis is 4 μM as concentration. The sets of "AMP binding" and "only oligo hybridization" could be fitted by an exponential dependence ($A = A_1 e^{-x/t} + A_0$) where A is % binding at concentration x, A_0: % binding at zero concentration, A_1 and t: variati on parameters (t: decay constant, A1: amplitude of % binding). The reduction or increase of t he frequency of the rupture events in the absence and in the presence of AMP, respectively, could be achieved by the fits.

At a concentration of 3.7 ± 2.5 μM we observed the crossover of both oligo hybridization (50%) and AMP binding (50%) events. The error is determined by averaging the errors of two closest data points. Therefore, the value (3.7 ± 2.5 μM) was attributed to the dissociation constant of the AMP binding split aptamer. This value, which was obtained on a single molecular level is in agreement with a measurement performed by ultrafiltration (6 ± 3 μM) [29].

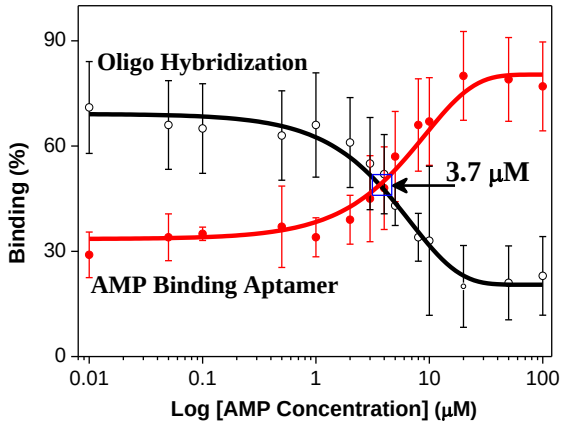

Figure 5.12. Plot of the fraction of oligo hybridization and AMP-split aptamer complex as functions of AMP concentration. The data is fitted with the first exponential decay and K_D is determined as the cross over point of two fitting curves.

5.6. Dependence of Rupture Forces on Loading Rates

In earlier studies [31, 155], by measuring the rupture force of a short dsDNA molecules at different velocities, the authors found that the rupture force increases logarithmically with the pull-off velocity. The increase in rupture force was attributed to cooperative thermal dissociation of short oligonuceotides. With an oligo 10 bp, Strunz et al. reported that the thermal off-rate value is about $10^{-1.5}$ s^{-1} [111]. The oligos in my study consist of two BP at the center. In order to understand if the oligos with BP behave similar to the oligos without BP reported by Strunz et al., I performed a set of measurement of rupture oligo a from oligo b at different pull-off speeds. The measurements were carried out in buffer T. The same cantilever was used to measure the rupture without AMP and with AMP. Measurements in pure buffer T were performed first and then the buffer T was replaced by buffer containing 100 μM AMP and measurements were performed again. The pull of speed was varied from 10 nm/s to 2000 nm/s. The most probable rupture force and the error bar from Gaussian fit at each speed were collected (Fig. 5.13 and Appendix A). At all loading rates, the rupture force of 'AMP binding' is higher than that of 'only oligo hybridization', as before.

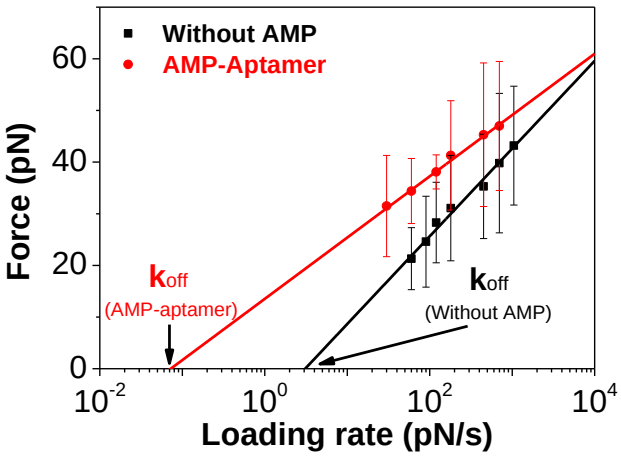

Figure 5.13. Dependence of rupture forces on loading rates for only oligo hybridization (black) and AMP-Split Aptamer complex (red). Thermal dissociation rates (k_{off}) are at the zero forces.

The most probable rupture forces of both 'AMP binding' and 'oligo hybridization' scale linearly with the logarithm of the force loading rates. This indicates that within the range of the employed pull-off velocity, a single energy barrier along the mechanical separation of oligo a from oligo b exists, similar to the behavior of oligos without any binding pocket [31, 111, 156]. It also means that the oligo with BP at the center in the presence and in the absence of AMP showed a cooperative thermal dissociation behavior similar to that of the short oligos.

However, having a close look at thermal off-rate values of 'only oligo hybridization' (~3.6 s^{-1}) and of 'AMP binding' (10^{-1} s^{-1}) (Fig. 5.13), those values are greater than that of oligo without binding pocket measured by Strunz et al ($10^{-1.5}$ s^{-1}) [111]. The greater thermal off-rate means that the aptamers with BP at the center is less stable than aptamers without binding pocket. When AMP enter the pockets, k_{off} is reduced closely to the one obtained by Strunz et al. This means that the AMP stabilizes the BP. However, the AMP-split aptamer complex is not as stable as the oligo without any BP studied by Strunz et al. In order to further understand the rupture mechanism of the split aptamer, I investigated the rupture forces at wide range of pull-off velocity, from 20 to 3000 nm/s. The most probable rupture forces are collected at each individual pull-off velocity (υ) and plotted against the loading rates (Fig. 5.14). In this force range, I did not observe the logarithmical increase of rupture force with the force loading rates. The data separated into two regimes. There is a linear regime (a) at low loading rates from 20 to 1000 nm/s and the second regime (b) at the higher loading rates.

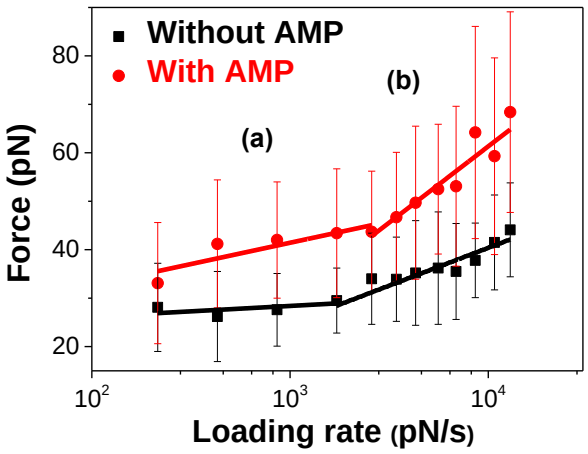

Figure 5.14. Dependence of rupture forces on wide range loading rates. The rupture force obtained from 'oligo hybridization' (black) is smaller than that of 'AMP binding' (red). Two separated force regimes are obtained in both cases. Drag forces were subtracted for all measurements.

In literature, the rupture forces of the oligonucleotides from their complementary strands are reported to increase linearly or logarithmically with an increase of pull-off velocities (from 8 to 1600 nm/s). Two regimes were not reported to my knowledge for ruptures of nucleic acids. For example, Strunz et al [111] measured the rupture force of 10, 20, and 30 bp dsDNA at different loading rate and reported that the rupture force of those oligonucleotides increased linearly with the increase of pull-off velocity. Within the range of pull-off velocity from 16- to 1600 nm/s, the most probable rupture forces increased from 21- to 41 pN for 10 bp, 35- to 50 pN for 20 bp and 43- to 54 pN for 30 bp. Morfill et al [101] or Gaub et al have also obtained the similar results as Strunz et al when they ruptured 20 or 30 bp dsDNA [31].

Regarding to the two distinguished regimes in the measurement of rupture force depending on pull-off velocity of biotin-streptavidin, Lo et al. found two distinguished slopes in the graph of rupture force *vs*. loading rate [70]. The author suggested that an existence of multiple energy barriers can be conducted from the two regimes. Also, De Paris et al. measure the rupture force of biotin-avidin complex at different pull-off velocities and also obtained two regimes in the graph of rupture force-loading rate dependence [157]. The first regime at low pull-off velocities is due to the unbinding of the biotin-avidin complex. The second regime at high force-loading rate is attributed to an intermediate transition in the dissociation process inside the binding pocket. The binding pocket belongs to streptavidin that allows biotin binds specifically to the streptavidin with non-covalent bonds. When the biotin is pulled from the streptavidin, the transition from the pockets of the streptavidin occurred. The transition means that the ribbons were extended during pulling. The author stated that the internal structure transition of the binding pocket occurs at high loading rate.

Looking back to our system, the rupture force of oligo a dissociates from oligo b at different loading rate also shows two regimes, i.e. at high loading rate (a) and low one (b). At the high loading rate regime, the rupture force significantly increases. Our result is totally different from previous studies on rupture of dsDNA which observed only one regime. Thus, the difference must occur at ssDNA parts which build the BP. It is known that the short dsDNAs behave as the stiff rods while ssDNAs fold in a worm like chain model [158, 159]. Therefore, under an additional pull-off force, the ssDNA parts can be extended to longer contour lengths. The extension of the ssDNA requires an additional force which may create the second regime in the rupture force *vs*. loading rate picture. To prove that the second regime in the force-loading rate graph is due to the pocket's transition, a reference experiment without any BP is tested. In these sequences, six bases at the pocket area are removed while 12 bases at two ends are kept (Tab. 5.5).

Table 5.5. The split aptamer without binding pockets

Oligo	HS-A^{20}-Sequences (5'→ 3')	Remark
a	CGTAGA-AGGTCA	without BP
b	TGACCT-TCTACG	

We found that with these sequences, the rupture force increase logarithmically with the increase of loading rate without the existence of the two distinguished regimes (Fig. 5.16 top) that were observed in the presence of BP (Fig. 16 bottom). The intercepts of the fits at zero force can be used to obtain the thermal dissociation constant k_{off} of this system. I found k_{off} to be in the range of 10^{-4} s^{-1} to 10^{-5} s^{-1}. A slight variation of k_{off} values obtained from 'with' and 'without' AMP is in the error range which have been described by De Paris et al that the error for calculations of k_{off} by this method can be varied from three orders of magnitude [157]. The result of the intercepts are in good agreement with the study by Strunz et al [111]. The author presented the k_{off} value was 10^{-2} s^{-1} for 10 bp oligonucleotide and it increased to 10^{-5} s^{-1} for 20 bp oligonucleotide. This means that the k_{off} reduces for longer sequences. In my split aptamer without pockets, the sequence contains 12 bp, so the k_{off} should be in the range between 10 bp and 20 bp of Strunz's result within the error bar. This result means that the BP plays an important role in the second regime of the 'force-loading rate graph, Fig. 5.14' at high loading rate.

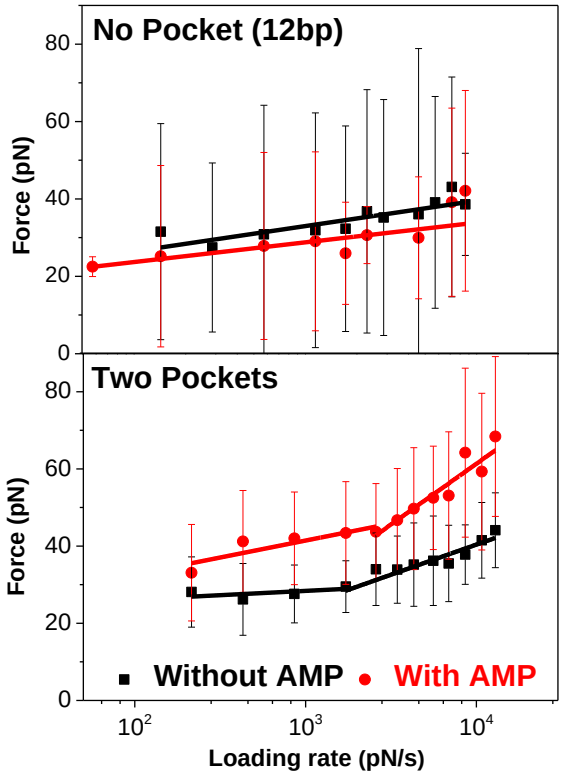

Figure 5.16. Comparison of most probable rupture forces at different loading rates between 'with' and 'without' BP. (top) 12 bp oligos without any binding pocket do not show two kinks as it has been observed in the 2 BP system (bottom) which was already presented in the figure 5.14. In the presence (red) or absence (black) of AMP, the rupture forces from 'without BP' increase logarithmically when the loading rate increases.

In order to further understand the pocket's transition at high loading rate, we analyze the rupture distances at different loading rates in the presence and in the absence of AMP (Fig. 5.17. Theoretical calculations for the lengths are ~17 nm and ~19 nm for no- and two- BP, respectively with a consideration of 0.34 nm per bp. In the system without BP (A), within the error bars we observe no increase in rupture distance. The length spacer A^{20} seems not to depend on the loading rate and the AMP does not interact with the split aptamer which contains no BP. In the two binding pocket system (B), the rupture distance increase logarithmically in the absence of AMP while it is constant in the presence of AMP. The constant rupture distance in the presence of AMP is attributed to the stabilization of the double helix when AMPs bind to the pockets. This difference in rupture distances (δ) can only be distinguishable at high loading rates because the ssDNAs at the pocket areas are only extended at high loading rate. The constant rupture distance in the presence of AMP means that the BP are not significantly stretched even high loading rate.

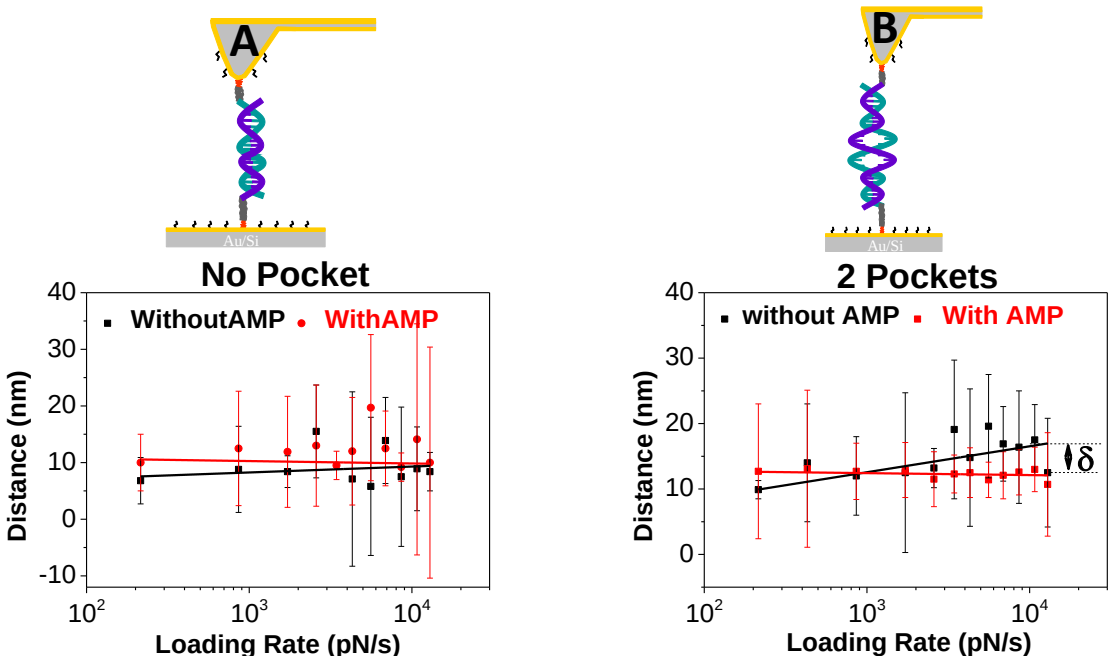

Figure 5.17. Pocket's transition analysis using the variation of rupture distances at different loading rates. (A) rupture distance does not change for the measurement of the sequences without BP while it slightly increases at 2 BP (B).

However, the binding of AMP to the BP of the split aptamer is different compared to the Watson-Crick pairs. We still see the kink in the rupture force-loading rate dependence in the presence of AMP. This observation may be due to numerous reasons. First, the number of H-bonds forming between two oligos at the BP area in the presence of AMP is less than the number of the H-bonds forming between them if the pockets are replaced by the Watson-Crick pairs. Thus, pulling the chain in the presence of AMP, the transition of the BP is still occurring, which leads to the appearance of the kink. Second, the AMP can enter the BP with a requirement of special steric structure. When the oligo is pulled, the Watson-Crick pairs are still stable at a certain distance but the formation of G-quartets may be lost, resulting in an unbinding of the AMP from the BP. After this unbinding, the pocket areas can then be stretched. The complicated transition and unbinding state may result in the kink in the force loading rate dependence. Third, it is also possible that at low pull-off speed, only the first Watson-Crick area at one end of the BP is ruptured and the second Watson-Crick area is then naturally ruptured at room temperature. At high pull-off speed, oligo a is separated very fast from oligo b and both Watson-Crick areas at both ends of the BP are ruptured at the same time, resulting in a high rupture force being measured. In the presence of AMP, the kink still appears which means that the binding of AMP to the pocket is localized and it is easy to be ruptured even under small loading rates.

The transition of the pockets means that two ssDNAs of the pocket are stretched (Fig.

5.18a). Those two ssDNA are much more flexible compared to the Watson-Crick parts which are considered to be the stiff rods. Under a loading force, the ssDNAs behave like two parallel springs being stretched. *The* ssDNAs at the pockets are first extended by a length l_1, and then stretched further by a length l_2. The stretching leads to an increase in the length of the oligos from *L to* $L+l_1+l_2$. The final measured rupture distance is $L+l_1+l_2$. In the presence of AMP, the BP are stabilized and no pocket transition occurs and the final rupture distance is the same as the original length (Fig. 5.18b).

Relating to the analysis of two force regimes at different loading rate, De Paris et al have utilized the Bell-Evans model for fitting and obtained the thermal off rate of the Biotin-streptavidin system [157]. I also used the Bell-Evans model for the two distinguished regimes to obtain information of the thermal kinetics of the AMP-split aptamer complex (Tab. 5.6).

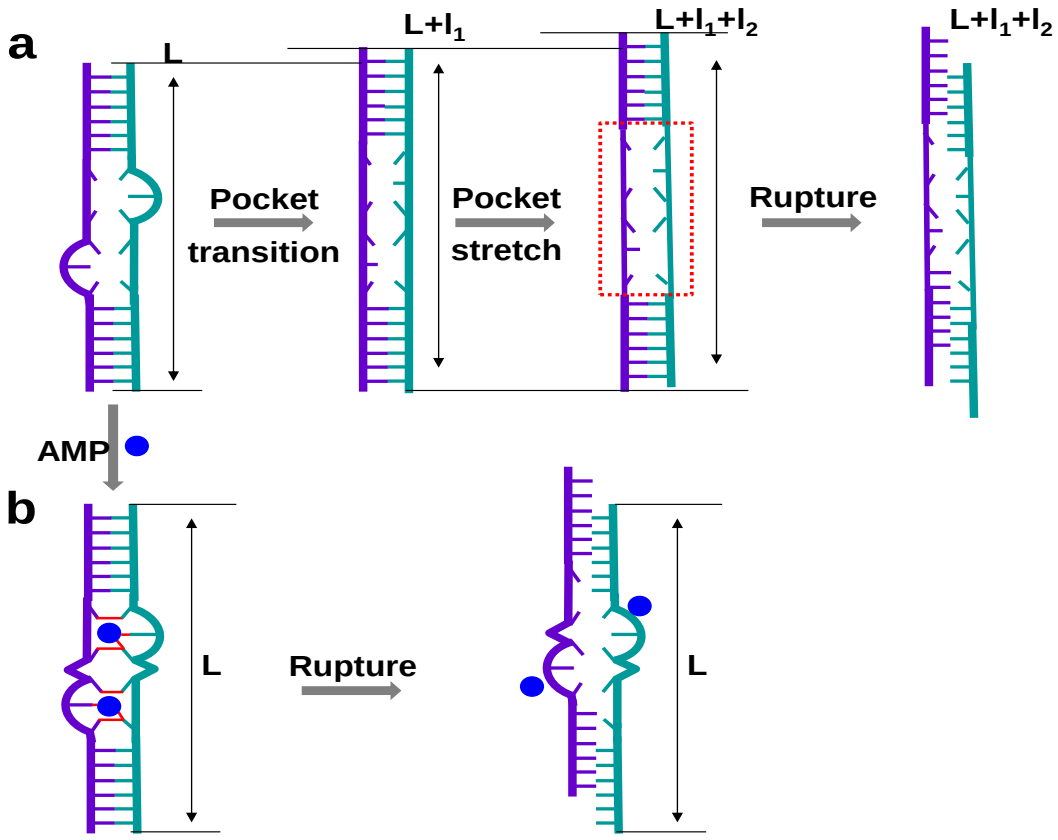

Figure 5.18. Pocket's transition in the absence (a) and in the presence (b) of AMP. After pocket transition, the oligo length is increased from *L* to $L+l_1+l_2$. The length does not change when AMPs enter the BP.

At low loading rates (a), the k_{off} values obtained in the absence of AMP (10^{-3} s^{-1}) are higher than that in the presence of AMP (10^{-5} s^{-1}). This means that in the presence of AMP, the split aptamer is more stable. The potential width follows an opposite trend, i.e. 19 nm in the

absence of AMP and 12 nm in the presence of AMP. Those values are reasonable compared with recent studies [31, 101, 111].

At high loading rates (b), the k_{off} significantly increase in the presence and absence of AMP while the potential width is reduced. These values are now much different compared with previous studies on the rupture of oligos. This indicates that some additional mechanisms occurred at high loading rates which I have discussed above. By studying the rupture force at various loading rate, the dynamics of the AMP binding aptamer and the BP transition could be understood.

Table 5.6: Fitting parameters obtained with the Bell-Evans models

regime	parameters	2P	2P-AMP complex
Flat (a)	k_{off} (s^{-1})	10^{-3}	10^{-5}
	Δx (nm)	19	12
Stiff (b)	k_{off} (s^{-1})	157	541
	Δx (nm)	3.0	1.3

6. Amplification of Rupture Force using a Series of Binding Pockets

The split aptamer concept was proved working on the level of small molecular interaction (chapter 5). However, on the aspect of measurement technique, the required rupture forces of only ~10 pN is at the limit of force resolution of AFS. In this chapter, the extension of the number of binding pockets (BP) in the split aptamer in order to amplify the measured rupture force will be described.

6.1. Four Binding Pockets

6.1.1. Design of Four Binding Pockets for AFS Measurement

The experimental design for measurement of aptamers with multiple BPs that bind multiple targets is in principle similar to the set-up for the standard system as described in the last chapter (Fig. 6.1). In order to form aptamers with multiple BPs, the standard oligos are lengthened from the 3'-end direction of the sequences while the BPare kept symmetrically in between the Watson Crick bases. In this section I present measurements on the split aptamer which is extended to 4 BP (Tab. 6.1 and Fig. 6.1). In the absence of AMP, the required force depends on the number of the Watson-Crick pairs in the sequences. When the oligos are lengthened the required rupture force increases.

Six Watson-Crick pairs are designed in between the pockets so that the BP can be easily formed after oligo hybridization. In the two BPs, two AMP molecules can enter the pockets when AMP

molecules are added to the buffer solution (Fig. 6.1a). When two more BPs are added to the split aptamer, four AMP molecules locate in those pockets and more H-bonds are formed between two oligos in the presence of AMP molecules (Fig. 6.1b).

Table 6.1. Split aptamer sequences with 4 BP

Oligo	**HS-AAAAAAAAAAAAAAAAAAAA(A^{20})-Sequences (5'→ 3')**					**BP**
C	TGACCT- GGAGGA-TCTACG-GGAGGA- TCGATC					4
D	GATCGA-GGAGGA-CGTAGA-GGAGGA-AGGTCA					
Characteristic						
Pocket	Sum Bases	Watson-Crick pairs	Number of A-T (bp)	Number of G-C (bp)	Total Length (nm)	Hybridization Force (pN)
4	30	18	9	9	24.8	33.3

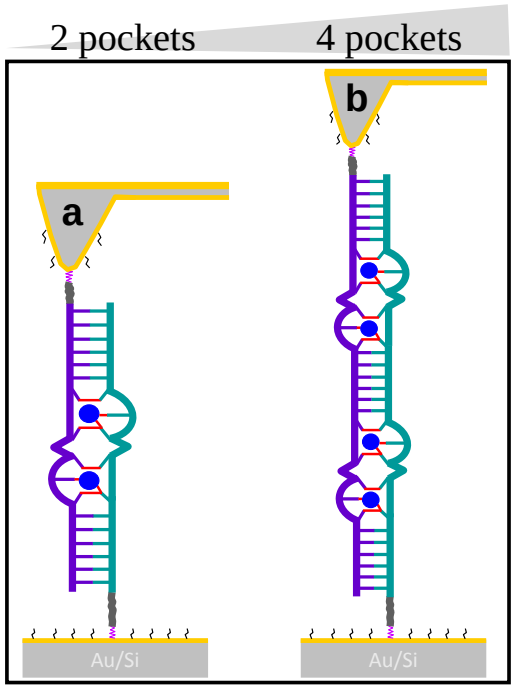

Figure 6.1. Scheme of the split AMP-split aptamer complex when more BP are added. The tip approaches the surface and the oligos hybridize to form 2 BPs (a) and 4 BPs for AMP (b).

6.1.2. Force-Distance Curve of Multiple Binding Pockets Aptamer

The measurements were carried out under the same conditions as in the case of the standard split aptamer, i.e. in buffer T, pull-off speed 400 nm/s and 100 μM AMP. At 100 μM, the about 80% measured rupture forces shifted to higher value which means that AMP bound the split aptamer. Thus, 100 μM is also selected for measurements of 4 BP system. Three measurements were carried out in the presence and absence of AMP and after rinsing.

Typical force-distance (F-D) curves in the absence (black) and presence (red) of AMP were obtained from 2 and 4 BP systems (Fig. 6.2). We found that the specific rupture events

varied depending on the length of the sequence. In the absence of AMP, the rupture force (F) and rupture distance (L) increases from 2- to 4- BP as theoretical calculation showed in table 6.1. In the presence of AMP, the rupture force and rupture distance are greater. Also, these parameters measured in 4-BP system are greater than those measured in 2-BP one. The difference in force and distance between two systems is attributed to the rupture of the additional H-bonds generated between AMP molecules and the aptamer with multiple BP.

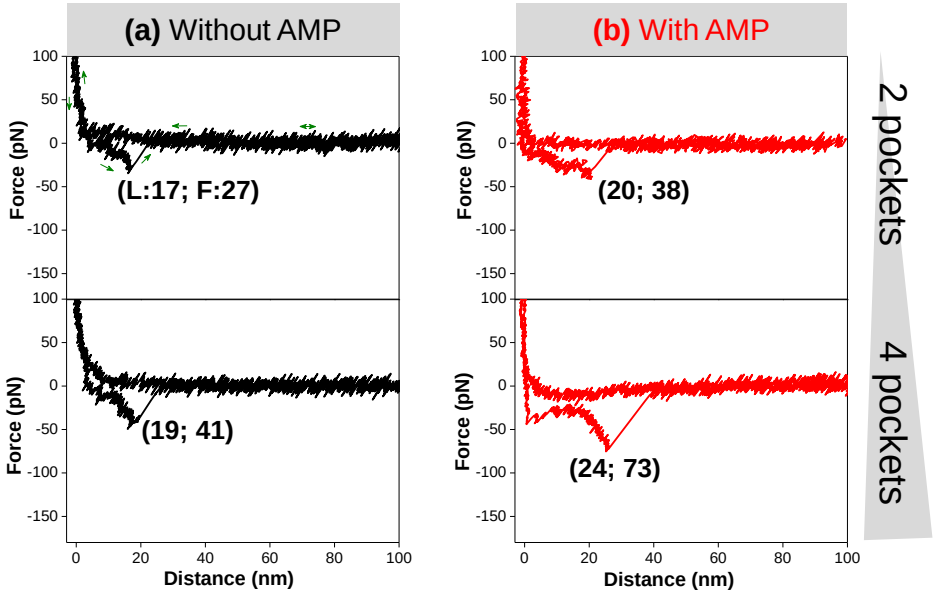

Figure 6.2. Comparison of F-D curves recorded at speed 400 nm/s between 2- (top) and 4- (bottom) BP systems. Rupture force (F) and rupture distance (L) collected at the tip/sample separation point increase from 2- to 4- BP and from the absence to the presence of AMP.

6.1.3. Amplification of Rupture Force

The most probable rupture force obtained from 2 BP and 4 BP are compared with the values obtained by Strunz et al [111] who have investigated the rupture forces of 10 and 20 bp (Fig. 6.3). A slight difference in the rupture forces between the author's data and our data can be due to some reasons such as different buffer, cantilever spring constant calibration or different structure of the oligos. This rupture forces are associated to the hydrogen bonds formed by 12 or 18 Watson Crick pairs (non-underlined sequence, Tab. 6.1). The most probable rupture force in the absence of AMP obtained from 2 BP is 27.3 ± 8.4 pN (Fig. 6.4 left, grey) and it increased to 38.7 ± 7.6 pN for 4 BP (Fig. 6.4 right, grey). Upon exchanging the buffer solution with a solution containing 100 µM AMP, an increase in the rupture force to 38.8 ± 5.2 pN (Fig. 6.4, lift, red) and 58.9 ± 14.1 pN (Fig. 6.4, right, red) was observed for 2- and 4- BP aptamers. However, significant rupture events appeared also at the low force regime and those events increased from 2- to 4 BP. In the 4-BP system, only ~70% events of

bound AMP-split aptamer were obtained while ~30% unbound events existed. Those values were estimated by calculating the rupture events under the Gaussian fit peaks (Fig. 6.4, green) at the low force regime (I) and at high force one (II).

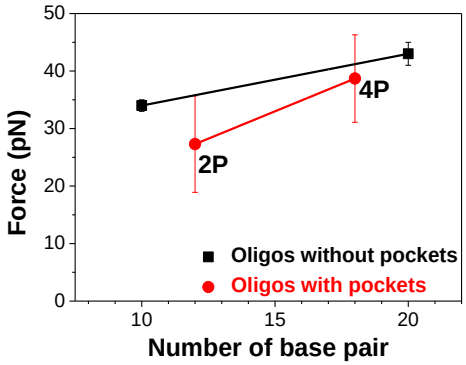

Figure 6.3. Comparison of rupture forces obtained from my measurements (red) and those reported by Strunz et al. (black) [111]. The rupture forces are comparable within the error bar.

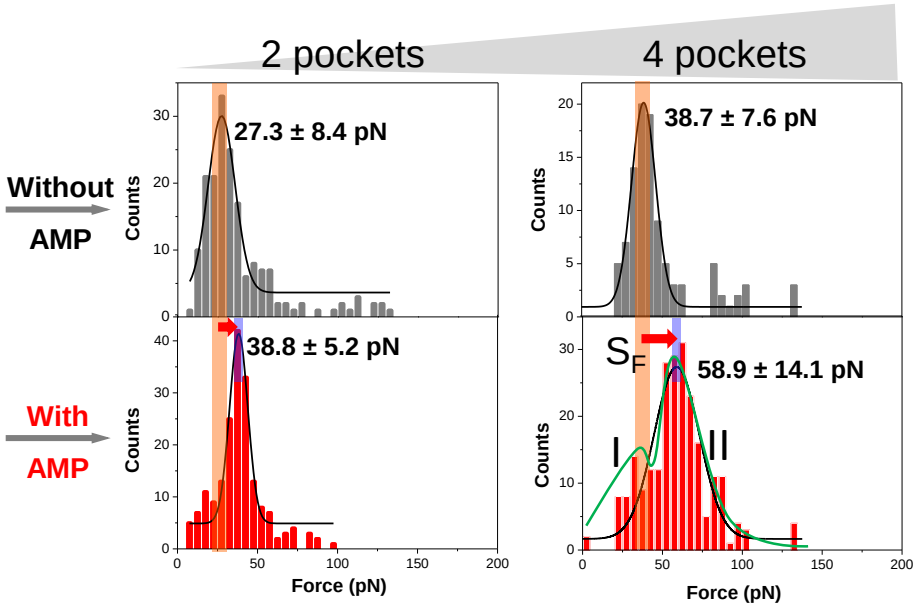

Figure 6.4. Histograms of the rupture forces obtained from multiple binding-pocket systems in the absence of AMP (top graphs) and in the presence of 100 μM AMP (bottom graphs). The most probable force is greater in the presence of AMP and increased with increasing number of BP. Red arrows show the shift in force (S_F).

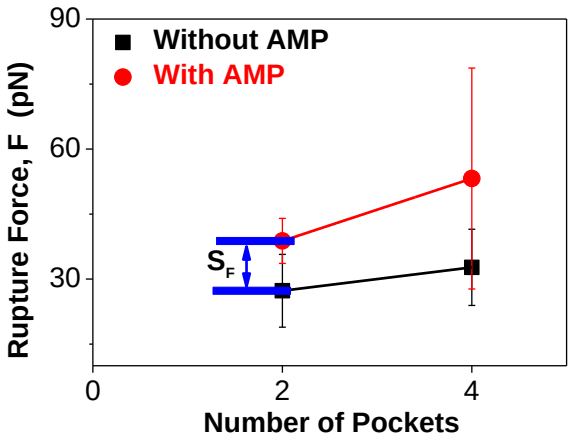

Figure 6.5. Summary of rupture force *vs*. number of BP. Since the oligos are lengthened, the force to break the Watson-Crick binding pairs also increases (black line). In the presence of AMP, the required force to rupture the additional H-bonds between AMPs and aptamers increases linearly from 2- to 4 BP (red line). The shift in rupture force from 2- to 4 BP is amplified by the factor of 2.

In order to quantify if the rupture force is amplified for 4- BP system, I subtracted the shift in the most probable rupture force (S_F) in the presence and absence of AMP (Fig. 6.5). I found that S_F increases by a factor of two within the error bar, i.e. the most probable rupture force is 11.5 pN for 2 BP and 20.2 pN for 4 BP. From the change in force, it can be concluded that the AMP entered the 4 BP of the split aptamer. The rupture force of AMP-split aptamer is amplified by adding BPs.

Next, I tried to add more BP in the split aptamer and measured the rupture force of AMP molecules to these split aptamers. Following that route, split aptamers with different number of BP such as 6, 8, and 16 pockets were designed (Tab. 6.3). With addition of more BP, the Watson-Crick pairs and the tip/surface length increase. The characteristic of those oligos are listed at the bottom of table 6.3.

Applying the same measurement protocol and data analysis method as before, the AMP-split aptamers binding can be measured. The AMP concentrations were increased of to 200 µM for 6- and 8 BP and 500 µM for 16 BP. Selection of high concentrations in the multiple BP because of the relation between bound factor and AMP concentration which will be described in the next section. The measured forces and their corresponding error bars were then plotted against the number of BP (Fig. 6.6). In the absence of AMP, the most probable rupture force increased proportional to the number of BPs (black) due to the increasing number of Watson-Crick pairs in the sequences. In the presence of AMP, the most probable rupture force also increased proportional to the number of BPs. Also, in the presence of AMP, the most probable rupture forces are higher.

Table 6.3. Aptamer sequences

Oligo	HS-AAAAAAAAAAAAAAAAAAAA(A^{20})-Sequences (5'→ 3')	BP
e	CGTAGAGGAGGATGCTGAGGAGGATCTCGAGGAGGATGACGT	6
f	ACGTCAGGAGGATCGAGAGGAGGATCAGCAGGAGGATCTACG	
g	CGTAGAGGAGGATGCTGAGGAGGATCTCGAGGAGGATGACGTGGAGGAAGTCTG	8
h	CAGACTGGAGGAACGTCAGGAGGATCGAGAGGAGGATCAGCAGGAGGATCTACG	
i	GCATCT-GGAGGA-TCTACG-GGAGGA-GTCATC-GGAGGA-CGTATC-GGAGGA-AGGTCT-GGAGGA-TTACGC-GGAGGA-AATGCA-GGAGGA-ACTCAC-GGAGGA-CAGTCA	16
k	TGACTG-GGAGGAGTGAGT-GAGGA-TGCATT-GGAGGA-GCGTAA-GGAGGA-AGACCT-GGAGGA-GATACG-GGAGGA-GATGAC-GGAGGA-CGTAGA-GGAGGA-AGATGC	

Characteristic

Pocket	Sum Bases	Watson-Crick pairs	Number of A-T (bp)	Number of G-C (bp)	Total Length (nm)
6	42	24	12	12	28.8
8	54	30	15	15	32.9
16	96	48	24	24	47.2

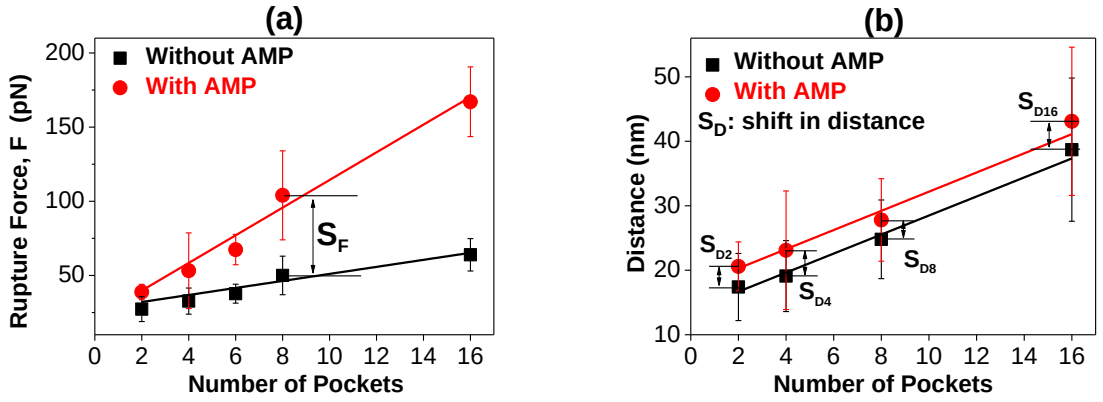

Figure 6.6. Summary of rupture forces and rupture distance *vs*. number of BP. Since the oligos are lengthened, the forces to break the Watson-Crick binding pairs (only hybridization) increased (black line) but they are lower than those in the presence of AMP (red line). (b) Shifts in rupture distance (S_D,) are ~3 nm and independent from number of pockets which is attributed to the stretching of the A^{20} spacers between oligos and surfaces. Both data sets increased linearly from 2 to 16 pockets. The shift in rupture force (S_F) was amplified when more BP are added. Different AMP concentrations were used such as 100 μM for 2- and 4 BP, 200 μM for 6 and 8 BP and 500 μM for 16 BP.

By subtracting the difference in most probable rupture force for each BP in the presence and in the absence of AMP, the shifts (S_F) were determined to be 13.0 ± 1.8 pN, 24.2 ± 5.0, 30.8 ± 10.0 pN, 44.5 ± 12.2 pN, and 94 ± 17.2 pN corresponding to the 2, 4, 6, 8, and 16 BP. From the increase of S_F, it can be concluded that the AMP entered into the multiple BPs and the ru pture force was amplified. The rupture distance measured in the presence of AMP increases by ~3 nm for 2 BP system which was contributed to the stretching of the involved oligonucleotides at the higher rupture force values that have been explained in chapter 5. However, in these experimental series using multiple BP, the increases in the rupture distances

were the same (~3 nm) for 2-, 4-, 6-, 8- and 16- BP (Fig. 6.6b). Therefore, we conclude that the increase in rupture length only comes from spacer A^{20} part.

6.2. Limitation of Multiple Binding Pockets

However, in the 4 BP system, only 80% events of bound AMP to aptamer were obtained while 20% unbound events existed. Those values were estimated by calculating the number of rupture events under the Gaussian fit peaks. These unbound events increase in the 6, 8 pockets system and they are more in the 16 pockets system. For example, among many measurements for 16 BP, a maximum of ~60% events of bound AMP to aptamer was obtained and the remaining events were at the low force regime (Fig. 6.7). The difference in the force distributions of 2-, 4-, 6-, 8- and 16 BP is attributed to a partial dissociation of some AMP molecules during rupturing the 6, 8 and 16 BP systems.

Besides two distributions of rupture forces, additional features can be observed directly from the recorded F-D curves with additional BP systems. The first feature is the appearance of multiple rupture steps in the measurement of 16 BP after the tip detaches from the surface (Fig. 6.8a, orange box). They appear frequently in the presence of 500 µM AMP (~40%) and less in the absence of AMP (~6-8%). More frequent appearance of multiple rupture steps in the presence of AMP may be due to the reformation of binding pocket during shearing oligo a from oligo b (Fig. 6.8a-top). In the presence of AMPs, AMPs can re-enter the new BPs so that the tip cannot instantly go back to the rest position. When the tip moves further from the substrate, this reformation of AMPs-pockets will be ruptured and then the tip can reach the rest position.

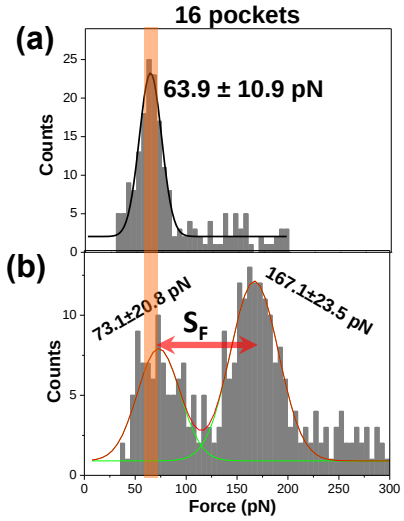

Figure 6.7. Histogram distributions of the rupture forces obtained from 16 BP systems in the absence of AMP (top graphs) and in the presence of 1 mM AMP (bottom graphs). The difference in rupture force, S_F, (shift in rupture force) is subtracted from 'with' and 'without' AMP.

The rupture forces and rupture distances can be collected as usual at the points at which the tip detaches from the surface. The rupture distances which oligo a separates from oligo b occur in the regime of about 42 nm (L), which is theoretically 47.2 nm, and the steps due to shearing's are observed at distances from 42 to 70 nm. The lengths of the steps vary from 1 to 7 nm (ΔL). The reformation of BP produces a complicated retraction curve, making it difficult to determine accurately the rupture force and rupture distance.

The second feature is BS transition of the long double strand oligonucleotides. At a force of 65-70 pN, the stretching of a dsDNA exhibits a highly cooperative transition, which refers to the conversion of B-DNA into an overstretched conformation so called S-DNA. This transition is called BS transition. I present here a typical F-D curve of the 16 BPs with a length of 102 bp (Fig. 6.8b-bottom). This BS transition occurs at the force of 66 pN. After BS transition, the oligo a separates from oligo b and the tip goes back to the rest position. The final rupture force, F, (Fig. 6.8b-bottom) consists of the ruptures of AMP from split aptamer, oligo hybridization and BS transition. The BS transition have been observed from stretching long dsDNA [158]. For a short dsDNA of less than 30 bp, it is hard to obtained BS transition because the short dsDNA molecule behaves like a stiff rod [160]. In my experiment, I did not obtain any BS transition from short sequences of 2, 4, 6 and 8 BP because of the different behaviors of the long and short dsDNA.

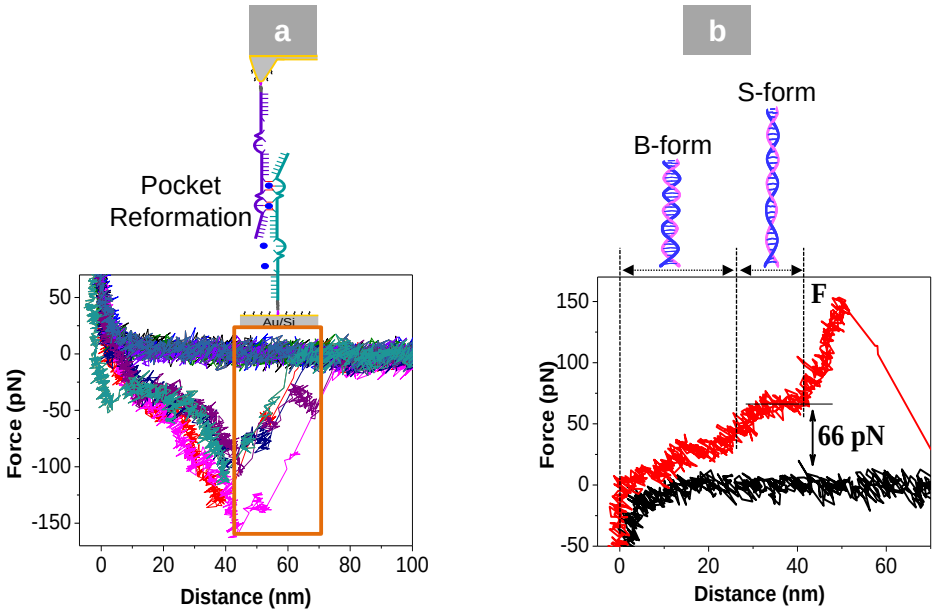

Figure 6.8. Limitation of 16 binding pockets obtained at speed 400 nm/s, contact time 2s. Multiple rupture steps due to reformation of BP and scheme of reformation of binding pocket during shearing (a). The oligos after hybridization transits from nature form (B-form) to the stretched form (S-form) in the presence of 500 μM AMP which is called BS transition process.

It is reported that among a set of measurement only ~ 30% rupture events with BS transition and more than 50% rupture events without BS transition can be observed [101, 161]. A mixture of data with and without BS transition can produce two distinguished distributions in a force histogram. In my specific experiment, the rupture events due to BS transition and in the presence of AMP can be overlapped or the force distribution can be more complicated and difficult to distinguish.

6.3. Loading Rate Dependence

In order to further understand the binding kinetics of the split aptamer itself with additional BP, the thermal off-rate parameter (k_{off}) of those systems was investigated.

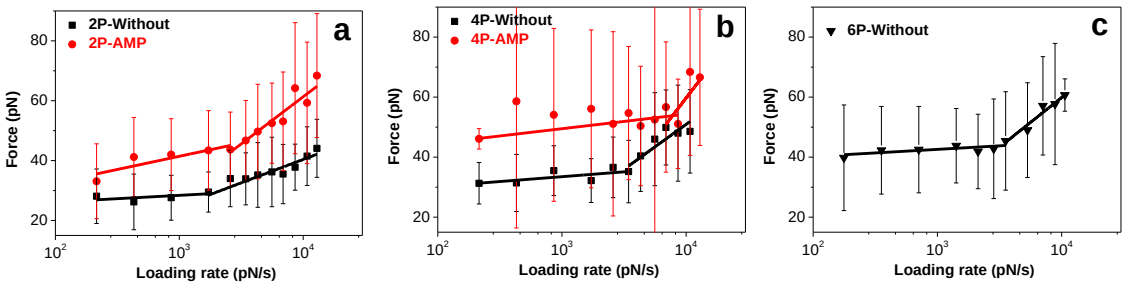

Figure 6.9. Influence of the loading rate on the rupture force for different BP systems. (a) The rupture force values obtained without AMP for two BP system (black) were measured to be lower than that of AMP-aptamer complexes (red) for 2- (a), 4- (b) and 6 BP (c). The graph of 2 BP (a), which was already presented in the figure 5.14, is again presented for comparison. The measurements were obtained with the same cantilever for each data set. The different regimes at low force (I) and high force (II) were observed for all systems.

Two distinguished regimes (Fig. 6.9) were always observed for 2- (Fig. 6.9a), 4- (Fig. 6.9b) and 6 BP (Fig. 6.9c). I attribute the kink in the force loading rate dependence on the stretching of the BP because I observed a difference in rupture distances in the presence and in the absence of AMP. Here, I analyze the rupture distance of 4 BP in the presence and in the absence of AMP. To have an overview about the rupture distance change in the different BP systems, the rupture distances obtained from no BP (Fig. 6.10A), 2 BP (Fig. 6.10B) and 4 BP (Fig. 6.10C) are compared in the same figure.

Theoretical calculation for the lengths are ~17 nm, ~19 nm and ~21 nm for no-, two- and four BP, respectively (0.34 nm/bp). In the 'No pocket' system (Fig. 6.10A), we observe no increase in rupture distance within the error bars. The rupture distance of no BP varies around 12 nm for both in the presence and absence of AMP and they do not change at different loading rates. In the '2P' system (Fig. 6.10B), the rupture distance seems to

separate to two regimes at low (smaller than ~ 500 pN/s) and high lading rates (higher than ~ 500 pN/s). At low loading rates, the rupture distances in the presence of AMP are similar (or higher) to those of in the absence of AMP. At high loading rates, the rupture distances are δ nm longer in the absence of AMP than those in the presence of AMP. In chapter 5, we saw ~ 3 nm increase in rupture distance in the presence of AMP at the loading rate of 400 nm/s and it was attributed to the stretching of A^{20} spacer at higher force. However, this observation was not clearly seen in those loading rate dependence measurements, which may be due to the large error bars. For the '4P' (Fig. 6.10C), the rupture distances in the absence of AMP are significantly larger than those in the presence of AMP. The difference of these two data sets (black and red) is now increased to about 2δ because the number of BP is doubled. This result implies that the longer rupture distance is due to the extension of the ssDNA in the pockets at high loading rate. When AMP enters the binding pocket, the double helix is stabilized. The constant rupture distance in the presence of AMP allows us to conclude that the pockets with AMP are not stretched even at high loading rates.

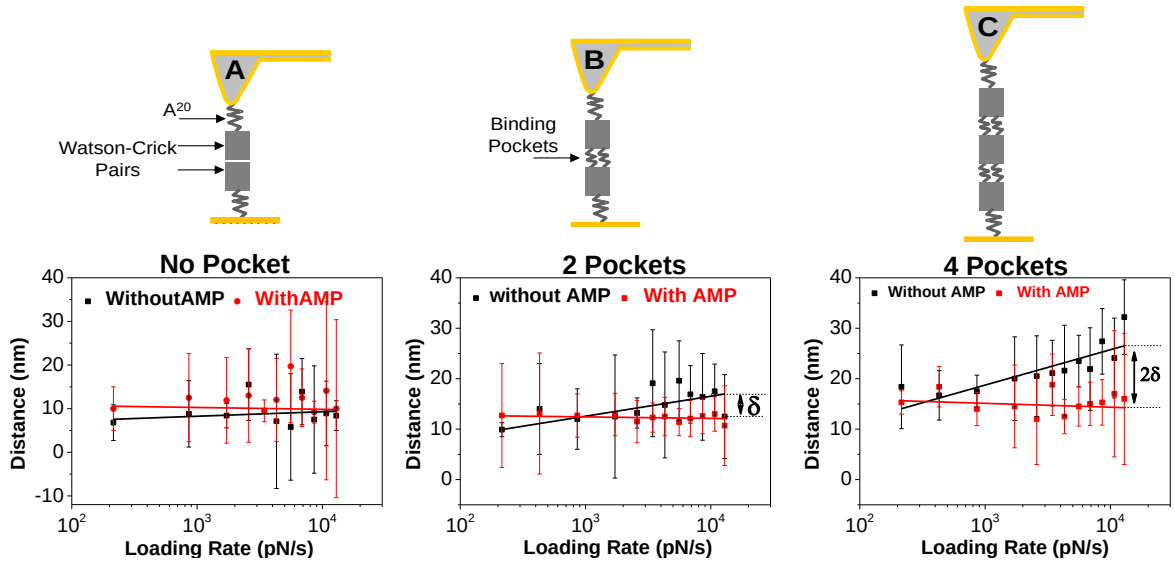

Figure 6.10. Pocket's transition analysis using the variation of rupture distances at different loading rates. (A) rupture distance does not change for the measurement of the sequences without BP while it slightly increases at 2 BP(B) and significantly increases at 4 BP(C). The kink appears at the loading rate of about 800 pN/s (blue box).

The logarithmic fits of two distinguished regimes at low and high loading rates (Fig. 6.9) provide information of thermal kinetics of the AMP-split aptamer with 4- and 6- (Tab. 6.2). At low loading rate, the dissociation rate of 6 BP split aptamer (10^{-9} s^{-1}) is lower than that of 4 BP (10^{-6} s^{-1}) which indicates that the long split aptamer is more stable than the shorter one. Similar to the 2 BP, the obtained potential width (Δx) is reasonable compared to previous

studies. At high loading rates, k_{off} (704 and 1320 s^{-1}) is unexpected high while the potential width (1.9 and 0.8 nm) is significantly reduced compared to previous studies. The appearance of the kink in the force loading rate dependence and the unexpected high k_{off} is caused by the stretching of the BP.

Table 6.2: Fitting parameters obtained with the Bell-Evans models

Regime	Parameters	4P	6P
Flat (a)	k_{off} (s^{-1})	10^{-6}	10^{-9}
	Δx (nm)	21	17
Stiff (b)	k_{off} (s^{-1})	704	1320
	Δx (nm)	1.9	0.8

7. Determination of Contribution of Single Hydrogen Bonds

In this chapter, a method to measure the rupture force of H-bonds forming between targets and the split aptamer will be introduced. The initial target is AMP which consists of three binding groups. The binding force between AMP and the split aptamer due to 8 H-bonds is ~11 pN as shown in chapter 6.

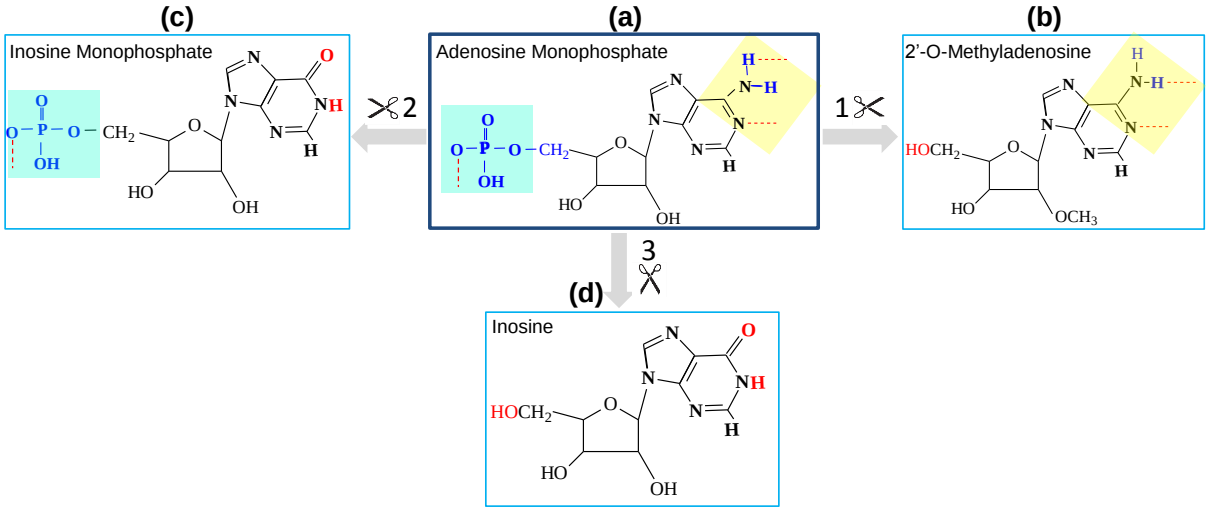

Figure 7.1. Removal of binding groups of the AMP. (a) phosphate (blue box) and amidine (yellow box) groups are the binding groups of AMP to the aptamer and the red-dashes lines indicate the formation of H-bonds with aptamer. (b) Replacing the phosphate group of AMP with hydroxyl group, leads to 2'-O-Methyladenosine which contains only two binding groups (yellow box). (c) IMP is formed when both amino and imine groups are replaced. A combination of both replacements of (b) and (c) produces Inosine target which contains no any binding group.

In order to understand the contributions of individual hydrogen bonds in the small molecule-split aptamer complex, the H-bonds of AMP are removed one by one. Starting from three specific binding sites denoted by red-dashed lines in the figure 7.1a, the binding groups were reduced to two (Fig 7.1b), to one (Fig 7.1c), and to zero (Fig 7.1d) corresponding to AMP, 2'-O-Methyladenosine (OMA), Inosine monophosphate (IMP), and Inosine, respectively. Detection of rupture forces of those targets that bind the split aptamer may meet the force resolution of AFS which is about 10 pN. In order to overcome this limitation, we used the split aptamers with multiple BP to amplify the rupture force as demonstrated in chapter 6.

By considering the most probable rupture forces between those different ligands and the aptamer, we could quantify how strong a single H-bond in this particular system is.

7.1. Experimental Scheme for Measurements of Single H-bonds

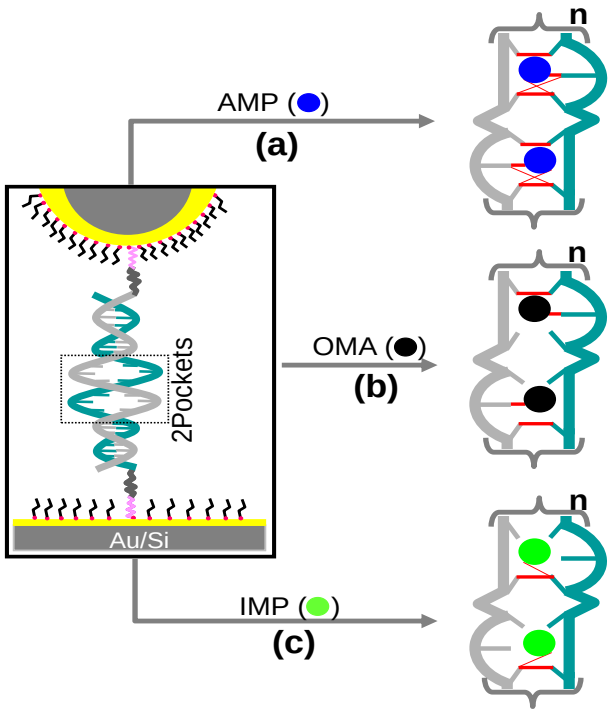

Figure 7.2. Schematic illustration of measuring rupture force of H-bonds in multiple BP systems by AFS. Assumptions of different targets that bind the same aptamer produce the corresponding H-bond network. (a) AMPs (blue) with 3 binding groups enter two BP and 8 additional H-bonds are formed per BP (red lines). (b) OMA (black) with 2 binding groups forms 4 additional H-bonds. (c) IMP (green) which consists of only one binding group forms three additional H-bonds with aptamer. Multiple BPs, **n**, is used to amplify the small measured rupture force when binding groups of the targets are removed.

The standard experimental setup is also applied to this investigation, i.e. 1000 F-D curves are first recorded in pure buffer T, then in a solution containing target molecules (AMP, OMA,

IMP or Inosine) with concentrations of 100 µM for 2- and 4 BP, 200 µM for 6- and 8 BP and 500 µM for 16 BP, and finally in buffer T again after rinsing.

When adding target molecules such as AMP, OMA or IMP to the buffer solution, they enter the pockets and different numbers of the H-bonds are formed (Fig. 7.2). For example, the AMP in the BP leads to 8 H-bonds (Fig 7.2a), 4 H-bonds for OMA (Fig 7.2b) and 3 H-bonds for IMP (Fig 7.2c).

7.2. Rupture Forces of Different Targets-Split Aptamer

To have an overview on the variation of rupture forces measured in the presence of different target molecules as well as multiple BPs, typical F-D curves for each investigation are presented (Fig. 7.3). The rupture force increases from Inosine (red) to IMP (green), OMA (black) and AMP (blue). Both rupture force (F) and rupture distance (L) increase with increasing number of BP. The rupture forces are amplified for every target molecule when multiple BPs are used, i.e. 2 BP (n=1, Fig. 7.3a), 4 BP (n=2, Fig. 7.3b) and 8 BP (n=4, Fig. 7.3c). The rupture lengths increased significantly from 2 to 8 BP because of the lengthening of aptamer to archive the multiple BP, i.e. ~ 17 nm, ~20 nm and ~30 nm corresponding to 2, 4 and 8 BP. Those values are reasonable compared with the theoretical values as mentioned in chapter 6.

The most probable rupture forces from the Gaussian fits of the data obtained from 2, 4 and 8 BP with target OMA are presented (Fig. 7.4). This force increased from the absence (top grey columns) to the presence of OMA (red columns). A mean rupture force of 30.2 ± 11.8 pN in the absence of OMA were determined from a fit of the main peak in the histogram by a Gaussian distribution for 2 BP. Upon the change from buffer T to 100 µM OMA, an increase in the rupture force to 36.7 ± 8.5 pN was detected (Fig. 7.4 a). After thoroughly rinsing the OMA target molecules out of the liquid cell with buffer, the mean rupture force also returned to original values within the given experimental error (bottom grey columns). Thus, the increase in rupture force is due to the binding of OMA molecules to the split aptamer.

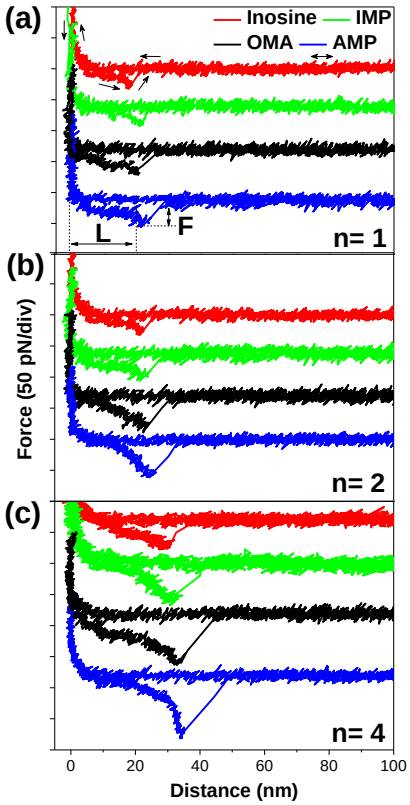

Figure 7.3. Typical rupture force distance curves recorded at 400 nm/s. F-D curves obtained from aptamer sequences containing 2 pockets (a), 4 pockets (b), and 8 pockets (c) in the presence of Inosine (red), IMP (green), OMA (black), and AMP (blue). The rupture force increased correspondingly from Inosine to AMP. The arrows present the direction of the approach and withdraw curves. Rupture force (F) and distance (L) at the tip/sample separation point are collected for analysis.

This series of measurements revealed that the rupture force is higher when multiple BP is used. For 4 BP, the most probable rupture force increases from 40.9 ± 13.2 pN to 52.6 ± 13.9 pN (Fig. 7.4 b) and from 52.1 ± 19.2 pN to 87.2 ± 18.0 pN for 8 BP (Fig. 7.4 c). A similar analysis was done for the targets Inosine, IMP or AMP (see details in appendix B). In order to summarize the variation of the most probable rupture forces in those measurements, the force shifts (S_F) were collected for further analysis. The S_F is subtracted from the most probable rupture force in the absence and in the presence of target molecule (Fig. 7.4., red arrow). The S_F values measured from aptamer-different target molecules binding are then plotted against the number of BP. For example, the S_F values for 2 BP split aptamer-OMA binding is ~ 6 pN, ~ 12 BP for 4 BP and ~35 pN for 8 BP. For 2- and 4- BP after rinsing, the most probable rupture force 29.8 ± 9.1 pN and 42.5 ± 8.5 pN are almost the same to that of the initial measurements, 30.2 ± 11.8 pN and 40.9 ± 13.2 pN within the error bars, respectively. However, this value increases in the 8 BP system, which is attributed to the use of high concentration of OMA in the buffer and the rinsing process did not removed all the OMA from the surrounding buffer.

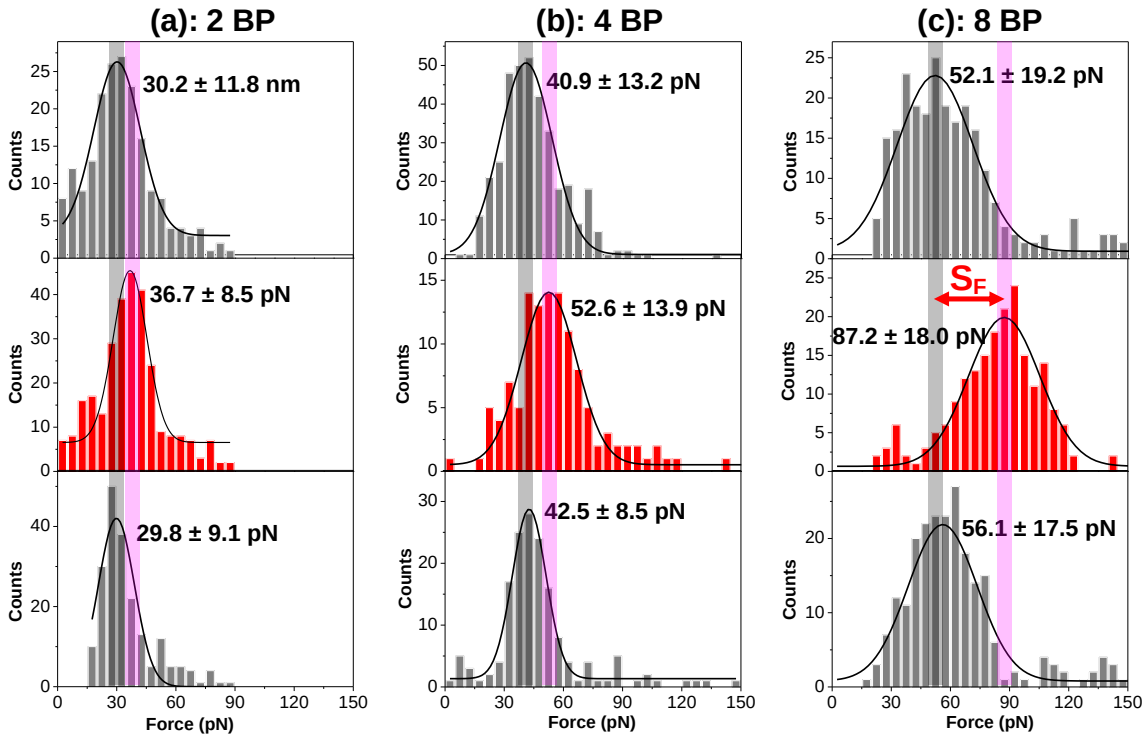

Figure 7.4. Histogram distributions of the rupture forces obtained for target OMA that binds the split aptamer with 2- (a), 4- (b) and 8 BP (c) in the absence (top-grey), presence (middle-red) and rinsing (bottom-grey). The difference in rupture force (S_F) between with and without OMA increased when the number of BP increased.

7.3. Amplification of Rupture Force for Detection of Single Binding Site

The small shifts in the most probable rupture forces in the presence of the targets are difficult to detect and analyze since many factors are involved. To get reliable shifts in the most probable rupture forces, I have repeated the experiments for each individual target and averaged all the data for each condition (Tab. 7.1). In addition, Inosine was also used as a reference target which contains no binding sites. I performed at least two repeated measurements for each condition and determined the S_F values. If the S_F value from the first measurement differed from the second one, I repeated the experiments more often. For example, for AMP with 6 BP, the S_F value varies from 22.7 pN to 50.0 pN and I have repeated this measurement seven times to get an average value S_F of 30.8 ± 10 pN. Among these measurements, a high S_F of 50.0 pN was obtained in only one measurement and it may be caused by multiple ruptures.

To compare the ruptures force among different target molecules, the shifts in forces (S_F) for different targets including Inosine, IMP, OMA, and AMP are plotted against the number of BP (Fig. 7.5). The shifts in force for every target increased linearly with an increase of the

number of BP (Fig. 7.5a). The highest S_F values were obtained from target AMP for all systems. This value is lowered for OMA and IMP. Without any binding group (Inosine), the shift in rupture force is around zero within the estimated error bars. Then I fitted the data of each individual target with line that provides the slope value and the associated error.

Table 7.1. Shift in rupture force (S_F)

No. of measurement		**Inosine (S_F, pN)**				**IMP (S_F, pN)**		
	2P	4P	6P	8P	2P	4P	6P	8P
1	-1.2	2.1	0.9	3.3	8.0	13.2	17.1	18.6
2	0	1.4	0	5.0	4.4	9.9	17.8	25.9
3	-0.4				7.6	13.1		
4					11.7	14.28		
5						13.2		
6						9.6		
S_F	**-0.5±0.6**	**1.8±0.5**	**0.5±0.6**	**4.5±1.2**	**7.9±3.0**	**12.2±2.0**	**17.5±0.5**	**22.3±5.2**
No. of measurement	**OMA (S_F, pN)**				**AMP (S_F, pN)**			
1	7.0	11.6	19.0	29.0	11.5	24.8	22.7	46.6
2	5.8	30.8	26.9	28.4	15.1	25.5	50.0	55.5
3		10.5		35.1	11.5	28.0	33.0	31.4
4					13.8	14.7	25.0	
5						23.3	33.0	
6						28.6	32.0	
7							20.0	
S_F	**6.4±0.8**	**17.6±11.4**	**23.0±5.6**	**30.8±3.7**	**13.0±1.8**	**24.2±5.0**	**30.8±10.0**	**44.5±12.2**

This resulted in a slope that changes from 0.20 ± 0.13 pN/BP for Inosine to 2.92 ± 0.04 pN/BP for IMP, 3.52 ± 0.192 pN/BP for OMA and 6.06 ± 0.29 pN/BP for AMP. The change of slopes means that rupture forces of the target binding the split aptamers are different. Higher value of slope indicate higher rupture force due to the target bindinig in one BP. Plotting the slopes value *vs*. targets, I found that they did not follow a linear dependence (Fig. 7.5b). The differences in the magnitudes of the slopes mean that the contribution of each binding group (phosphate, amino and imine) to the total H-bond network when the target enters the BP was not equal. In the presence of phosphate group, the slope is 2.72 pN/BP and the difference in slope in the presence of both amino and imine group is only 0.6 pN/BP. The difference indicates that more H-bonds were formed in the presence of phosphate group compared to that in the presence of the other two groups of amidine. In the presence of phosphate group in IMP or AMP, the slope changes are approximately equal, i.e. 2.72 pN/BP for the IMP and 2.54 pN/BP for the AMP.

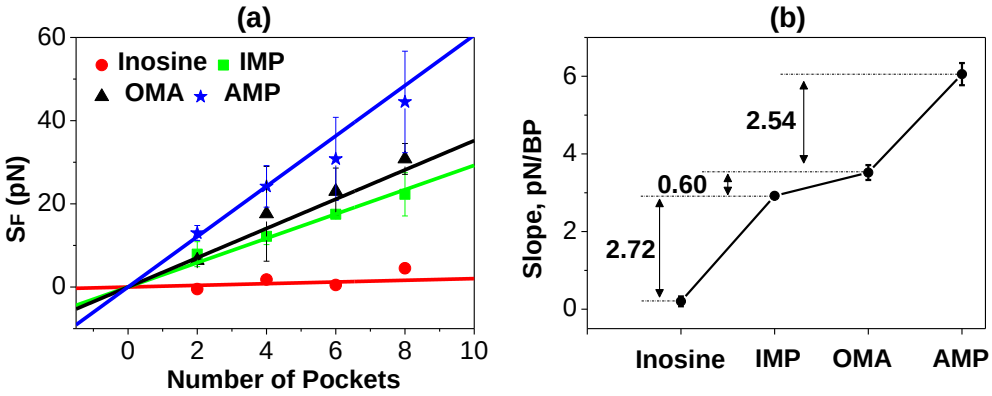

Figure 7.5. The shift in rupture forces S_F of targets with reduction of binding sites that bind multiple BP aptamer. Highest rupture forces (blue) were observed for target AMP and lower values were observed for OMA (black), IMP (green) and Inosine (red) (a). The rupture forces are amplified when multiple BP are utilized. Each data set follows a linear model but slopes of the fits do not follow this model (b).

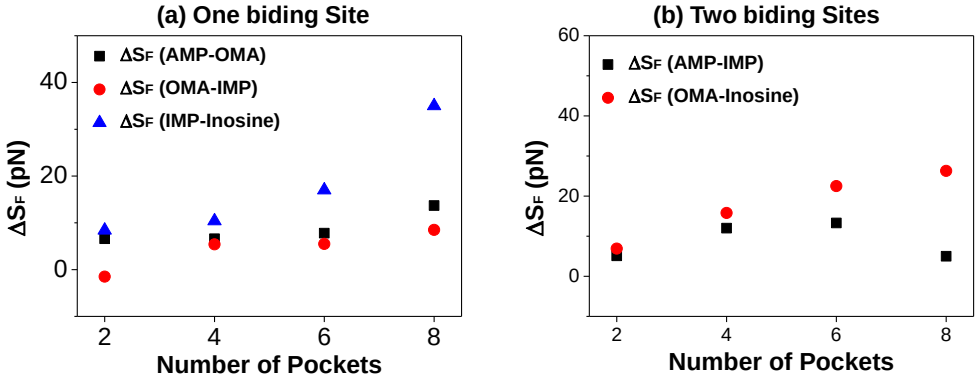

Figure 7.6. Contribution of one (a) and two (b) binding sites to the rupture forces. The rupture force generated by each binding site at different position to the split aptamer is not same.

In order to quantify the contribution of each binding site to the total H-bonds, I subtracted the difference in ΔS_F value among the targets (Fig. 7.6). For example, to get the influence of only one binding site to the BP, the difference in S_F between AMP and OMA, OMA and IMP, and IMP and Inosine were subtracted (Fig. 7.6 a). In a similar way, to see if the contribution of two binding sites to the pocket is the same, differences in the ΔS_F between AMP and IMP or OMA and Inosine were subtracted (Fig. 7.6 b). The data did not overlap each other for both cases. It means that existence of the binding sites at different position form different H-bond networks with the split aptamer.

In conclusion, with this advanced experimental design, we could observe the rupture force of targets with only one or two binding sites to the split aptamer. We also quantify that the contribution of each individual binding site to the H-bond network between the target and the split aptamer is not equal.

7.4. Loading Rate Dependence for Different Target Molecules

In order to understand the change of thermal kinetics of AMP-aptamer binding when AMP's binding sites are removed, I made a series of measurements of speed dependence for different targets, i.e., AMP to OMA, IMP and Inosine using the same cantilever. The most probable rupture forces follow a linear dependence with the pull-off velocity (Fig. 7.7). At all speeds, the most probable rupture forces in the presence of AMP were always higher than that of the other targets. The rupture forces in the absence of target molecules and in the presence of Inosine are similar within error bars and they are smallest compared to other cases. The rupture forces become higher in the presence of IMP, OMA and AMP. The increase in rupture force is attributed to cooperative thermal dissociation of AMP-, OMA-, and IMP-split aptamer. It would be very interesting if we can obtain the variation of thermal off rates k_{of} of those molecules that bind the split aptamer. However, within the error bars in our measurements, it seems to be impossible to further interpret the difference in thermal kinetic of these systems since the k_{off} for those targets varied over a wide range, ~10^{-4} to ~10^{-7} s^{-1}.

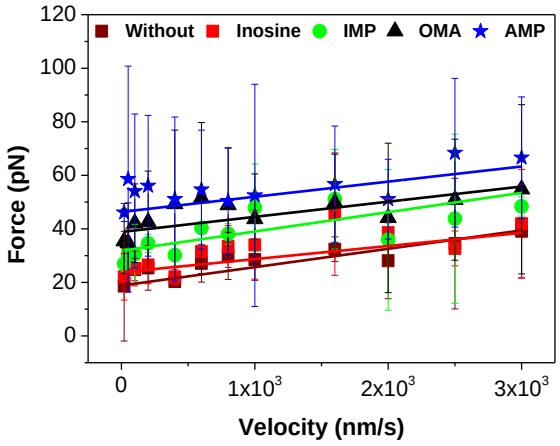

Figure 7.7. Dependence of rupture forces on pull-off velocities. The most probable rupture forces due to only oligo hybridization (wine) are similar to the target Inosine (red) but they are lower than those from target IMP (green), OMA (black) or AMP (blue).

There are two points which can be understood from speed dependence measurements. First, the data directly supported the previous investigations (sections 7.1 to 7.3) since the similar trends of rupture forces in the presence of different targets were observed. The rupture forces reduced when the binding groups of the targets were reduced. Second, the aptamer forming complexes with IMP, OMA and AMP also followed the same rule of cooperative thermal dissociation as normal oligos in the previous studies [31, 101, 111].

Conclusion and Outlook

Within this thesis, I studied a new concept for binding small molecules to binding pockets (BP) formed by aptamers. The concept is based on splitting an aptamer into two stands, which can be immobilized on an AFM tip and a surface, respectively. Atomic force spectroscopy showed that the Watson-Crick pairs and the aptamer BP formed when the tip was brought close to the surface. Adding excess target molecules led to an increase in rupture forces of both strands. Thus, the presence of target molecules in the BP could be detected. Within my thesis, I proved that adenosine monophosphate (AMP), cocaine and tetracycline could be detected by using different aptamer systems. Thus, the split aptamer concept could be a general approach to detect small molecules in a label-free way.

Furthermore, this approach allowed me to measure extremely small rupture forces (~10 pN) of target molecules. The ability to measure these rupture forces using AFS makes our split aptamer concept a valuable approach since target modification was always required for immobilization or optical labeling in previous studies. Since many macromolecules that bind aptamers are known, such as proteins, tissues and cells, it would be interesting for future studies to apply this concept and measure their rupture forces. When these molecules are immobilized on the surfaces, their binding groups can be hidden and only the groups which can contact with the aptamer are functional. By using the split aptamer concept, the macromolecules can form complexes with aptamers in three dimensions, allowing their complete binding characteristics to be measured.

Dissociation constants (K_D) have been measured in bulk by various techniques such as titration and filtration. However, those techniques require a significant quantity of sample and the results have a large error [162]. In the present study, a method to determine K_D of an AMP-split aptamer complex by analyzing the rupture force distributions at different AMP concentrations has been introduced. The exponential fits for the sets of data in the presence

and in the absence of AMP allowed us to obtain an accurate K_D value. We obtained a K_D of 3.7 ± 2.5 μM, which was in the range of values reported in literature. To the best of my knowledge, the method of determining K_D on a single molecule level by analyzing rupture force distributions has been shown in this study for first time.

Furthermore, I demonstrated that the rupture force of the AMP-split aptamer complex could be amplified by adding a series of BP. In the absence of the target molecule, the most probable rupture forces increased with additional BP owning to the presence of more Watson-Crick pairs. In the presence of excess of the target molecules, we obtained a further increase in rupture forces for the systems having a series of BP. The results suggest that the rupture forces were amplified when additional BP were utilized. Increases in the shifts of the rupture forces due to the presence of AMP proved that the target molecules could enter the multiple BP systems.

In addition, the split aptamer allowed me to investigate the role of the different H-bonds formed between the target molecules and the BP of the aptamer. This was done by replacing AMP, which contains three binding groups (phosphate, amino and imine) with its derivative molecules such as 2'-O-Methyladenosine (OMA), Inosine monophosphate (IMP) or Inosine containing two (amino and imine), one (phosphate) or no binding groups, respectively. By adding excess of those molecules, increases in rupture forces were recorded for OMA and IMP but not for Inosine. This observation revealed that the OMA and IMP bound in the BP. Reduction in rupture forces from AMP- to OMA- and to IMP-split aptamer allowed me to estimate the force contribution of single H-bonds in the AMP molecule. Assuming only contribution of H-bonds to the binding between AMP and the split aptamer, the rupture forces of several involved H-bonds were quantified in the range of only few pN. I found that the shifts in rupture forces of all target molecules at different number of BP followed linear dependences. The difference in slope indicated that the contribution of each binding group in the AMP molecule to the total rupture force was not the same. In the presence of the phosphate group the slope was about 2.7 pN/BP while it was reduced to only around 0.6 pN/BP in the presence of the amino and imine groups. Thus, I concluded that the phosphate group plays the most important role in the formation of the H-bond network between AMP and aptamer.

Thermal kinetics of the AMP-split aptamer complex could be obtained by measuring rupture forces at different loading rates. I obtained a slight increase in the thermal off-rate of the split aptamer system when it is exposed to excess of the AMP molecule. This result showed that the split aptamer was stabilized in the presence of AMP. Furthermore, I found two distinguishable regimes in the results of rupture force-loading rate dependence measurements. From this behavior, I concluded that an additional mechanism occurred

during pulling the split aptamer. By considering the structure of the split aptamer, I proposed a model to explain the appearance of the two regimes which described the transition of the BP at high loading rates. My model in principle was based on the sequences at the BP which were flexible and they behaved like two parallel springs. The proposed model was proven accurate by observation of the change in rupture distances at different loading rates. At high loading rates, I found that the rupture distance increased in the absence of the AMP molecules but was constant in the presence of AMP molecules. These results suggested that the BP areas of the split aptamer were stretched to longer lengths in the absence of AMP. This behavior did not occur in the presence of AMP due to the stabilization of AMP in the BP. The model was further clarified when we investigated these rupture distances for a 4 BP system. The characteristics of the rupture distances at high loading rates were similar to those observed in the 2 BP system. However, the difference in the rupture distance (δ) in the presence and in the absence of AMP was amplified twice, i.e. δ for 2 BP and about 2δ for 4 BP system. The amplification of δ in the 4 BP system supported the proposed model. In the 4 BP system, the number of flexible parts was twice that of the 2 BP system. Stretching these flexible parts at high loading rates resulted in an increase in δ in the 4 BP system. To the best of my knowledge, mechanics of the split aptamer carrying multiple BP was here investigated and reported for the first time.

Bibliography

1. Tuerk, C. and L. Gold, *Systematic evolution of ligands by exponential enrichment: RNA ligands to bacteriophage T4 DNA polymerase.* Science, 1990. **249**(4968): p. 505-10.
2. Ellington, A.D. and J.W. Szostak, *In vitro selection of RNA molecules that bind specific ligands.* Nature, 1990. **346**(6287): p. 818-22.
3. Du, J.A., D.Z. Fang, J. Lin, L.Y. Xiao, X.D. Zhou, S. Shigdar, and W. Duan, *TaqIB polymorphism in the CETP gene modulates the impact of HC/LF diet on the HDL profile in healthy Chinese young adults.* Journal of Nutritional Biochemistry, 2010. **21**(11): p. 1114-1119.
4. Keefe, A.D., S. Pai, and A. Ellington, *Aptamers as therapeutics.* Nature Reviews Drug Discovery, 2010. **9**(7): p. 537-550.
5. Luzi, E., M. Minunni, S. Tombelli, and M. Mascini, *New trends in affinity sensing: aptamers for ligand binding.* Trac-Trends in Analytical Chemistry, 2003. **22**(11): p. 810-818.
6. Kusser, W., *Chemically modified nucleic acid aptamers for in vitro selections: evolving evolution.* J Biotechnol, 2000. **74**(1): p. 27-38.
7. Pieken, W.A., D.B. Olsen, F. Benseler, H. Aurup, and F. Eckstein, *Kinetic Characterization of Ribonuclease-Resistant 2'-Modified Hammerhead Ribozymes.* Science, 1991. **253**(5017): p. 314-317.
8. Heidenreich, O. and F. Eckstein, *Hiv-1 Ltr Rna Cleavage by Hammerhead Ribozymes.* Biological Chemistry Hoppe-Seyler, 1991. **372**(9): p. 673-673.
9. Velasco-Garcia, M.N. and S. Missailidis, *New trends in aptamer-based electrochemical biosensors.* Gene Therapy and Molecular Biology, 2009. **13**(1): p. 1-9.
10. Nakamoto, K., M. Tsuboi, and G.D. Strahan, *Drug-DNA interactions: structures and spectra.* Methods Biochem Anal, 2008. **51**: p. 1-366.
11. Nunn, C.M., L. Vanmeervelt, S. Zhang, M.H. Moore, and O. Kennard, *DNA Drug-Interactions - the Crystal-Structures of D(Tgtaca) and D(Tgatca) Complexed with Daunomycin.* J Mol Biol, 1991. **222**(2): p. 167-177.
12. Zlatanova, J., S.M. Lindsay, and S.H. Leuba, *Single molecule force spectroscopy in biology using the atomic force microscope.* Progress in Biophysics & Molecular Biology, 2000. **74**(1-2): p. 37-61.
13. Williams, M.C. and I. Rouzina, *Force spectroscopy of single DNA and RNA molecules.* Current Opinion in Structural Biology, 2002. **12**(3): p. 330-336.
14. Neuman, K.C. and A. Nagy, *Single-molecule force spectroscopy: optical tweezers, magnetic tweezers and atomic force microscopy.* Nat Methods, 2008. **5**(6): p. 491-505.
15. Binnig, G., C.F. Quate, and C. Gerber, *Atomic force microscope.* Phys Rev Lett, 1986. **56**(9): p. 930-933.
16. Ros, R., R. Eckel, F. Bartels, A. Sischka, B. Baumgarth, S.D. Wilking, A. Puhler, N. Sewald, A. Becker, and D. Anselmetti, *Single molecule force spectroscopy on ligand-DNA complexes: from molecular binding mechanisms to biosensor applications.* J Biotechnol, 2004. **112**(1-2): p. 5-12.
17. Tessmer, I., C.G. Baumann, G.M. Skinner, J.E. Molloy, J.G. Hoggett, S.J.B. Tendler, and S. Allen, *Mode of drug binding to DNA determined by optical tweezers force spectroscopy.* Journal of Modern Optics, 2003. **50**(10): p. 1627-1636.
18. Boland, T. and B.D. Ratner, *Direct Measurement of Hydrogen-Bonding in DNA Nucleotide Bases by Atomic-Force Microscopy.* Proc Natl Acad Sci U S A, 1995. **92**(12): p. 5297-5301.
19. Lee, G.U., L.A. Chrisey, and R.J. Colton, *Direct Measurement of the Forces between*

Complementary Strands of DNA. Science, 1994. **266**(5186): p. 771-773.
20. Noy, A., D.V. Vezenov, J.F. Kayyem, T.J. Meade, and C.M. Lieber, *Stretching and breaking duplex DNA by chemical force microscopy.* Chem Biol, 1997. **4**(7): p. 519-527.
21. Sattin, B.D., A.E. Pelling, and M.C. Goh, *DNA base pair resolution by single molecule force spectroscopy.* Nucleic Acids Res, 2004. **32**(16): p. 4876-83.
22. Rief, M., H. Clausen-Schaumann, and H.E. Gaub, *Sequence-dependent mechanics of single DNA molecules.* Nat Struct Biol, 1999. **6**(4): p. 346-9.
23. Samori, B., *Stretching, tearing, and dissecting single molecules of DNA.* Angewandte Chemie-International Edition, 1998. **37**(16): p. 2198-2200.
24. Bockelmann, U., B. Essevaz-Roulet, P. Thomen, and F. Heslot, *Mechanical opening of DNA by micro manipulation and force measurements.* Comptes Rendus Physique, 2002. **3**(5): p. 585-594.
25. Nguyen, T.H., S.M. Lee, K. Na, S. Yang, J. Kim, and E.S. Yoon, *An improved measurement of dsDNA elasticity using AFM.* Nanotechnology, 2010. **21**(7).
26. Cocco, S., J. Yan, J.F. Leger, D. Chatenay, and J.F. Marko, *Overstretching and force-driven strand separation of double-helix DNA.* Phys Rev E Stat Nonlin Soft Matter Phys, 2004. **70**(1 Pt 1): p. 011910.
27. Storm, C. and P.C. Nelson, *Theory of high-force DNA stretching and overstretching.* Phys Rev E Stat Nonlin Soft Matter Phys, 2003. **67**(5 Pt 1): p. 051906.
28. Nguyen, T.H., S.S. Choi, D.W. Kim, and Y.U. Kim, *Study on the binding force between lambda-DNA and various types of substrates.* Journal of the Korean Physical Society, 2007. **50**(6): p. 1942-1946.
29. Huizenga, D.E. and J.W. Szostak, *A DNA Aptamer That Binds Adenosine and Atp.* Biochemistry, 1995. **34**(2): p. 656-665.
30. Diamandis, E.P. and T.K. Christopoulos, *The Biotin (Strept)Avidin System - Principles and Applications in Biotechnology.* Clin Chem, 1991. **37**(5): p. 625-636.
31. Gaub, B.M., C. Kaul, J.L. Zimmermann, T. Carell, and H.E. Gaub, *Switching the mechanics of dsDNA by Cu salicylic aldehyde complexation.* Nanotechnology, 2009. **20**(43).
32. Ho, D., K. Falter, P. Severin, and H.E. Gaub, *DNA as a Force Sensor in an Aptamer-Based Biochip for Adenosine.* Anal Chem, 2009. **81**(8): p. 3159-3164.
33. Rief, M. and H. Grubmuller, *Force spectroscopy of single biomolecules.* Chemphyschem, 2002. **3**(3): p. 255-61.
34. Leng, F.F., J.B. Chaires, and M.J. Waring, *Energetics of echinomycin binding to DNA.* Nucleic Acids Res, 2003. **31**(21): p. 6191-6197.
35. Steinbock, L., in *Institute of Phamarcy and Molecular Biotechnology*2006, University of Heidelberg. p. 109.
36. Kim, Y., Z. Cao, and W. Tan, *Molecular assembly for high-performance bivalent nucleic acid inhibitor.* Proc Natl Acad Sci U S A, 2008. **105**(15): p. 5664-5669.
37. de Franciscis, V., C.L. Esposito, S. Catuogno, L. Cellai, and L. Cerchia, *Aptamers as Innovative Diagnostic and Therapeutic Agents in the Central Nervous System.* Cns & Neurological Disorders-Drug Targets, 2009. **8**(5): p. 393-401.
38. Farokhzad, O.C., J.J. Cheng, B.A. Teply, I. Sherifi, S. Jon, P.W. Kantoff, J.P. Richie, and R. Langer, *Targeted nanoparticle-aptamer bioconjugates for cancer chemotherapy in vivo.* Proc Natl Acad Sci U S A, 2006. **103**(16): p. 6315-6320.
39. Savran, C.A., S.M. Knudsen, A.D. Ellington, and S.R. Manalis, *Micromechanical detection of proteins using aptamer-based receptor molecules.* Anal Chem, 2004. **76**(11): p. 3194-3198.
40. Hwang, K.S., S.M. Lee, K. Eom, J.H. Lee, Y.S. Lee, J.H. Park, D.S. Yoon, and T.S. Kim, *Nanomechanical microcantilever operated in vibration modes with use of RNA aptamer as receptor molecules for label-free detection of HCV helicase.* Biosens Bioelectron, 2007. **23**(4): p. 459-465.
41. Famulok, M. and D. Faulhammer, *Specific Binding of Antibodies to DNA through*

Combinatorial Antibody Libraries. Angewandte Chemie-International Edition in English, 1994. **33**(18): p. 1827-1829.
42. Famulok, M., *Molecular Recognition of Amino-Acids by Rna-Aptamers - an L-Citrulline Binding Rna Motif and Its Evolution into an L-Arginine Binder.* J Am Chem Soc, 1994. **116**(5): p. 1698-1706.
43. Gebhardt, K., A. Shokraei, E. Babaie, and B.H. Lindqvist, *RNA aptamers to S-adenosylhomocysteine: Kinetic properties, divalent cation dependency, and comparison with anti-S-adenosylhomocysteine antibody.* Biochemistry, 2000. **39**(24): p. 7255-7265.
44. Haller, A.A. and P. Sarnow, *In vitro selection of a 7-methyl-guanosine binding RNA that inhibits translation of capped mRNA molecules.* Proc Natl Acad Sci U S A, 1997. **94**(16): p. 8521-8526.
45. Tuerk, C. and L. Gold, *Systematic Evolution of Ligands by Exponential Enrichment - Rna Ligands to Bacteriophage-T4 DNA-Polymerase.* Science, 1990. **249**(4968): p. 505-510.
46. Juli Atherton, N.B., Ben Brown, Nobuo Ogawa, Stuart M. Davidson, Michael B. Eisen, Mark D. Biggin, and Peter Bickel, *A model for sequential evolution of ligands by exponential enrichment (SELEX) data.* Annals of Applied Statistics, 2012. **6**.
47. Ponomarenko, J.V., G.V. Orlova, A.S. Frolov, M.S. Gelfand, and M.P. Ponomarenko, *SELEX_DB: a database on in vitro selected oligomers adapted for recognizing natural sites and for analyzing both SNPs and site-directed mutagenesis data.* Nucleic Acids Res, 2002. **30**(1): p. 195-199.
48. Ponomarenko, J.V., G.V. Orlova, M.P. Ponomarenko, S.V. Lavryushev, A.S. Frolov, S.V. Zybova, and N.A. Kolchanov, *SELEX_DB: an activated database on selected randomized DNA/RNA sequences addressed to genomic sequence annotation.* Nucleic Acids Res, 2000. **28**(1): p. 205-208.
49. Nonin-Lecomte, S., C.H. Lin, and D.J. Patel, *Additional hydrogen bonds and base-pair kinetics in the symmetrical AMP-DNA aptamer complex.* Biophys J, 2001. **81**(6): p. 3422-3431.
50. Lin, C.H. and D.J. Patel, *Structural basis of DNA folding and recognition in an AMP-DNA aptamer complex: distinct architectures but common recognition motifs for DNA and RNA aptamers complexed to AMP.* Chem Biol, 1997. **4**(11): p. 817-832.
51. Xiao, H., T.E. Edwards, and A.R. Ferre-D'Amare, *Structural Basis for Specific, High-Affinity Tetracycline Binding by an In Vitro Evolved Aptamer and Artificial Riboswitch.* Chem Biol, 2008. **15**(10): p. 1125-1137.
52. Volkow, N.D., G.J. Wang, M.W. Fischman, R. Foltin, J.S. Fowler, D. Franceschi, M. Franceschi, J. Logan, S.J. Gatley, C. Wong, Y.S. Ding, R. Hitzemann, and N. Pappas, *Effects of route of administration on cocaine induced dopamine transporter blockade in the human brain.* Life Sciences, 2000. **67**(12): p. Pl1507-Pl1515.
53. Neves, M.A.D., O. Reinstein, M. Saad, and P.E. Johnson, *Defining the secondary structural requirements of a cocaine-binding aptamer by a thermodynamic and mutation study.* Biophysical Chemistry, 2010. **153**(1): p. 9-16.
54. Baker, B.R., R.Y. Lai, M.S. Wood, E.H. Doctor, A.J. Heeger, and K.W. Plaxco, *An electronic, aptamer-based small-molecule sensor for the rapid, label-free detection of cocaine in adulterated samples and biological fluids.* Journal of the American Chemical Society, 2006. **128**(10): p. 3138-9.
55. Tobias, R.S., *The determination of stability constants of complex inorganic species in aqueous solutions.* J. Chem. Educ., 1958. **35**(12): p. 592.
56. Meites, T. and L. Meites, *Theory of titration curves-VII The properties of derivative titration curves for strong acid-strong base and other isovalent ion-combination titrations.* Talanta, 1970. **17**(6): p. 525-36.
57. Langer, M.R., C.J. Fry, C.L. Peterson, and J.M. Denu, *Modulating acetyl-CoA binding in the GCN5 family of histone acetyltransferases.* Journal of Biological Chemistry, 2002. **277**(30): p. 27337-27344.

58. Langer, M.R., C.J. Fry, C.L. Peterson, and J.M. Denu, *Modulating acetyl-CoA binding in the GCN5 family of histone acetyltransferases.* J Biol Chem, 2002. **277**(30): p. 27337-44.
59. Jeffrey G. A., and Saenger W., *Hydrogen Bonding in Biological Structures.* Springer-Verlag Berlin Heidelberg New York, 1991.
60. Karahalil, B., V.A. Bohr, and D.M. Wilson, *Impact of DNA polymorphisms in key DNA base excision repair proteins on cancer risk.* Hum Exp Toxicol, 2012. **31**(10): p. 981-1005.
61. Loureiro, M.E., A. D'Antuono, J.M.L. Macleod, and N. Lopez, *Uncovering Viral Protein-Protein Interactions and their Role in Arenavirus Life Cycle.* Viruses-Basel, 2012. **4**(9): p. 1651-1667.
62. Kastantin, M., R. Walder, and D.K. Schwartz, *Identifying Mechanisms of Interfacial Dynamics Using Single-Molecule Tracking.* Langmuir, 2012. **28**(34): p. 12443-12456.
63. Ritort, F., *Single-molecule experiments in biological physics: methods and applications.* Journal of Physics-Condensed Matter, 2006. **18**(32): p. R531-R583.
64. Binnig, G. and H. Rohrer, *Scanning Tunneling Microscopy.* Ibm Journal of Research and Development, 1986. **30**(4): p. 355-369.
65. Ramachandran, S. and R. Lal, *Scope of atomic force microscopy in the advancement of nanomedicine.* Indian Journal of Experimental Biology, 2010. **48**(10): p. 1020-1036.
66. Lyubchenko, Y.L., L.S. Shlyakhtenko, and T. Ando, *Imaging of nucleic acids with atomic force microscopy.* Methods, 2011. **54**(2): p. 274-283.
67. Hansma, H.G., R.L. Sinsheimer, M.Q. Li, and P.K. Hansma, *Atomic Force Microscopy of Single-Stranded and Double-Stranded DNA.* Nucleic Acids Res, 1992. **20**(14): p. 3585-3590.
68. Allen, M.J., E.M. Bradbury, and R. Balhorn, *AFM analysis of DNA-protamine complexes bound to mica.* Nucleic Acids Res, 1997. **25**(11): p. 2221-6.
69. Fang, Y. and J.H. Hoh, *Cationic silanes stabilize intermediates in DNA condensation.* FEBS Lett, 1999. **459**(2): p. 173-6.
70. Lo, Y.S., Y.J. Zhu, and T.P. Beebe, *Loading-rate dependence of individual ligand-receptor bond-rupture forces studied by atomic force microscopy.* Langmuir, 2001. **17**(12): p. 3741-3748.
71. Merkel, R., P. Nassoy, A. Leung, K. Ritchie, and E. Evans, *Energy landscapes of receptor-ligand bonds explored with dynamic force spectroscopy.* Nature, 1999. **397**(6714): p. 50-53.
72. Cocco, S., R. Monasson, and J.F. Marko, *Force and kinetic barriers to unzipping of the DNA double helix.* Proc Natl Acad Sci U S A, 2001. **98**(15): p. 8608-8613.
73. Ivanovska, I.L., P.J. de Pablo, B. Ibarra, G. Sgalari, F.C. MacKintosh, J.L. Carrascosa, C.F. Schmidt, and G.J.L. Wuite, *Bacteriophage capsids: Tough nanoshells with complex elastic properties.* Proc Natl Acad Sci U S A, 2004. **101**(20): p. 7600-7605.
74. Morii, T., R. Mizuno, H. Haruta, and T. Okada, *An AFM study of the elasticity of DNA molecules.* Thin Solid Films, 2004. **464**: p. 456-458.
75. Suresh, S., *Nanomedicine - Elastic clues in cancer detection.* Nature Nanotechnology, 2007. **2**(12): p. 748-749.
76. Ionescu-Zanetti, C., R. Khurana, J.R. Gillespie, J.S. Petrick, L.C. Trabachino, L.J. Minert, S.A. Carter, and A.L. Fink, *Monitoring the assembly of Ig light-chain amyloid fibrils by atomic force microscopy.* Proc Natl Acad Sci U S A, 1999. **96**(23): p. 13175-13179.
77. Berquand, A., M.P. Mingeot-Leclercq, and Y.F. Dufrene, *Real-time imaging of drug-membrane interactions by atomic force microscopy.* Biochimica Et Biophysica Acta-Biomembranes, 2004. **1664**(2): p. 198-205.
78. Albrecht, T.R., S. Akamine, T.E. Carver, and C.F. Quate, *Microfabrication of Cantilever Styli for the Atomic Force Microscope.* Journal of Vacuum Science & Technology a-Vacuum Surfaces and Films, 1990. **8**(4): p. 3386-3396.
79. Cappella, B. and G. Dietler, *Force-distance curves by atomic force microscopy.*

Surface Science Reports, 1999. **34**(1-3): p. 1-+.
80. Hutter, J.L. and J. Bechhoefer, *Calibration of Atomic-Force Microscope Tips (Vol 64, Pg 1868, 1993).* Review of Scientific Instruments, 1993. **64**(11): p. 3342-3342.
81. Heim, L.O., M. Kappl, and H.J. Butt, *Tilt of atomic force microscope cantilevers: Effect on spring constant and adhesion measurements.* Langmuir, 2004. **20**(7): p. 2760-2764.
82. Hutter, J.L., *Comment on tilt of atomic force microscope cantilevers: effect on spring constant and adhesion measurements.* Langmuir, 2005. **21**(6): p. 2630-2632.
83. Cleveland, J.P., S. Manne, D. Bocek, and P.K. Hansma, *A Nondestructive Method for Determining the Spring Constant of Cantilevers for Scanning Force Microscopy.* Review of Scientific Instruments, 1993. **64**(2): p. 403-405.
84. Bank, T.L., A. Dosen, R.F. Giese, E.M. Haase, and H.T. Sojar, *Atomic Force Spectroscopy Evidence of Non-Specific Adhesion of Aggregatibacter actinomycetemcomitans.* Journal of Nanoscience and Nanotechnology, 2011. **11**(10): p. 8450-8456.
85. Bizzarri, A.R. and S. Cannistraro, *The application of atomic force spectroscopy to the study of biological complexes undergoing a biorecognition process.* Chemical Society Reviews, 2010. **39**(2): p. 734-749.
86. Butt, H.J., B. Cappella, and M. Kappl, *Force measurements with the atomic force microscope: Technique, interpretation and applications.* Surface Science Reports, 2005. **59**(1-6): p. 1-152.
87. Israelachvili, J.N., *Intermolecular and Surface Forces.* Academic Press, 1992.
88. Bell, G.I., *Models for Specific Adhesion of Cells to Cells.* Science, 1978. **200**(4342): p. 618-627.
89. Evans, E. and K. Ritchie, *Dynamic strength of molecular adhesion bonds.* Biophys J, 1997. **72**(4): p. 1541-1555.
90. Neuert, G., C. Albrecht, E. Pamir, and H.E. Gaub, *Dynamic force spectroscopy of the digoxigenin-antibody complex.* FEBS Lett, 2006. **580**(2): p. 505-509.
91. Rüdiger Berger, Gutmann J., Rolf Schäfer, *SCANNING PROBE METHODS: FROM MICROSCOPY TO SENSING.* 2011: p. 12.
92. Friedsam, C., A.K. Wehle, F. Kuhner, and H.E. Gaub, *Dynamic single-molecule force spectroscopy: bond rupture analysis with variable spacer length.* Journal of Physics-Condensed Matter, 2003. **15**(18): p. S1709-S1723.
93. Noy, A., *Strength in numbers: Probing and understanding intermolecular bonding with chemical force microscopy.* Scanning, 2008. **30**(2): p. 96-105.
94. Alessandrini, A. and P. Facci, *AFM: a versatile tool in biophysics.* Measurement Science & Technology, 2005. **16**(6): p. R65-R92.
95. Frisbie, C.D., L.F. Rozsnyai, A. Noy, M.S. Wrighton, and C.M. Lieber, *Functional-Group Imaging by Chemical Force Microscopy.* Science, 1994. **265**(5181): p. 2071-2074.
96. Hinterdorfer, P., W. Baumgartner, H.J. Gruber, K. Schilcher, and H. Schindler, *Detection and localization of individual antibody-antigen recognition events by atomic force microscopy.* Proc Natl Acad Sci U S A, 1996. **93**(8): p. 3477-3481.
97. Dammer, U., M. Hegner, D. Anselmetti, P. Wagner, M. Dreier, W. Huber, and H.J. Guntherodt, *Specific antigen/antibody interactions measured by force microscopy.* Biophys J, 1996. **70**(5): p. 2437-2441.
98. Florin, E.L., V.T. Moy, and H.E. Gaub, *Adhesion Forces between Individual Ligand-Receptor Pairs.* Science, 1994. **264**(5157): p. 415-417.
99. Ebner, A., J. Madl, F. Kienberger, L.A. Chtcheglova, T. Puntheeranurak, R. Zhu, J.L. Tang, H.J. Gruber, G.J. Schutz, and P. Hinterdorfer, *Single molecule force microscopy on cells and biological membranes.* Current Nanoscience, 2007. **3**(1): p. 49-56.
100. Nguyen, T.H., Y.U. Kim, K.J. Kim, and S.S. Choi, *Investigation of Structural Transition of dsDNA on Various Substrates Studied by Atomic Force Microscopy.* Journal of Nanoscience and Nanotechnology, 2009. **9**(3): p. 2162-2168.
101. Morfill, J., F. Kuhner, K. Blank, R.A. Lugmaier, J. Sedlmair, and H.E. Gaub, *B-S*

transition in short oligonucleotides. Biophys J, 2007. **93**(7): p. 2400-2409.
102. Eckel, R., S.D. Wilking, A. Becker, N. Sewald, R. Ros, and D. Anselmetti, *Single-molecule experiments in synthetic biology: an approach to the affinity ranking of DNA-binding peptides.* Angew Chem Int Ed Engl, 2005. **44**(25): p. 3921-4.
103. Lee, M. and S.W. Kim, *Polyethylene glycol-conjugated copolymers for plasmid DNA delivery.* Pharmaceutical Research, 2005. **22**(1): p. 1-10.
104. Berquand, A., *Common Approaches to Tip Functionalization for AFM-Based Molecular Recognition Measurements.* Bruker Nano Surfaces Business, 2010: p. 6.
105. #130, B.N.S.A.N., *Common Approaches to Tip Functionalization for AFM-Based Molecular Recognition Measurements.*
106. Shlyakhtenko, L.S., A.A. Gall, A. Filonov, Z. Cerovac, A. Lushnikov, and Y.L. Lyubchenko, *Silatrane-based surface chemistry for immobilization of DNA, protein-DNA complexes and other biological materials.* Ultramicroscopy, 2003. **97**(1-4): p. 279-87.
107. Grandbois, M., M. Beyer, M. Rief, H. Clausen-Schaumann, and H.E. Gaub, *How strong is a covalent bond?* Science, 1999. **283**(5408): p. 1727-1730.
108. Hegner, M., P. Wagner, and G. Semenza, *Ultralarge Atomically Flat Template-Stripped Au Surfaces for Scanning Probe Microscopy.* Surface Science, 1993. **291**(1-2): p. 39-46.
109. Getz, E.B., M. Xiao, T. Chakrabarty, R. Cooke, and P.R. Selvin, *A comparison between the sulfhydryl reductants tris(2-carboxyethyl)phosphine and dithiothreitol for use in protein biochemistry.* Anal Biochem, 1999. **273**(1): p. 73-80.
110. Ikai, A., R. Afrin, H. Sekiguchi, T. Okajima, M.T. Alam, and S. Nishida, *Nano-mechanical methods in biochemistry using atomic force microscopy.* Curr Protein Pept Sci, 2003. **4**(3): p. 181-93.
111. Strunz, T., K. Oroszlan, R. Schafer, and H.J. Guntherodt, *Dynamic force spectroscopy of single DNA molecules.* Proc Natl Acad Sci U S A, 1999. **96**(20): p. 11277-11282.
112. Kada, G., F. Kienberger, and P. Hinterdorfer, *Atomic force microscopy in bionanotechnology.* Nano Today, 2008. **3**(1-2): p. 12-19.
113. Krautbauer, R., M. Rief, and H.E. Gaub, *Unzipping DNA oligomers.* Nano Lett, 2003. **3**(4): p. 493-496.
114. Hinterdorfer, P., W. Baumgartner, H.J. Gruber, K. Schilcher, and H. Schindler, *Detection and localization of individual antibody-antigen recognition events by atomic force microscopy.* Proc Natl Acad Sci U S A, 1996. **93**(8): p. 3477-81.
115. Ho, D., J.L. Zimmermann, F.A. Dehmelt, U. Steinbach, M. Erdmann, P. Severin, K. Falter, and H.E. Gaub, *Force-driven separation of short double-stranded DNA.* Biophys J, 2009. **97**(12): p. 3158-67.
116. Kufer, S.K., E.M. Puchner, H. Gumpp, T. Liedl, and H.E. Gaub, *Single-molecule cut-and-paste surface assembly.* Science, 2008. **319**(5863): p. 594-596.
117. Noy, A., D.V. Vezenov, and C.M. Lieber, *Chemical force microscopy.* Annual Review of Materials Science, 1997. **27**: p. 381-421.
118. Noy, A., D.V. Vezenov, J.F. Kayyem, T.J. Meade, and C.M. Lieber, *Stretching and breaking duplex DNA by chemical force microscopy.* Chem Biol, 1997. **4**(7): p. 519-27.
119. Folkers, J.P., P.E. Laibinis, and G.M. Whitesides, *Self-Assembled Monolayers of Alkanethiols on Gold - Comparisons of Monolayers Containing Mixtures of Short-Chain and Long-Chain Constituents with Ch3 and Ch2oh Terminal Groups.* Langmuir, 1992. **8**(5): p. 1330-1341.
120. Ling, L.S., H.J. Butt, and R. Berger, *Rupture force changes between the third strand and the double strand within an oligonucleotide-directed triplex in the presence of intercalative molecules.* Applied Physics Letters, 2006. **89**(11).
121. Ling, L.S., H.J. Butt, and R. Berger, *Rupture force between the third strand and the double strand within a triplex DNA.* Journal of the American Chemical Society, 2004. **126**(43): p. 13992-13997.

122. Vezenov, D.V., A. Noy, L.F. Rozsnyai, and C.M. Lieber, *Force titrations and ionization state sensitive imaging of functional groups in aqueous solutions by chemical force microscopy.* Journal of the American Chemical Society, 1997. **119**(8): p. 2006-2015.
123. Laibinis, P.E., M.A. Fox, J.P. Folkers, and G.M. Whitesides, *Comparisons of Self-Assembled Monolayers on Silver and Gold - Mixed Monolayers Derived from Hs(Ch2)21x and Hs(Ch2)10y (X, Y = Ch3, Ch2oh) Have Similar Properties.* Langmuir, 1991. **7**(12): p. 3167-3173.
124. Nuzzo, R.G. and D.L. Allara, *Adsorption of Bifunctional Organic Disulfides on Gold Surfaces.* J Am Chem Soc, 1983. **105**(13): p. 4481-4483.
125. Lee, C.K., Y.M. Wang, L.S. Huang, and S. Lin, *Atomic force microscopy: determination of unbinding force, off rate and energy barrier for protein-ligand interaction.* Micron, 2007. **38**(5): p. 446-61.
126. Yuan, C., A. Chen, P. Kolb, and V.T. Moy, *Energy landscape of streptavidin-biotin complexes measured by atomic force microscopy.* Biochemistry, 2000. **39**(33): p. 10219-23.
127. Stevens, M.M., S. Allen, M.C. Davies, C.J. Roberts, E. Schacht, S.J.B. Tendler, S. VanSteenkiste, and P.M. Williams, *The development, characterization, and demonstration of a versatile immobilization strategy for biomolecular force measurements.* Langmuir, 2002. **18**(17): p. 6659-6665.
128. Hegner, M., P. Wagner, and G. Semenza, *Immobilizing DNA on Gold Via Thiol Modification for Atomic-Force Microscopy Imaging in Buffer Solutions.* Febs Letters, 1993. **336**(3): p. 452-456.
129. Zhang, W., R. Barbagallo, C. Madden, C.J. Roberts, A. Woolford, and S. Allen, *Progressing single biomolecule force spectroscopy measurements for the screening of DNA binding agents.* Nanotechnology, 2005. **16**(10): p. 2325-2333.
130. Wolf, L.K., Y. Gao, and R.M. Georgiadis, *Sequence-dependent DNA immobilization: Specific versus nonspecific contributions.* Langmuir, 2004. **20**(8): p. 3357-3361.
131. Bain, C.D., E.B. Troughton, Y.T. Tao, J. Evall, G.M. Whitesides, and R.G. Nuzzo, *Formation of Monolayer Films by the Spontaneous Assembly of Organic Thiols from Solution onto Gold.* J Am Chem Soc, 1989. **111**(1): p. 321-335.
132. Rong, W., W. Ding, L. Madler, R.S. Ruoff, and S.K. Friedlander, *Mechanical properties of nanoparticle chain aggregates by combined AFM and SEM: isolated aggregates and networks.* Nano Lett, 2006. **6**(12): p. 2646-55.
133. Neundlinger, I., A. Poturnayova, I. Karpisova, C. Rankl, P. Hinterdorfer, M. Snejdarkova, T. Hianik, and A. Ebner, *Characterization of enhanced monovalent and bivalent thrombin DNA aptamer binding using single molecule force spectroscopy.* Biophys J, 2011. **101**(7): p. 1781-7.
134. Koltover, I., K. Wagner, and C.R. Safinya, *DNA condensation in two dimensions.* Proc Natl Acad Sci U S A, 2000. **97**(26): p. 14046-51.
135. McConnell, K.J. and D.L. Beveridge, *DNA structure: what's in charge?* J Mol Biol, 2000. **304**(5): p. 803-20.
136. Wenner, J.R., M.C. Williams, I. Rouzina, and V.A. Bloomfield, *Salt dependence of the elasticity and overstretching transition of single DNA molecules.* Biophys J, 2002. **82**(6): p. 3160-3169.
137. Verwey, E.J.W., *Theory of the Stability of Lyophobic Colloids.* Journal of Physical and Colloid Chemistry, 1947. **51**(3): p. 631-636.
138. Derjaguin, B., *Citation-Classic - Theory of the Stability of Strongly Charged Lyophobic Sols and of the Adhesion of Strongly Charged-Particles in Solution of Electrolytes.* Current Contents/Physical Chemical & Earth Sciences, 1987(32): p. 20-20.
139. Baumann, C.G., S.B. Smith, V.A. Bloomfield, and C. Bustamante, *Ionic effects on the elasticity of single DNA molecules.* Proc Natl Acad Sci U S A, 1997. **94**(12): p. 6185-6190.
140. Sitko, J.C., E.M. Mateescu, and H.G. Hansma, *Sequence-dependent DNA condensation*

and the electrostatic zipper. Biophys J, 2003. **84**(1): p. 419-431.
141. Stevens, M.J., *Simple simulations of DNA condensation.* Biophys J, 2001. **80**(1): p. 130-139.
142. Fang, Y. and J. Yang, *Two-dimensional condensation of DNA molecules on cationic lipid membranes.* Journal of Physical Chemistry B, 1997. **101**(3): p. 441-449.
143. Deng, H. and V.A. Bloomfield, *Structural effects of cobalt-amine compounds on DNA condensation.* Biophys J, 1999. **77**(3): p. 1556-1561.
144. Chen, H., S.P. Meisburger, S.A. Pabit, J.L. Sutton, W.W. Webb, and L. Pollack, *Ionic strength-dependent persistence lengths of single-stranded RNA and DNA.* Proc Natl Acad Sci U S A, 2012. **109**(3): p. 799-804.
145. Iversen, H.W. and R. Balent, *A Correlating Modulus for Fluid Resistance in Accelerated Motion.* Journal of Applied Physics, 1951. **22**(3): p. 324-328.
146. Janovjak, H., J. Struckmeier, and D.J. Muller, *Hydrodynamic effects in fast AFM single-molecule force measurements.* European Biophysics Journal with Biophysics Letters, 2005. **34**(1): p. 91-96.
147. Ke, C.H., Y. Jiang, M. Rivera, R.L. Clark, and P.E. Marszalek, *Pulling geometry-induced errors in single molecule force spectroscopy measurements.* Biophys J, 2007. **92**(9): p. L76-L78.
148. Ke, C., Y. Jiang, M. Rivera, R.L. Clark, and P.E. Marszalek, *Pulling geometry-induced errors in single molecule force spectroscopy measurements.* Biophys J, 2007. **92**(9): p. L76-8.
149. Nguyen, T.H., L.J. Steinbock, H.J. Butt, M. Helm, and R. Berger, *Measuring Single Small Molecule Binding via Rupture Forces of a Split Aptamer.* J Am Chem Soc, 2011. **133**(7): p. 2025-2027.
150. Chen, J.W., J.H. Jiang, X. Gao, G.K. Liu, G.L. Shen, and R.Q. Yu, *A New Aptameric Biosensor for Cocaine Based on Surface-Enhanced Raman Scattering Spectroscopy.* Chemistry-a European Journal, 2008. **14**(27): p. 8374-8382.
151. Stojanovic, M.N. and D.W. Landry, *Aptamer-based colorimetric probe for cocaine.* J Am Chem Soc, 2002. **124**(33): p. 9678-9679.
152. Liu, J.W. and Y. Lu, *Fast colorimetric sensing of adenosine and cocaine based on a general sensor design involving aptamers and nanoparticles.* Angewandte Chemie-International Edition, 2006. **45**(1): p. 90-94.
153. Zhou, J.W., A.V. Ellis, H. Kobus, and N.H. Voelcker, *Aptamer sensor for cocaine using minor groove binder based energy transfer.* Anal Chim Acta, 2012. **719**: p. 76-81.
154. Swensen, J.S., Y. Xiao, B.S. Ferguson, A.A. Lubin, R.Y. Lai, A.J. Heeger, K.W. Plaxco, and H.T. Soh, *Continuous, Real-Time Monitoring of Cocaine in Undiluted Blood Serum via a Microfluidic, Electrochemical Aptamer-Based Sensor.* J Am Chem Soc, 2009. **131**(12): p. 4262-4266.
155. Gaub, B.M., C. Kaul, J.L. Zimmermann, T. Carell, and H.E. Gaub, *Switching the mechanics of dsDNA by Cu salicylic aldehyde complexation.* Nanotechnology, 2009. **20**(43): p. 434002.
156. Green, N.H., P.M. Williams, O. Wahab, M.C. Davies, C.J. Roberts, S.J.B. Tendler, and S. Allen, *Single-molecule investigations of RNA dissociation.* Biophys J, 2004. **86**(6): p. 3811-3821.
157. Roberto De Paris, T.S., Krisztina Oroszlan, Hans-Joachim Güntherodt and a.M. Hegner, *Force Spectroscopy and Dynamics of the Biotin-Avidin Bond Studied by Scanning Force Microscopy.* Single Mol. , 2000. **1**(4): p. 5.
158. Bustamante, C., S.B. Smith, J. Liphardt, and D. Smith, *Single-molecule studies of DNA mechanics.* Current Opinion in Structural Biology, 2000. **10**(3): p. 279-285.
159. Murphy, M.C., I. Rasnik, W. Cheng, T.M. Lohman, and T.J. Ha, *Probing single-stranded DNA conformational flexibility using fluorescence spectroscopy.* Biophys J, 2004. **86**(4): p. 2530-2537.
160. Deniz, A.A., M. Dahan, J.R. Grunwell, T. Ha, A.E. Faulhaber, D.S. Chemla, S. Weiss, and P.G. Schultz, *Single-pair fluorescence resonance energy transfer on freely*

diffusing molecules: observation of Forster distance dependence and subpopulations. Proc Natl Acad Sci U S A, 1999. **96**(7): p. 3670-5.
161. Williams, M.C., J.R. Wenner, I. Rouzina, and V.A. Bloomfield, *Effect of pH on the overstretching transition of double-stranded DNA: evidence of force-induced DNA melting.* Biophys J, 2001. **80**(2): p. 874-81.
162. Niazi, J.H., S.J. Lee, Y.S. Kim, and M.B. Gu, *ssDNA aptamers that selectively bind oxytetracycline.* Bioorg Med Chem, 2008. **16**(3): p. 1254-1261.

Appendix

Appendix A: Speed Dependence for 2- BP system

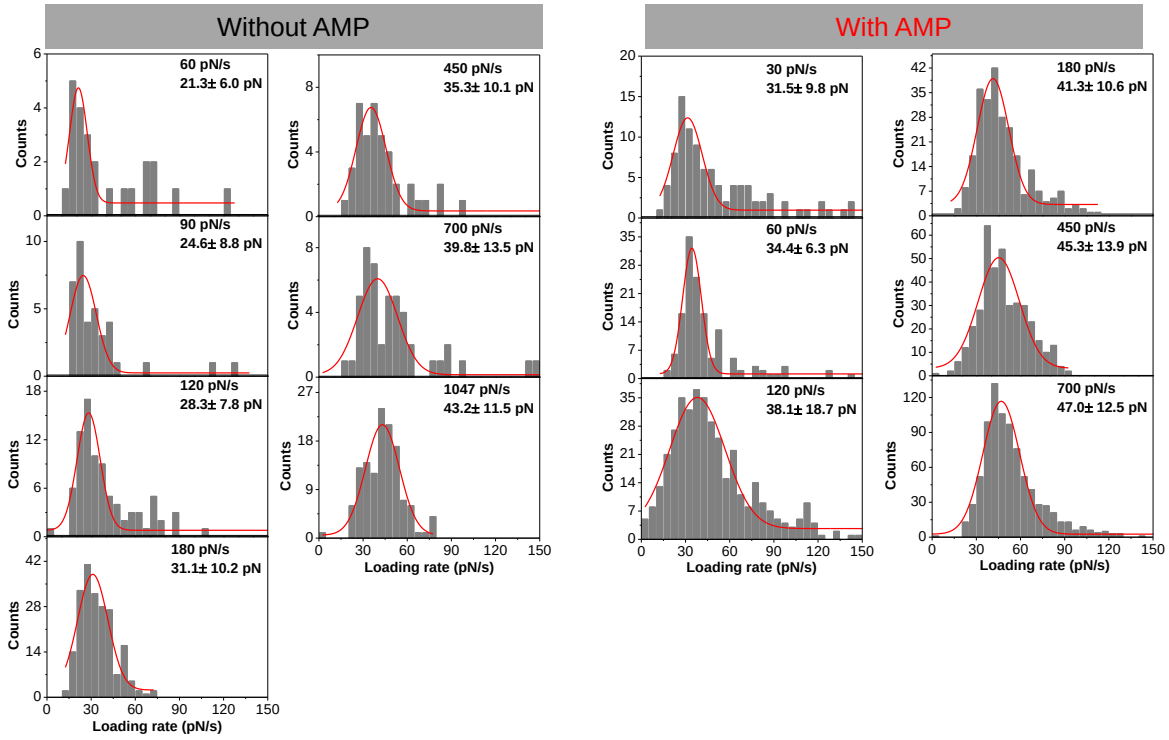

Figure A.1. Rupture forces at loading rates from 30 to 1047 pN/s in the absence of AMP (left) and in the presence of AMP (right).

Appendix B: Substitution of binding group

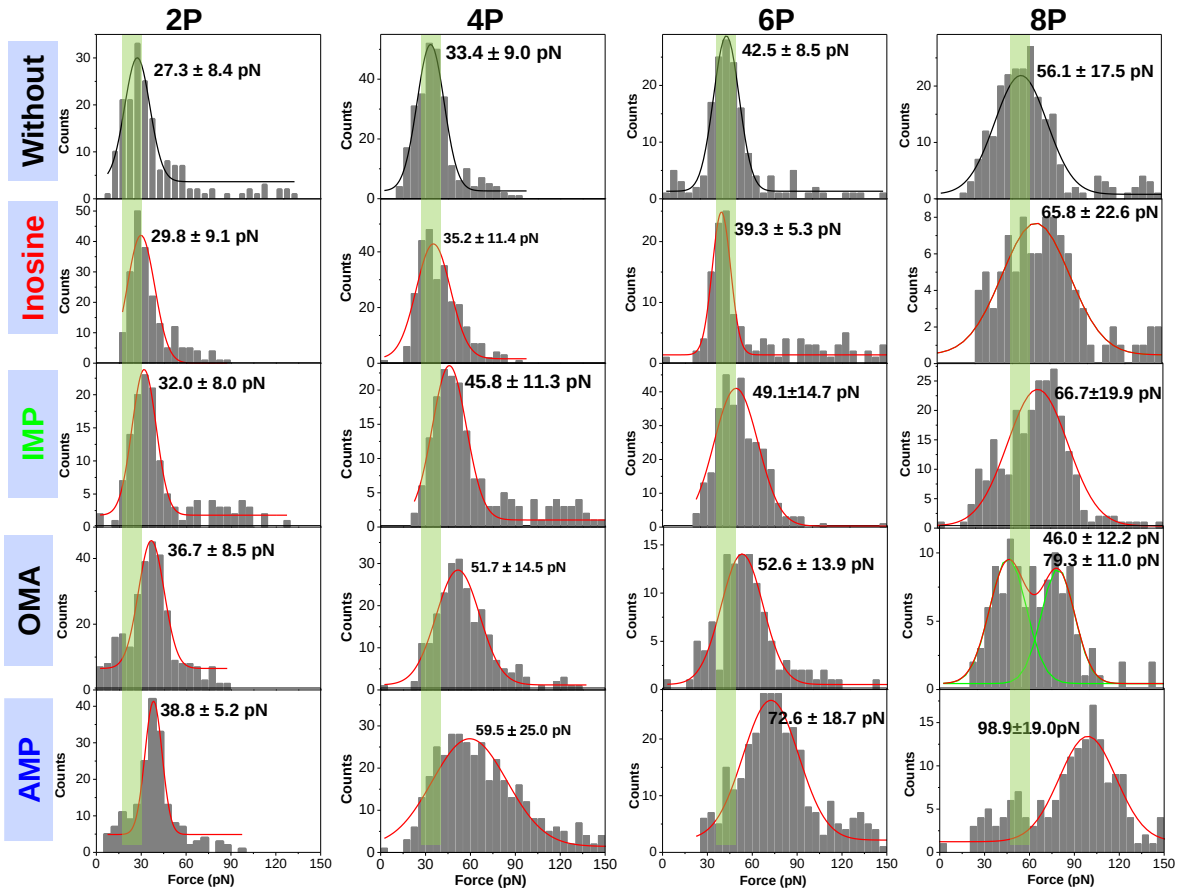

Figure B.1. A set of measurement of rupture forces of targets Inosine, IMP, OMA and AMP that bind aptamers containing different number of pockets. The most probable rupture forces shift to higher values from top to bottom due to the increase of binding group of the target. Many sets of measurements were averaged in figure 7.5, depending on each measurement as described in the table 7.1.